University of Massachusetts Medical School

eScholarship@UMMS

2012-05-30

Small Molecule Investigation of KCNQ Potassium Channels: A Dissertation

Karen Mruk
University of Massachusetts Medical School

Let us know how access to this document benefits you.

Follow this and additional works at: https://escholarship.umassmed.edu/gsbs_diss

Part of the Amino Acids, Peptides, and Proteins Commons, Bacteria Commons, Biochemistry, Biophysics, and Structural Biology Commons, Biological Factors Commons, Inorganic Chemicals Commons, and the Investigative Techniques Commons

SMALL MOLECULE INVESTIGATION OF KCNQ POTASSIUM CHANNELS

A Dissertation Presented

By

Karen Mruk

Submitted to the Faculty of the University of Massachusetts Graduate School of Biomedical Sciences, Worcester in partial fulfillment of the requirements for the degree of

DOCTOR OF PHILOSOPHY

May 30, 2012

BIOCHEMISTRY AND MOLECULAR PHARMACOLOGY

SMALL MOLECULE INVESTIGATION OF KCNQ POTASSIUM CHANNELS

A Dissertation Presented
By
Karen Mruk

The signature of the Dissertation Defense Committee signify completion and approval as
to style and content of the Dissertation

_____
William R. Kobertz, Ph.D, Thesis Advisor

_____
Steven A. N. Goldstein, M.D., Ph.D., Member of the Committee

_____
José R. Lemos, Ph.D, Member of the Committee

_____
Celia A. Schiffer, Ph.D., Member of the Committee

_____
William Royer, Ph.D., Member of the Committee

The signature of the Chair of the Committee signifies that the written dissertation meets
the requirements of the Dissertation Committee

_____
Stephen C. Miller, Ph.D., Chair of Committee

The signature of the Dean of the Graduate School of Biomedical Sciences signifies that
the student has met all graduation requirements of the school.

_____
Anthony Carruthers, Ph.D.,
Dean of the Graduate School of Biomedical Sciences

Biochemistry and Molecular Pharmacology

May 30, 2012

DEDICATION

I dedicate this thesis in memory of my grandmother Helen Mruk and to my grandmother Frances Bollwage. Thank you for being my two biggest cheerleaders.

ACKNOWLEDGEMENTS

First and foremost, I would like to thank my thesis advisor, Bill Kobertz. His enthusiasm for science is contagious and his patience truly endless: a winning combination for any mentor to have. I would also like to thank my labmates, past and present, for all of their help, guidance, silly conversations, and of course helping to edit this thesis. In particular, Jess Rocheleau and Trevor Morin taught me how to do extract oocytes. They in addition to Heidi Hafemann provided electrophysiological support. Yuan Gao, there will never be another lab manager like you. Thank you to Kshama Chandrasekhar for countless discussions. There hasn't been another Kobertz lab dance party since you've graduated. Also, a great big thank you to my bay mates, Anatoli Lvov and Zhengmao Hua who have listened to me yell at my computer for the past 4 months and served as a wealth of information as well as my support system through this difficult process.

I would like to thank my committee members, José Lemos, Bill Royer, Celia Schiffer, and my committee chair, Steve Miller for their feedback and suggestions throughout the duration of my thesis research. Also, many thanks to Steve Goldstein for serving as my external examiner.

I have been extremely fortunate to be part of the Biochemistry family. Thank you to the faculty, post-docs, technicians, students, and administrative staff for many discussions, suggestions, and of course reagents. I only hope that someday the softball team will carry on in all its glory. In particular, thank you to Steven Pauff and Kate

Harwood, my lab neighbors, for offering your shoulders and ears to me whenever I needed to vent or share a silly story.

Finally, as no one gets through grad school without some sort of support system, I am extremely grateful for mine. To my bowling buddies, thank you for being a constant source of welcome distraction. To my parents and sister, I could not have got through this process without your constant love and support. Thank you to my best friend Erica Sanchez and "the Drew Crew" for countless phone dates and for listening, laughing, and crying with me every step of the way. Lastly, a great big thank you to all the great friends I've made in my time here.

ABSTRACT

Voltage-gated K^+ channels associate with multiple regulatory proteins to form complexes with diverse gating properties and pharmacological sensitivities. Small molecules which activate or inhibit channel function are valuable tools for dissecting the assembly and function of these macromolecular complexes. My thesis focuses on the discovery and use of small molecules to probe the structure and function of the KCNQ family of voltage-gated K^+ channels.

One protein that obligatorily assembles with KCNQ channels to mediate proper assembly, trafficking, and gating is the calcium sensor, calmodulin. Although resolution of the crystal structures of calmodulin associated with isolated peptide fragments from other ion channels has provided some insight into how calmodulin interacts with and modulates KCNQ channels, structural information for calmodulin bound to a fully folded ion channel in the membrane is unknown. In Chapter II, I developed an intracellular tethered blocker approach to determine the location of calmodulin binding with respect to the KCNQ ion-conducting pathway. Using distance restraints from a panel of these intracellular tethered blockers we then generated models of the KCNQ-calmodulin complex. Our model places calmodulin close to the gate of KCNQ channels, providing structural insight into how CaM is able to communicate changes in intracellular calcium levels to KCNQ channel complexes.

In addition to pore blockers, chemical modification of ion channels has been used to probe ion channel function. During my initial attempt to chemically activate KCNQ channels, I discovered that some boronates modulate KCNQ complexes. In Chapter III,

the activating derivative, phenylboronic acid, is characterized. Characterization of activation by phenylboronic acid showed that it targeted the ion conduction pathway of KCNQ channels with some specificity over other voltage-gated K^+ channels. The commercial availability of thousands of boronic acid derivatives provides a large class of compounds with which to systematically dissect the mechanisms of KCNQ gating and may lead to the discovery of a potent activator of KCNQ complexes for the treatment of channelopathies.

All of the electrophysiological studies presented in this thesis were conducted in *Xenopus* oocytes. Unexpectedly, during the studies described above, the quality of our *Xenopus* oocytes declined. The afflicted oocytes developed black foci on their membranes, had negligible electric resting potentials, and poor viability. Culturing the compromised oocytes determined that they were infected with multi-drug resistant *Stenotrophomonas maltophilia, Pseudomonas fluorescens* and *Pseudomonas putida*. Antibiotic testing showed that all three species of bacteria were susceptible to amikacin and ciprofloxacin, which when included in the oocyte storage media prevented the appearance of black foci and resulted in oocytes that were usable for electrophysiological recordings. This study provides a solution to a common issue that plagues many electrophysiologists who use *Xenopus* oocytes.

Taken together, these findings provide new insights into activation of KCNQ channel complexes and provide new tools to study the structure-function relationship of voltage-gated K^+ channels.

TABLE OF CONTENTS

LIST OF TABLES

LIST OF FIGURES

LIST OF SYMBOLS AND ABBREVIATIONS

$>$	Greater than
Δg_{max}	Change in maximal current
$\approx$	Approximately equal to
1-5-10	Calmodulin binding motif containing hydrophobic residues at positions 1, 5, and 10
1-8-14	Calmodulin binding motif containing hydrophobic residues at positions 1, 8, and 14
AKAP	A-kinase anchoring protein
apoCaM	Non-calcified calmodulin
BFNC	Benign familial neonatal convulsions
BFNE	Benign familial neonatal epilepsy
Ca^{2+}	Calcium ion
CaM	Calmodulin
CaM_{12}	Calmodulin with mutations in both EF hands of the N lobe
CaM_{1234}	Calmodulin with mutations in sll four EF hands
CaM_{34}	Calmodulin with mutations in both EF hands of the C lobe
cAMP	Cyclic adenosine monophosphate
Cav	Voltage-gated calcium channel
Cl^{-}	Chloride ion
Cs^{+}	Cesium Ion
CTX	Charybdotoxin
$d_{1/2}$	Length of the tether that results in half maximal inhibition
DFNA2	Nonsyndromic sensorineural deafness type 2
DIDS	4,4'-Diisothiocyano-2,2'-stilbenedisulfonic acid
E1	KCNE1
E2	KCNE2
E3	KCNE3
E4	KCNE4
E5	KCNE5
EC_{50}	Half maximal effective concentration
EF hand	Helix-loop-helix structural domain
ESI	Electrospray ionization
F	Farraday's constant
hERG	Human ether-a-go-go potassium channel
IC_{50}	Half maximal inhibitory concentration
I_{Kn}	Outwardly rectifying potassium current found in outer hair cells
I_{Ks}	Slow delayed rectifier potassium current found in cardiac myocytes
I_{M}	M-current

IQ-like motif	Calmodulin binding motif starting with residues Isoleucine and Glutamine
K^+	Potassium Ion
KcsA	Potassium channel from *Streptomyces lividans*
Kv	Voltage-gated potassium channel
KvAP	Voltage-gated potassium channel from *Aeropyrum Pernix*
LQTS	Long QT Syndrome
ND96-ACT	Ooocyte storage buffer supplemented with amikacin, ciprofloxacin, and tetracycline
ND96-GT	Oocyte storage buffer supplemented with gentamicin and tetracycline
NEM	N-ethylmaleimide
PBA	Phenylboronic Acid
PBS	Phosphate buffered saline
PIP_2	Phosphatidyliniositol 4,5-biphosphate
PKA	Protein kinase A
pKa	Logarithmic measure of the acid dissociation constant
PKC	Protein kinase C
PNH	Peripheral nerve hyperexcitability
PY motif	Proline-rich sequence
Q1	KCNQ1
Q2	KCNQ2
Q3	KCNQ3
Q4	KCNQ4
Q5	KCNQ4
QA	Quaternary ammonium
R	Universal gas constant
Rb^+	Rubidium Ion
rKv1.2	Voltage-gated potassium channel from *Rattus norvegicus*
R-L3	(3-R)-1,3-dihydro-5-(2-fluorophenyl)-3-(1H-indol-3-ylmethyl)-1-methyl-2H-1,4-benzodiazepin-2-one
SEM	Standard error of the mean
Shaker-IR	Inactivation removed *Shaker* potassium channel
SK channel	Small conductance calcium-activated potassium channel
SQTS	Short QT Syndrome
T	Temperature in Kelvin
T1	Tetramerization domain
TCEP	*tris*(2-carboxyethyl)phosphine
TEA	Tetraethylammonium
TFA	Trifluoroacetic acid
$V_{1/2}$	Potential of half-maximal activation
VDW	Van der Waals
z	Slope factor

α	Alpha
β	Beta
Δ	Delta
τ	Tau

Standard one or three letter code was used to abbreviate amino acids. Mutated residues were abbreviated by position number. All measurement values are in standard SI units.

PREFACE

The experimental work in Chapter II has been written up as a manuscript for publication at the time of this thesis preparation. I developed the intracellular tethered blocker approach to locate the position of CaM binding to KCNQ channels. Dr. Shiven Shandilya is credited with authorship on the manuscript for his work generating the quaternary models of the KCNQ-CaM complex using the distance restraints from the panel of tethered blockers. Authorship is also credited to Dr. Robert Blaustein as we used his short glycine linkers for the initial tethered blocker controls.

The experimental work in Chapters III and IV have been published in peer-reviewed journals. References to publications that represent the work contained within these chapters:

Mruk, K. and Kobertz, W.R. 2009. Discovery of a Novel Activator of KCNQ1-KCNE1 K$^+$ Channel Complexes. *PLoS One* 4(1):e4236.

O'Connell D*, Mruk K*, Rocheleau JM, Kobertz WR. 2011. *Xenopus laevis* Oocytes Infected with Multi-Drug-Resistant Bacteria: Implications for Electrical Recordings. *J Gen Physiol*. 138(2):271-7.

Chemicals not directly generated by author:

The chromanol linker shown in Chapter V were synthesized by Dr. Zhengmao Hua.

CHAPTER I: INTRODUCTION

Efflux of K^+ ions is critical for controlling neuronal excitability and maintaining cardiac rhythmicity, in addition to regulating hormone and electrolyte homeostasis in non-excitable cell types [1]. To achieve proper spatiotemporal release of K^+ ions, cells employ voltage-gated potassium (Kv) channels. These membrane embedded proteins open and close in response to changes in membrane potential permitting the passive diffusion of K^+ ions down their electrochemical gradient and across the lipid bilayer. Accordingly, inadequate Kv function causes multiple diseases including epilepsy, cardiac arrhythmia, deafness, and diabetes [2]. Thus, examining the relationship between the structure and function of Kv channels is essential for understanding their role in human physiology.

Kv Channel Structure

Kv channels are tetramers of pore-forming α-subunits. Each α-subunit is composed of six transmembrane α-helices (S1-S6) (Figure I-1). Assembly into a tetramer forms two essential and coupled domains: a voltage sensing domain (S1-S4) and pore domain (S5-S6). Upon changes in a cell's membrane potential, the voltage-sensing domain moves, resulting in conformational changes that cause the intracellular gate within the pore domain to open allowing K^+ ions to flow down their concentration gradient.
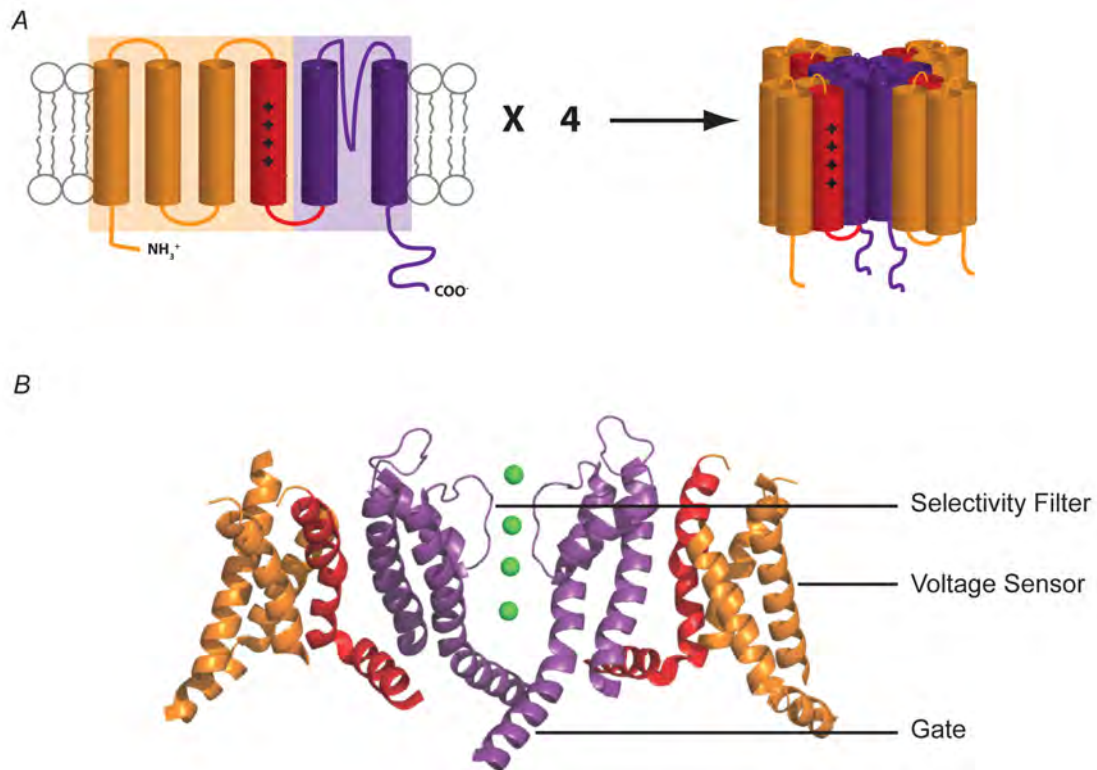
Figure I-1. Structure of voltage-gated potassium channels
(A) Topology schematic of KCNQ channels. The first four transmembrane domains (colored yellow and red) comprise the voltage sensing domain with the fifth and sixth transmembrane domains (colored purple) forming the inner pore domain. (B) Ribbon representation of the crystal structure of a voltage-gated K^+ channel with the front and back subunits removed for clarity. The transmembrane domains are colored as in (A).

Schematic of KCNQ topology generated by K. Mruk. Structure of voltage-gated K^+ channel generated from PDB: 2R9R. Reference: Long, SB, Tao, X, Campbell, EB, MacKinnon, R. *Nature* **450**, 376-382 (2007).

The Pore Domain

The S5 and S6 helices of each α-subunit form the inverted tepee-shaped ion-conducting pore domain (Figure I-2) [3]. The pore domain contains two regulatory modules: the selectivity filter and the intracellular channel gate. Kv channels are selectively permeable to potassium over the smaller cations sodium and lithium. This selectivity is achieved through a sequence of amino acids near the extracellular side of the ion conducting pathway (Thr-Val-Gly-Tyr-Gly) (Figure I-2) [3-5]. The backbone carbonyls of these amino acids coordinate to mimic the hydration shell of potassium ions. The positioning of these carbonyls prevents proper coordination of hydrated smaller cations; however, it does allow for permeation of the larger rubidium (Rb^+) which is nearly a perfect K^+ analog [3].

Unlike the selectivity filter, the channel gate is located at the cytoplasmic face of the membrane. The intracellular gate opens and closes to allow ion flow through the ion conduction pathway. The gate is located at a kink in the C-terminal end of the S6 helixes termed the helix bundle crossing [6]. In eukaryotes, this kink is formed through a Pro-X-Pro or Pro-X-Gly motif (where X is any amino acid) that bends the S6 helix to open and close the channel (Figure I-1) [7,8].
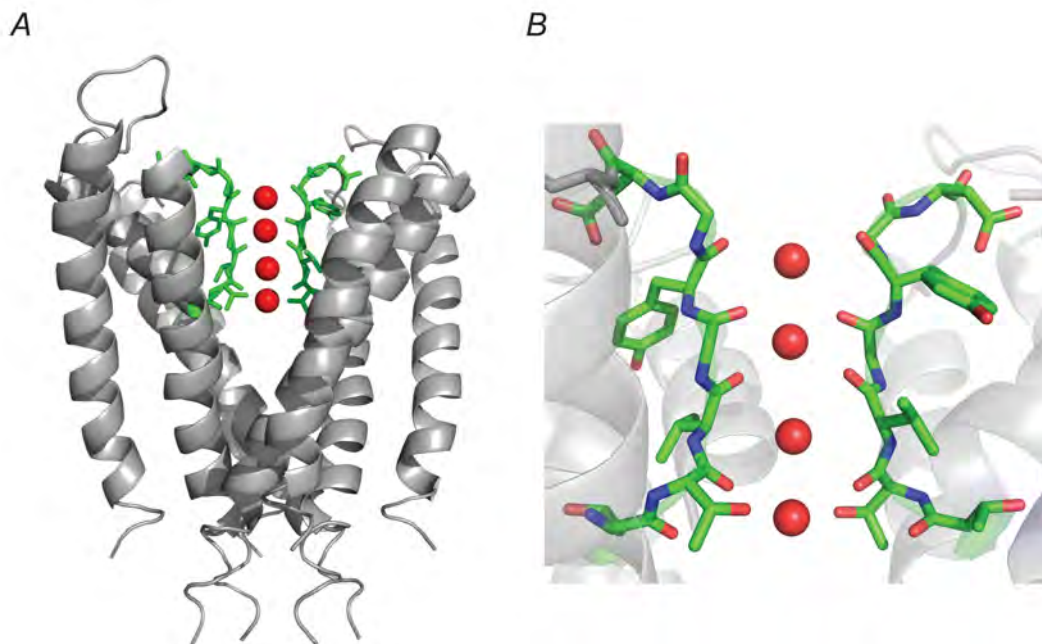
Figure I-2. The structure of the pore and selectivity filter of a K$^+$ channel
(A) Ribbon representation of the crystal structure of the bacterial KcsA K+ channel. The front and back selectivity filter loops are removed for clarity. The selectivity filter is highlighted in green and contains four K$^+$ions. (B) Close-up view of two subunits forming the selectivity filter. Backbone carbonyl atoms form four K$^+$ ion coordination sites.

Structures of the pore domain and selectivity filter are generated from PBD: 1JVM.
Reference: Morais-Cabral, J, Zhou, Y, and MacKinnon, R. *Nature* **414**, 37-42 (2001).

The Voltage Sensing Domain

The voltage sensing domain is comprised of the S1-S4 helices of the α-subunits and is responsible for detecting changes in membrane potential. The voltage sensing domain of one subunit surrounds the pore forming helices of the adjacent subunit, leading to tight coupling between voltage sensor movement and gate opening [9]. Upon membrane depolarization, the positively charged S4 helices move out toward the cell exterior, resulting in a widening of the ion conduction entryway (Figure I-3). Membrane repolarization causes the S4 helices to move back into the membrane, forcing the downward displacement of the linker helix between the S4 and S5 transmembrane helices (Figure I-3). This movement towards the intracellular side of the cell compresses the gate and prevents ions from entering the ion conduction pathway.
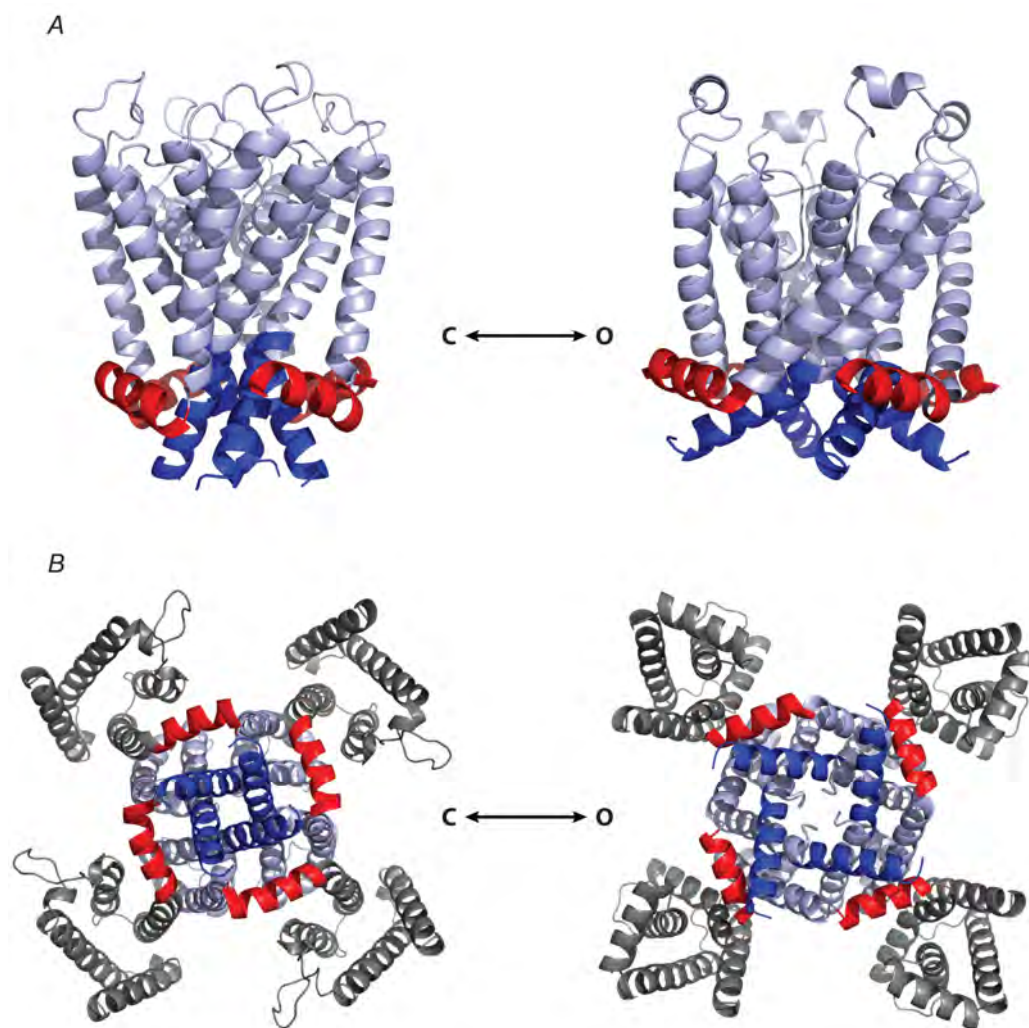
Figure I-3. Model of the coupling between the voltage sensor and intracellular gate
(A) Membrane view of a model of the KCNQ1 K^+ channel in the proposed closed (left) and open (right) conformations. S4-S5 linkers are in red, the kink in the gate is in blue, the rest of the pore subunits are tinted. The voltage-sensing domain is removed for clarity. (B) Cytosolic view of the models from above. The voltage sensor is depicted in grey, the rest of the colors are the same as above. Notice the differences in the voltage-sensing domain and the gate between the open and closed conformations.

Closed and open state models were generated from the PDBs attached as supplemental material from the following paper: Smith, JA, Vanoye, CG, George, AL, Meiler, J, and Sanders, CR, *Biochemistry*, **46** 14141–14152 (2007).

KCNQ K$^+$ Channels

KCNQ channels are a subfamily of Kv channels (Kv7) that are vital for regulating membrane excitability, cardiac rhythmicity, and salt and water homeostasis. Similar to other Kv channels, KCNQ α-subunits share the standard topology of six transmembrane segments comprising the voltage sensing domain (S1-S4) and pore domain (S5-S6). However, KCNQ channels diverge from classical Kv channels outside of the core membrane embedded structure. KCNQ channels have a short cytoplasmic N-terminus (~100 residues) and therefore lack a *bona fide* tetramerization (T1) domain. Instead, KCNQ channel subunits contain a large C-terminal domain (300-500 residues) which secondary structure algorithms predict to contain 4 α-helices [10] (Figure I-4). The two proximal helices (A & B) act as a scaffold for cytoplasmic regulatory molecules [11] whereas the last two helices (C & D) act as an assembly domain to direct subunit oligomerization [12-15]. Subsequent resolution of the isolated helix D peptide structure from two different KCNQ channels confirmed that this domain forms a self-assembled tetrameric coiled-coil structure [16,17]. The specific protein-protein interactions found in the two crystal structures also provided a structural basis for why KCNQ1 channels preferentially form homomeric channels over the heteromeric complexes typically found for KCNQ2-KCNQ5 channels [11,14]. The fact that structural determination of a small part of the C-terminus can explain their physiological assembly in native cells emphasizes the role structure-function studies play in understanding KCNQ physiology.
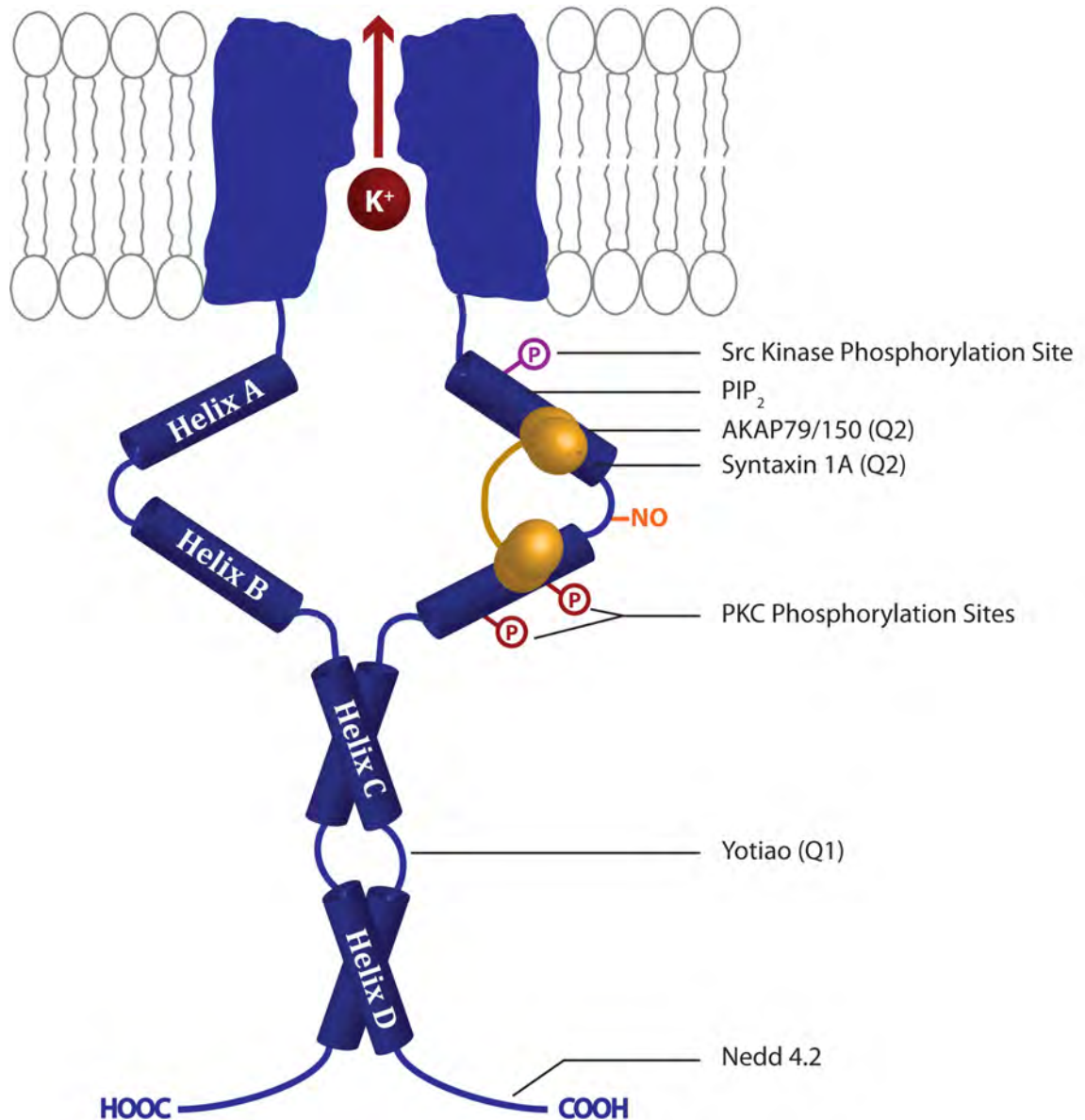
Figure I-4. Cartoon representation of the KCNQ C-terminus.
Only two subunits are shown for clarity. Helices are represented as cylinders.
Calmodulin is depicted in yellow, phosphorylation sites are depicted with circles.
Predicted location of cytosolic regulatory factors binding sites are indicated with lines.

Schematic generated by K. Mruk.

The KCNQ family of K$^+$ channels contains five members (KCNQ1-KCNQ5; Kv7.1–Kv7.5) which are characterized primarily by their tissue expression. KCNQ1 (Q1) channels are expressed throughout the body, but absent from the central nervous system where KCNQ2-5 channels are primarily found (Table I-1) [1]. Although KCNQ α-subunits can form functional homotetrameric channels in heterologous expression systems, often these homomeric channels do not faithfully recapitulate physiological currents. This is because in native tissues, KCNQ subunits form heteromeric channel complexes.

KCNQ1

The KCNQ1 (Q1) gene was first mapped through a genetic linkage study from a family of individuals suffering from the common inherited arrhythmia, Long QT Syndrome (LQTS) [18]. When Q1 is expressed in heterologous systems, functional channels produce rapidly activating current (Figure I-5). Q1 channels can also undergo voltage-dependent inactivation which can be visualized by a "hook" in tail current recordings (Figure I-5). This hook is due to Q1 channels passing rapidly from the inactive state to the open state faster than the channels close [19]. However, this inactivation is never observed in currents from native tissues as Q1 α-subunits obligatorily co-assemble with KCNE β-subunits which relieve channel inactivation.

Table I-1. Characteristics of the KCNQ channel family.

Gene	KCNQ1	KCNQ2	KCNQ3	KCNQ4	KCNQ5
Chromosome Locus	11p15.5	20q13.3	8q24	1p34	6q14
mRNA Location	Crypt Cells Heart Kidney Lung Stria Vascularis Pituitary Placenta	Nervous System Pituitary SCG Testis	Nervous System Cochlea Pituitary SCG Neurons Spleen	Auditory Pathway Cochlea Outer Hair Cells Vestibular Hair Cells	Nervous System Skeletal Muscle SCG Neurons
Disease Association	Cardiac Arrhythmia	Benign Neonatal Familial Epilepsy	Benign Neonatal Familial Epilepsy	Nonsyndromic Hearing Loss	Unknown
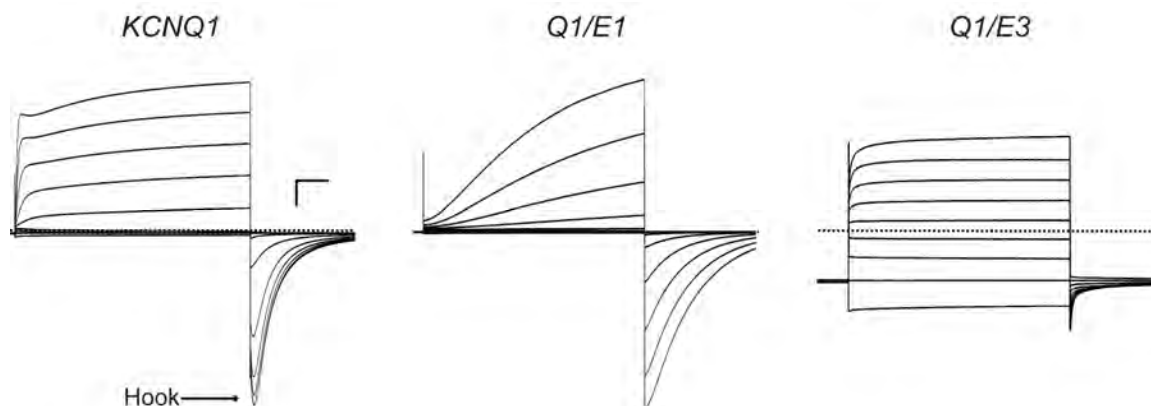
Figure I-5. Electrophysiological properties of KCNQ1 homomeric and Q1-KCNE heteromeric complexes
Families of macroscopic currents were recorded in high extracellular K^+ (50 mM) to accentuate the differences in deactivation kinetics. Currents were elicited by 4 s test potentials from –100 to +60 mV in 20 mV increments from a holding potential of –80 mV followed by a tail pulse to –80 mV. The arrow indicates the hook in tail currents of Q1 homomeric channels indicative of inactivation which is absent in currents from Q1-KCNE complexes. Q1/E1 complexes have slow gating kinetics and do not fully close within the same amount of time as Q1 channels. Scale bars indicate 1 µA and 500 ms. Dashed line equals zero current.

Families of currents were recorded by K. Mruk.

KCNE β-Subunits

KCNE β-subunits (KCNE1-KCNE5) are small (~100–170 amino acids), single transmembrane spanning proteins with extracellular N-termini [20]. Co-assembly of Q1 with KCNE peptides lead to dramatic changes in channel conductance, gating kinetics, and pharmacology allowing for Q1 channels to function in diverse tissues (Figure I-5) [21]. Although KCNE peptides promiscuously assemble with multiple Kv channels in native cells, the biophysical properties of Q1-KCNE heteromeric complexes are well established. Q1 subunits form channel complexes with KCNE1 (E1) peptides in the heart and inner ear. These complexes are responsible for maintaining cardiac rhythm and providing an avenue for K^+ to enter the endolymph [22,23]. Both Q1/E2 and Q1/E3 complexes are constitutively conducting and contribute to K^+ recycling in epithelial cells of the gastrointestinal tract [24,25]. When Q1 co-assembles with E4, current is dramatically reduced [26]. Although the physiological role for Q1/E4 complexes is unclear, two independent studies showed that E4 can co-assemble with Q1/E1 complexes [27,28] suggesting E4 may fine tune Q1/E1 channel function. E5 shifts the voltage activation of Q1 channels towards more positive potentials and increases the rate of deactivation [29]. Similar to E4, the physiological role for Q1/E5 complexes is not established.

Q1/E1 Pathophysiology

In the heart, Q1 channels co-assemble with E1 in the heart to generate the slow delayed rectifier K$^+$ current (I$_{Ks}$) [22,23]. I$_{Ks}$ is responsible for shaping the repolarization phase of cardiac action potentials (Figure I-6). Decreases in I$_{Ks}$ impair membrane repolarization, prolonging the duration of cardiac action potentials. Similarly, increases in I$_{Ks}$ lead to a reduction in the plateau phase causing an overall shortening of the cardiac action potential (Figure I-6). Accordingly, individuals with mutations in either Q1 or E1 which affect proper channel function suffer from cardiac arrhythmias [30-32].

Over 200 loss-of-function mutations in Q1 subunits and 20 in E1 subunits have been identified in patients suffering from the arrhythmia, Long QT Syndrome (LQTS) characterized by an elongation in the QT interval on an electrocardiogram (Figure I-6). More than 70% of these mutations are due to a single amino acid change highlighting the drastic effect a small change in the Q1/E1 complex can have on physiological processes [33]. Biophysical and biochemical investigation of these loss-of-function mutations group them into two categories: (1) improper biogenesis and (2) altered voltage-sensitivity of the channel [34]. Gain-of-function mutations in Q1 channels are associated with the cardiac arrhythmia, Short QT Syndrome (SQTS) characterized by a short QT interval and sharp T wave (Figure I-6). SQTS is less prevalent than LQTS and only two point mutations have been identified in Q1 subunits [33]. Both of these mutations increase the activation kinetics of Q1/E1 complexes, leading to larger currents. Together, the LQTS and SQTS-associated mutations in Q1/E1 complexes emphasize the critical influence the channel has on regulating the cardiac action potential.

Cardiac Action Potential

Potassium current (I_{to})

Calcium current (I_{Ca})

Potassium current (I_{Ks})

Sodium current (I_{Na})

Potassium current (I_{Kr})

Normal Electrocardiogram

R

Q S

T

Long QT Syndrome

R

Q S

T

Short QT Syndrome

R

Q S

T
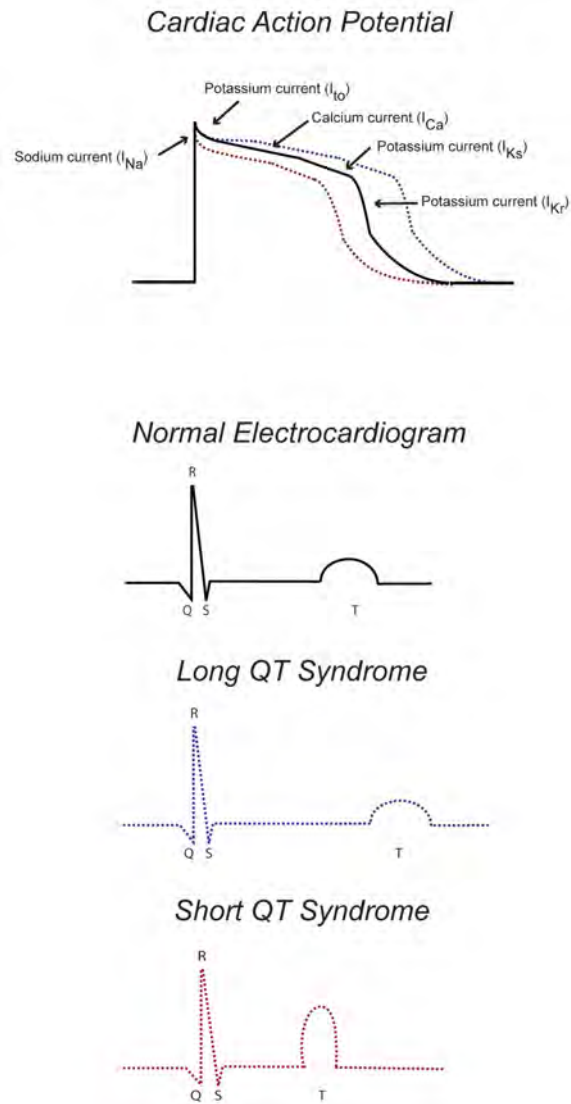
Figure I-6. Cardiac action potential
Top: Schematic of ion channel current associated with each phase of the cardiac action potential. Bottom: Representation of a normal electrocardiogram compared to that for long and short QT syndrome respectively. The QRS complex reflects ventricular depolarization and the T wave ventricular repolarization. The changes in the action potential that cause cardiac arrhythmia are color coded with the respective electrocardiogram.

Schematics generated by K. Mruk.

Q1/E1 channel complexes are also located in the inner ear and provide the sole avenue for transport of K^+ into the endoplymph [35-37]. Individuals suffering from the autosomal recessive form of LQTS are also deaf. These mutations are primarily frameshift or deletion mutations [33] suggesting that the loss of hearing is due to a lack of assembled Q1/E1 complexes and not just a reduction in voltage-sensitivity of these channels. Studies using $KCNQ1^{-/-}$ [38] or $KCNE^{-/-}$ [36] knockout mice demonstrate that an inability of K^+ to enter the inner ear leads to a collapse of the endolymphatic space in an adult mouse. As a result, knockout mice present with symptoms of deafness. These mutations underscore the importance of K^+ flux within the inner ear.

KCNQ2 and KCNQ3 Channels

The genes for KCNQ2 (Q2) and KCNQ3 (Q3) were identified as Q1 homologues by positional cloning in infants with benign familial neonatal epilepsy [39,40]. Both of these channels can be expressed individually in *Xenopus* oocytes and mammalian cells; however, the properties of these homomeric channels do not faithfully recapitulate the properties of the non-inactivating K^+ current (M-current, I_M) found in neurons. Expression of both Q2 and Q3 subunits lead to larger currents, altered gating kinetics, and different pharmacological sensitivities than homomeric channels suggesting that these heteromeric channels are responsible for the native M-current [41]. Unlike Q1 channels, Q2/Q3 channel complexes activate slowly, do not inactivate, and inward rectify at positive potentials (Figure I-7). This produces smaller currents upon increases in

voltage even though the driving force for K^+ transport is increasing. Q2/Q3 complexes do not physiologically interact with KCNE subunits as their tissue expression is different.

Q2/Q3 Pathophysiology

Because Q2/Q3 channels do not inactivate, they generate a steady voltage-dependent outward current in neurons. This constant K^+ current serves as a "brake" for neuronal firing by stabilizing the membrane potential in the presence of depolarizing currents. Accordingly, mutations in Q2/Q3 channels which affect generation of the neuronal M-current are associated with benign familial neonatal epilepsy (BFNE, formerly BFNC) and peripheral nerve hyperexcitability (PNH) [42]. There are over 30 BFNE-associated Q2 mutations and 4 BFNE-associated Q3 mutations which exhibit reductions in Q2/Q3 heteromeric channel current [43]. Similar to Q1, mutations in Q2 are found throughout the protein and affect either channel biogenesis or voltage sensitivity. The four mutations in Q3 channels fall within the pore region of the Q3 subunit but have not been biochemically or biophysically characterized [42]. PNH-associated mutations are located within the voltage-sensor of Q2 channels and exert a dominant-negative effect on wild type subunits, causing a significant decrease (>70%) in the M-current [39,44].
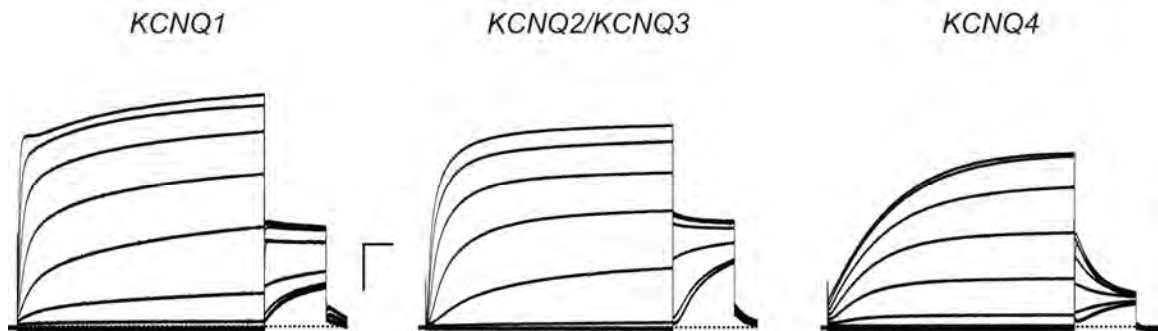
Figure I-7. Electrophysiological properties of KCNQ channels.
Families of current from Q1 homomeric, Q2/Q3 heteromeric, and Q4 homomeric channel complexes were recorded in physiological levels of extracellular K^+ (2 mM). Currents were elicited by 4 s test potentials from –100 to +60 mV in 20 mV increments from a holding potential of –80 mV followed by a tail pulse to –30 mV. Dashed line indicates zero current. Scale bars represent 1 µA and 0.5 s.

Families of currents were recorded by K. Mruk.

KCNQ4

The gene for KCNQ4 (Q4) was cloned and characterized after being mapped to the DFNA2 locus in individuals with nonsyndromic hearing loss [45]. Q4 tissue expression is limited to the inner ear and brainstem [46]. Q4 channels are predominantly homomeric and are responsible for the potassium current activated at negative potentials in hair cells of the inner ear ($I_{K,n}$) [47]. Q4 channels also activate slowly, display no inactivation, and inwardly rectify at positive potentials (Figure I-7). Q4 subunits can co-assemble with Q3 but it is unlikely that these heteromeric channel complexes contribute to the M-current in neurons as Q4's tissue expression is limited in neurons. Although co-expression of Q4 with KCNE peptides in heterologous expression systems does lead to changes in channel kinetics and current amplitude, [48] these complexes have not been shown to exist in native tissues.

Q4 Pathophysiology

Multiple mutations within the *KCNQ4* gene have been associated with inherited nonsyndromic progressive hearing loss. Single point mutations in Q4 map to the pore domain of Q4 subunits and cause dominant negative effects on wild type subunits [49]. Two deletion mutations have also been identified which result in truncated nonfunctional Q4 subunits [49]. Studies using *KCNQ4*$^{-/-}$ knock-out mice and heterozygous mutant mice *KCNQ4*$^{G285S/+}$ demonstrate that a lack of K^+ efflux leads to chronic depolarization of the hair cells causing degeneration of outer hair cells [50]. The role of Q4 function in

congenital deafness once again highlights the role KCNQ channels play as a "brake" to regulate cellular excitability.

KCNQ5

KCNQ5 (Q5) is the only member of the KCNQ family not associated with a disease and as such the gene was found through a GenBank homology search instead of genetic linkage analysis and positional cloning [51]. The tissue expression pattern for Q5 is similar to both Q2 and Q3 [52]. Q5 α-subunits can co-assemble with Q3 leading to speculation that Q5 may contribute to the M-current. Q5 homomers have the slowest activation kinetics of all the KCNQ members and also exhibit "crossover" at positive membrane potentials indicative of inward rectification. Similar to Q4 channels, Q5 channels do not display inactivation and interact with KCNE β subunits in expression systems but have not been shown to physiologically interact with KCNE β subunits [53].

KCNQ Modulation

Although KCNQ channels are voltage-gated, many small cytoplasmic signaling molecules can modulate the channels' response to changes in membrane potential. Many of these molecules do not directly bind to KCNQ channels. Rather, intracellular proteins act as sensors for these molecules and in turn bind to KCNQ channels to modulate channel function. The interaction between KCNQ channels and cytoplasmic proteins is critical as mutations in KCNQ channels that disrupt these protein-protein interactions are often associated with KCNQ channelopathies.

cAMP, phosphorylation, and A-kinase anchoring proteins

It was first demonstrated that cAMP levels modulate KCNQ channels when the Kass laboratory showed that addition of cAMP analogs to ventricular cells could increase cardiac I_{Ks}, and that this increase in I_{Ks} was mediated through protein kinase A (PKA) [54]. Later, electrophysiological studies using cloned α- and β-subunits in *Xenopus* oocytes demonstrated that cAMP increased Q1/E1 currents through PKA activation [55]. PKA does not directly bind to Q1 but rather forms a macromolecular signaling complex with the regulatory phosphatase PP1 and the AKAP protein Yotiao (AKAP9) [55]. Yotiao binds to a leucine zipper motif on Q1 channels in between helices C and D of the C-terminus (Figure I-4). Anchoring of the complex by Yotiao is critical for PKA phosphorylation of serine 27 in the N-terminus of Q1 subunits which in turn activates Q1 channels and increases channel current. This activation is short lived as PP1 rapidly dephosphorylates serine 27 [56]. Mutations in the leucine zipper motif of the Q1 C-terminus which disrupt Yotiao binding to Q1/E1 channels are associated with LQTS [57]. Genetic mutations in Yotiao which reduce interactions with Q1 channels have also been identified in LQTS patients [58] further demonstrating the physiological importance of the Q1/E1-Yotiao complex.

Similar to cardiac I_{Ks}, the M-current, and outer hair cell $I_{K,n}$ are also regulated by cAMP levels [59,60]. Studies using cloned α-subunits determined that increases in cAMP levels elevate current levels from heteromeric Q2/Q3 channels and homomeric Q4 channels [59-61]. As with Q1/E1 complexes, this increase in current is mediated by

PKA. Q2 channels contain a consensus site for PKA phosphorylation at serine 52. The site of cAMP mediated phosphorylation on Q4 channels has not been mapped as no obvious consensus sites are contained within the amino acid sequence. Whether PKA can directly bind to Q2/Q3 and Q4 channels or is localized through AKAP binding is unknown.

Phosphorylation by PKC

In addition to activation by cAMP, the M-current is suppressed by activation of muscarinic receptors. It was suggested that suppression occurs through activation of protein kinase C (PKC) as activators of PKC can suppress the M-current in neurons but inhibitors of PKC do not promote receptor-induced inhibition of the M-current [62-65]. Therefore, it was proposed that suppression of I_M may involve macromolecular signaling complexes, a likely candidate being the neuronal anchoring protein, AKAP79/150, which binds to helix A in the C-terminus of Q2 channels (Figure I-4) [66,67]. AKAP79/150 contains a binding site for PKC and was later shown to form a trimeric complex with Q2 channels [68]. Further examination of the Q2 C-terminus revealed two PKC dependent phosphorylation sites, serine 534 and serine 541 [69]. Inhibition of Q2 currents through phosphorylation requires the presence of the trimeric Q2/PKC/AKAP complex. Q3-Q5 channels may be subject to the same modification as they contain a conserved threonine residue at position 541 and directly bind AKAP79/150 [70]; however, PKC-dependent phosphorylation at this residue has not been investigated in those channels.

PIP₂

KCNQ currents quickly run-down in excised patches leading to the hypothesis

that KCNQ channels are also modulated by levels of the membrane phospholipid

phosphatidyliniositol 4,5-biphosphate (PIP_2). Although both Q1/E1 and Q2/Q3

complexes as well as Q4 homomers run-down upon PIP_2 hydrolysis, PIP_2 activates

KCNQ channels through different mechanisms [60,71,72]. PIP_2 activates Q1/E1

complexes by slowing the deactivation kinetics of the channel and shifting the voltage

dependence to more negative potentials, suggesting that PIP_2 modulates the voltage

sensitivity of the Q1/E1 complex [71,73]. In contrast, PIP_2 increases the open probability

of Q2-Q5 homomeric channels and Q2/Q3 complexes [74]. Two lines of evidence

suggest that PIP_2 directly binds to the C-terminus of KCNQ channels. First, the C-

terminus of KCNQ channels contains a cluster of conserved basic amino acid residues

which has been shown to direct PIP_2 binding to other ion channels [75]. Second, three

LQTS-associated genetic mutations within this region of Q1 channels have reduced

affinity for PIP_2 [76,77]. However, to date, the exact PIP_2 binding site has not been

mapped onto KCNQ channels.

Ubiquitin and Nedd4-2 Ligase

Ubiquitin is a small regulatory protein that is attached to proteins to target them

for degradation. The Nedd4-2 ubiquitin ligase binds to the C-terminus of KCNQ

channels to regulate their cell surface expression [78,79]. Ubiquitination of Q1 channels

requires Nedd4-2 to bind to the PY motif downstream of Helix D in the C-terminus

(Figure I-4). Similarly, Nedd4-2 ubiquitinates both Q2 and Q3 homomeric channels but binding to Q3 subunits is required for downregulation of both Q2/Q3 and Q3/Q5 complexes. However, whether Nedd4-2 interacts with Q3 subunits through a PY motif or a macromolecular signaling complex remains unclear. Overexpression of the ubiquitin-specific protease 2 (USP2) increases the total and surface-expressed amount of Q1 protein, protects Q1 from ubiquitination, and counteracts the effect of Nedd4-2 [80]. This interplay between Nedd4-2 and USP2 is well-established for other ion channels and further investigation into their modulation of KCNQ channels may provide insight into disease-associated mutations which affect channel stability.

Ca^{2+} and calmodulin

Fluctuations in Ca^{2+} concentration differentially modulate KCNQ function. Increases in Ca^{2+} activate both homomeric Q1 channels and Q1/E1 complexes [81]. Furthermore, upon stimulation of cardiac myocytes, I_{Ks} increases in a Ca^{2+}-dependent manner leading to shorter action potentials [82]. In contrast to I_{Ks}, increases in Ca^{2+} lead to suppression of the M-current [83]. Although KCNQ channels are modulated by intracellular calcium, they do not directly bind calcium. Instead, they employ the ubiquitous Ca^{2+} sensor, calmodulin (CaM). CaM promotes channel modulation directly by binding to KCNQ channels or indirectly by regulating the binding of additional factors to the C-terminus.

CaM directly binds to two CaM binding motifs in the C-terminus of KCNQ channels: a Ca^{2+} independent (IQ-like) motif and a Ca^{2+} dependent (1-5-10) motif,

located in helices A and B respectively (Figure I-4) [10]. CaM can bind to either of these isolated sites *in vitro*, but both binding sites must be intact for CaM to interact with full-length KCNQ channels [84]. Fittingly, genetic mutations in either of these binding motifs that perturb CaM binding reduce channel current and are associated with both LQTS and BFNE, suggesting that CaM binding is required for proper KCNQ function [81,85-87]. CaM binds to KCNQ channels in the presence or absence of Ca^{2+} which is similar to what is observed for other ion channels [88]. *In vitro*, CaM binding to KCNQ channels promotes solubility of the isolated C-terminal domain suggesting that the KCNQ-CaM interaction is required for proper channel assembly and trafficking to the plasma membrane [17,81]. However, the Villaroel lab showed that a Q2 mutant containing a single point mutation in the C-terminus which abrogates CaM binding can still traffic normally to the cell surface, suggesting that CaM is not constitutively tethered to KCNQ channels during channel biogenesis [84]. As seen with other ion channels, calcification of either the N- or C- lobe of CaM allows for the modular regulation of KCNQ channels. Overexpression of calcified but not apoCaM leads to overall decreases in Q2, Q4, and Q5 currents but not Q1 or Q3, consistent with what is seen when intracellular Ca^{2+} levels in native cells increase [89]. This observed Ca^{2+} sensitivity requires calcification of only the N-lobe of CaM.
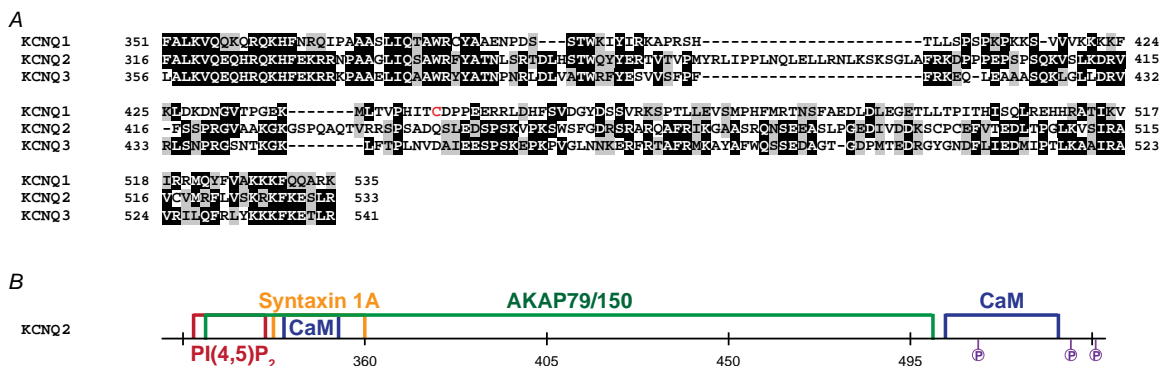
Figure I-8. The proximal C-terminus of KCNQ channels.

(A) Sequence alignment of the first two helices of the KCNQ C-termimus. Identical residues are marked with black background, similar residues in grey. The nitrosylated cysteine in Q1 is highlighted in red. (B) The Q2 carboxy-terminal tail contains overlapping binding sites for multiple regulatory molecules. PI(4,5)P2, phosphatidylinositol-4,5-bisphosphate (red); AKAP, A-kinase anchoring protein (green); CaM, calmodulin (blue); S511, S534, and S541, residues phosphorylated (purple), syntaxin 1A (yellow).

Schematics generated by K. Mruk.

In addition to acting as a Ca^{2+} sensor, CaM binding to KCNQ channels affects the ability of other cytoplasmic factors to bind to the C-terminus. Because the AKAP79/150 binding site overlaps with the first CaM binding motif in helix A of the C-terminus of Q2-Q5 channels, it was postulated that CaM and AKAP79/150 may interact with KCNQ channels through a macromolecular signaling complex (Figure I-8). Indeed, calcified CaM, but not apoCaM, disrupts AKAP79/150 binding to Q2-Q5 channels by competing for an overlapping binding site on KCNQ channels [70]. Furthermore, overexpression of wild type CaM disrupts the functional effect AKAP79/150 has on heteromeric Q2/Q3 channels, suggesting that CaM prevents phosphorylation by PKC.

CaM binding to the isolated CaM binding motifs from KCNQ channels is reduced in the presence of PIP_2, suggesting that they too share overlapping binding sites [90]. However, competition experiments between CaM and PIP_2 on full length KCNQ channels have not been attempted. Modulation of Q2-Q5 channels by PIP_2 and CaM is reciprocal but additive for Q1/E1 complexes, suggesting that PIP_2 and CaM may possess overlapping functionality to modulate KCNQ function [74]. Interestingly, the proposed site for PIP_2 binding to KCNQ channels also overlaps with the AKAP79/150 binding site (Figure I-8). The Shapiro lab has shown that AKAP79/150 can decrease PIP_2 affinity for KCNQ channels, suggesting that the three molecules (CaM, AKAP, and PIP_2) may form heteromeric signaling complexes [70].

In addition to regulating the binding of cytoplasmic factors that modulate all members of the KCNQ family, CaM can interfere with subunit specific regulators

including the SNARE protein, syntaxin 1A and the signaling molecule, nitric oxide.

Syntaxin 1A binds to Q2 channels at helix A to modulate channel current [91] (Figure I-

8). CaM binding to Q2 channels is increased in the presence of syntaxin 1A. However,

in the presence of either calcified CaM or apoCaM, the modulatory effects of syntaxin

1A on Q2 channels are lost [92]. This suggests that there is functional interplay between

CaM and syntaxin 1A upon binding to Q2 channels to modulate channel function. Nitric

oxide binds to Q1/E1 channel complexes at residue cysteine 445, which is located in the

linker region between helices A and B of the Q1 C-terminus [93] (Figure I-4 and I-8). In

the presence of calcified CaM, Q1 channels are nitrosylated. Overexpression of apoCaM

prevents nitrosylation suggesting that the binding of calcified CaM is required for

nitrosylation of Q1 channels [93]. Binding of calcified CaM to Q1 channels may cause

structural changes in the C-terminus such that cysteine 445 becomes exposed and

available for nitrosylation.

Currently, what is known about the protein interactions between CaM, KCNQ

channels, and additional regulatory factors is limited to functional studies. Although

crystallographic studies have provided molecular insight into how CaM binds to target

peptides, the location and orientation of CaM bound to fully folded ion channels in the

membrane is unknown. Without additional structural information, it is difficult to discern

the molecular mechanisms that govern CaM regulation of the binding of additional

cytoplasmic factors to KCNQ channels.

Tools to Study Kv Channels

Kv channel complexes are difficult to study by traditional biochemical methods due to their membranous lipid environment and large size. Instead, Kv channel complexes have been investigated using chemical probes in combination with electrical recordings allowing for the simultaneous probing of Kv structure and function. This combinatorial approach not only provides insight into modulation of Kv channels but also aids in the discovery of therapeutic compounds to treat Kv channelopathies.

Pharmacology and Screening Libraries

Most genetic mutations in KCNQ channels that are linked to human disorders arise from an overall decrease in K^+ current [43]. Therefore, small molecule modulators of KCNQ channel complexes that increase K^+ current provide a new avenue of pharmacological treatment. Although inhibitors of KCNQ channels are abundant, small molecule activators are rare [94], challenging to synthetically derivatize, and are often less effective on the physiologically relevant heteromeric KCNQ complexes as compared to KCNQ homomeric channels [95-97]. Furthermore, since ion channels share a common core topology, many Kv channel activators cross-react with other channels [98] relegating them to an investigative tool instead of suitable drug candidates.

In an attempt to discover small molecule modulators of Kv channels, two high-throughput approaches have been utilized. The first is a fluorescence-based approach in which a dye that is sensitive to changes in membrane potential is applied to mammalian cells expressing the Kv channel of interest [99,100]. Small molecules that modulate Kv

channel function are physiologically associated with changes in membrane potential that can then be visualized as changes in fluorescence. This approach was successfully used to identify specific Kv channel inhibitors from a library of 20,000 compounds [99]. The second assay uses atomic absorption spectroscopy to measure nonradioactive Rb^+ flux from mammalian cells expressing ion channels. This approach allows for identification of both Kv inhibitors and activators as most Kv channels readily conduct Rb^+ ions which provide a direct measurement of channel function. This approach was used to identify the KCNQ specific activator, zinc pyrithione, out of over 20,000 compounds [95].

Although these high-throughput screening methods have increased the number of compounds that can be tested on Kv channels, only a few activators have been identified. In fact, many activators, such as the benzodiazepine R-L3, are often found randomly when screening for Kv channel blockers [96] instead of through screens for activators. One of the main hindrances in screening for activators is a lack of structural data available for Kv channels. Mutagenesis studies have revealed that most activators of KCNQ channels bind deep within the pore region to small binding pockets, such that additional chemical modifications render the molecules unable to bind to the KCNQ channels [101]. Therefore, increasing the amount of structural data in combination with functional data of Kv channels could aid in the discovery of channel activators.

Tethered Blockers

Channel blockers bind to sites on either end of the selectivity filter where they get physically stuck and block the passage of K^+ ions. The two most commonly used

channel blockers are quaternary ammoniums (QAs) and peptide toxins. Kv channel block by QAs is rapid, reversible, and subunit specific, allowing for the probing of Kv channel complex assembly. The differential sensitivity of KCNQ subunits was used to show that in hippocampal neurons, the M-current is primarily generated through Q2/Q3 complexes with a minor contribution from Q3/Q5 complexes [102] and later to show that the stoichiometry of the Q2/Q3 complex in superior cervical ganglia neurons is 2:2 [103]. Increased sensitivity to QAs can be engineered into channel subunits through single point mutations allowing for the biophysical characterization of the ion conducting pathway in otherwise insensitive Kv channels. Indeed, the Kass laboratory employed this technique to show that coassembly of Q1 with E1 β-subunits, which leads to a decrease in QA sensitivity, did not change the structure of the outer vestibule of the Q1 channel [104]. In contrast to QAs, peptide toxins bind to Kv channels with high affinity. The scorpion toxin, charybdotoxin (CTX), has been used to determine the stoichiometry of the *Shaker* Kv channel [105] and later to further investigate inactivation in these channels [106]. Although, KCNQ channels are not sensitive to CTX, mutagenesis studies have allowed toxin sensitivity to be engineered into these and other otherwise insensitive channels. Using a Q1 CTX-sensitive channel, our lab and others have determined the stoichiometry of the Q1/E1 channel complex to be 4 α-subunits:2 β-subunits [107,108].

In order to gain more knowledge about the structural architecture of K^+ channels, labs have turned to using tethered blockers. Typically, tethered blockers contain a QA or toxin that is linked to a cysteine-modifying group which allows for covalent attachment to the channel of interest (Figure I-9). Because QAs have low affinity for K^+ channels,

inhibition is highly dependent on the effective concentration generated by the length of the linker between the cysteine-modifying group and the QA. Therefore, QA-tethered blockers are often used as molecular calipers to measure distances between extracellular segments of K^+ channels to the entrance of the pore [109]. More recently, tethered blockers containing QAs have expanded beyond probing channel structure to controlling Kv channel function in native tissues [110,111]. In one approach, the tether contained an azobenzene linker which adopts an extended *trans* conformation in visible light but a condensed *cis* confirmation under UV light (Figure I-9). These linkers allow for the temporal control of channel function through the use of light which can be used to study the roles that Kv channels, including the KCNQs, play in native cells [112]. Because CTX binds to Kv channels with high affinity, unlike QAs, channel inhibition by CTX is insensitive to linker length. Therefore, the cysteine-reactive moiety reacts with the Kv channel before CTX can unbind, creating a covalently tethered blocker which precludes additional blockers from binding to the channel. This essentially irreversible inhibition has been used to demonstrate that Q1 channels can form heteromeric complexes with multiple KCNE β-subunits [27]. Additionally, our lab has shown that using a chemically cleavable linker can allow for multiple rounds of sequential labeling, providing a method to deliver chemical handles to functional channels [113]. Although tethered blockers have been widely successful in gathering structural information about Kv channels, to date, their use has been limited to probing the extracellular surface of Kv channels.
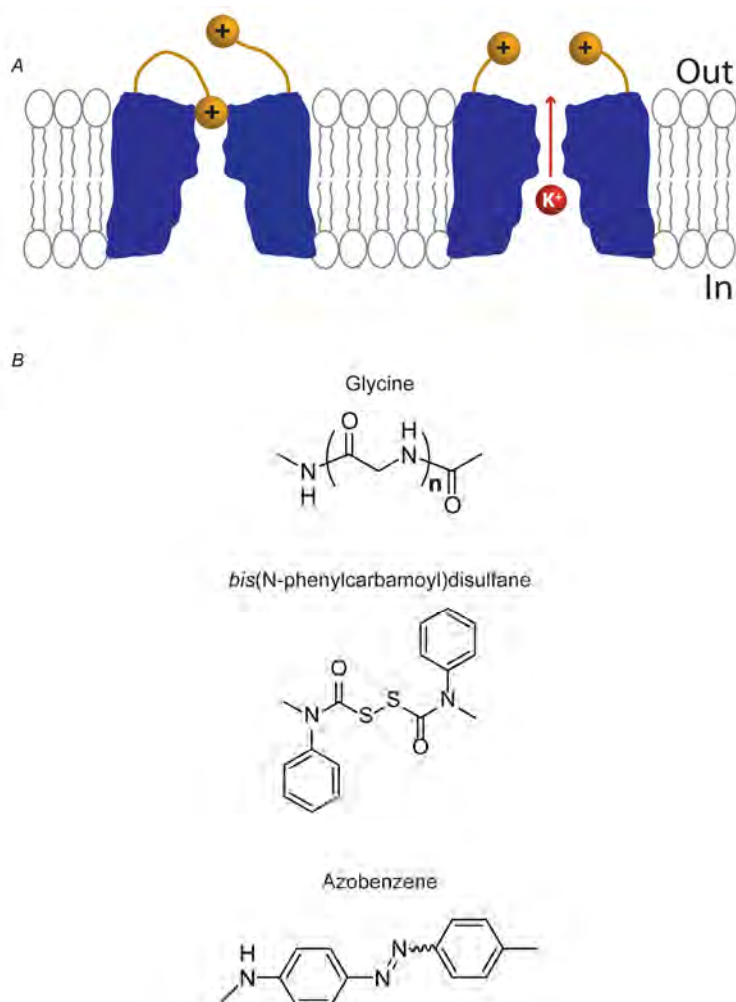
Figure I-9. Tethered Blockers
(A) Cartoon of the tethered blocker strategy using a quaternary ammonium. If the tether is long enough, the blocker will reach its binding site and block K^+ conduction whereas shorter tethers prevent the blocker from effectively inhibiting channel function. Because the effective concentration of the blocker is dependent on tether length, the magnitude of inhibition provides a distance between the chemically modified residue and the internal blocker site. (B) Chemical linkers used in tethered blocker studies. The glycine linker allows for changes in length. The bis(N-phenylcarbamoyl)disulfane linker is cleavable allowing for delivery of small molecules. The azobenzene linker isomerizes in response to light, allowing for photocontrol of channel block.

Figures generated by K. Mruk.

The Oocyte Expression System

Intact oocytes extracted from *Xenopus laevis* are a versatile expression system for the structural and functional investigation of ion channels and transporters. One advantage of using oocytes over mammalian cells is that they do not express a large number of endogenous ion channels. In addition to rapid co-expression of mRNA, microinjection also allows for facile incorporation of unnatural amino acids [114], as well as examination of recombinant proteins [115] and isolated membranes from native cells [116]. Microinjection also allows for precise control of protein subunit expression which is critical for heteromeric Kv channels [117]. Channel function can be investigated electrophysiologically in the traditional whole-cell configuration (two-electrode voltage clamp - TEVC) or in excised patches of membrane [118]. The large size of the oocyte also makes single cell biochemistry possible, enabling the direct comparison of cell surface expression and electrical recordings [119-121].

Although many studies are easier to do in *Xenopus* oocytes than mammalian cells, oocytes also have some experimental disadvantages. The vitelline envelope of the oocyte can cause decreases in small molecule potency and must be removed for many experiments [118] resulting in decreased viability. Furthermore, the cellular trafficking of oocytes is different from native cells, precluding the study of channel mutations which affect trafficking [122]. In addition, oocyte quality can be variable based on husbandry conditions and season, rendering them unusable at times for electrophysiological recordings [122-126]. The inconsistency of oocyte quality has caused many labs to turn

to mammalian expression systems which are less amenable to the currently available tools to study Kv channels.

Structural Prediction and Bioinformatics

Out of the 30 identified homomeric mammalian Kv channels, only the crystal structure of one mammalian Kv channel (rKv1.2) is known. However, based on the high resolution structures of the bacterial K^+ channels (KcsA and KvAP) as well as rKv1.2, structural features of other Kv channels have been predicted. There are two main techniques used to predict the structure of Kv channels. The first uses structural bioinformatics tools and the second uses molecular dynamics simulations [127]. The bioinformatics approach relies on a combination of secondary structure predictions and homology modeling to construct structural models that are homologous to known K^+ channel structures. This method was used to generate both open and closed state models of Q1 channels using the crystal structures of rKv1.2 and KcsA respectively [128]. These models were used in subsequent studies to model the interaction between Q1 α-subunits and E1 β-subunits [129]. Unlike structural bioinformatics, molecular dynamics explores the conformational space of proteins within a pre-defined environment. For ion channels, molecular dynamic simulations are typically run in a membrane mimetic environment [130] allowing for a wealth of information to be collected about the movement and energetics of K^+ permeation through the selectivity filter. Typically, these two methods are used together to generate models of the interactions formed between small molecule and peptide toxins with Kv channels [131-134]. More recently, the Seebohm lab used

structural bioinformatics to create a homology model of the Q1/E1 channel complex and applied molecular dynamic simulations to ascertain the stability of the complex [135]. As more high resolution structures of ion channel accessory subunits are solved, structural bioinformatics provides an avenue to piece together this structural data with functional data in an attempt to fully understand modulation of Kv channels.

Outline of Thesis

My thesis work focuses on the discovery and use of small molecules to probe the assembly and function of heteromeric KCNQ channel complexes.

Chapter II illustrates the synthesis and utilization of a modified version of the tried-and-true tethered blocker approach allowing for the study of the intracellular structure of KCNQ channels. Using the distance restraints generated from our intracellular tethered blockers and structural bioinformatics, we built models of the KCNQ-CaM complex. Our models place CaM close to the gate of KCNQ channels where it is able to communicate changes in intracellular calcium levels to modulate KCNQ current levels.

Chapter III describes the serendipitous discovery of an activator of KCNQ complexes, phenylboronic acid (PBA). PBA activates both homomeric KCNQ channels as well as the physiologically relevant Q1/E1 and Q2/Q3 channel complexes. Although the potency of PBA is weak (millimolar), the commercial availability to thousands of PBA derivatives provides a large class of compounds to systematically dissect the mechanisms of KCNQ gating.

Chapter IV addresses the common problem of microbial contamination of *Xenopus* oocytes after surgical removal. Microbial contaminated oocytes have negligible electric resting potentials and poor viability resulting in eggs that are unsuitable for electrophysiological recordings. We identified multi-drug resistant bacteria as the source of the contamination and developed an antibiotic cocktail to treat compromised oocytes.

The development of the tools used in this thesis, provides new reagents to further our understanding of Kv channel complexes.

CHAPTER II: STRUCTURAL INSIGHTS INTO NEURONAL KCNQ-CALMODULIN COMPLEXES

Abstract

Calmodulin (CaM) is a ubiquitous intracellular calcium sensor that directly binds to and modulates a wide variety of ion channels. Despite the large repository of high resolution structures of CaM bound to peptide fragments derived from ion channels, there is no structural information about CaM bound to a fully folded ion channel at the plasma membrane. To determine the location of CaM docked to a functioning KCNQ K^+ channel, we developed an intracellular tethered blocker approach to measure distances between CaM residues and the ion conducting pathway. Combining these distance restraints with structural bioinformatics, we generated the first quaternary structural model of an ion channel-CaM complex in the open state. These structural models place CaM strikingly close to the cytoplasmic gate where it is well-positioned to modulate channel function.

Introduction

Voltage-gated ion channels respond to fluctuations in Ca^{2+} concentration in order to regulate membrane excitability, cardiac rhythm, and synaptic transmission between neurons. Although many ion channels are regulated by intracellular calcium, most voltage-gated channels do not directly bind calcium; instead, they employ the ubiquitous Ca^{2+} binding protein, calmodulin (CaM). CaM consists of two globular domains (N- and C-lobes), each of which contains two calcium binding EF hand structures permitting the binding of up to four Ca^{2+} ions. CaM communicates changes in intracellular Ca^{2+} levels by binding to consensus sites known as CaM binding motifs (e.g. IQ, 1-5-10, 1-8-14) [136] in both the presence and absence of Ca^{2+} leading to changes in channel function (calmodulation) [137-140]. Furthermore, calcification of either the N- or C- lobe of CaM allows for the modular regulation of channel assembly and gating through lobe specific interactions of CaM with voltage-gated ion channels [141,142].

For the KCNQ family of potassium channels (Q1 – Q5; Kv7.1 – Kv7.5), CaM binds to the intracellular C-terminus to regulate channel assembly [17,81], trafficking [85,86], and function [81,87,89]. The KCNQ C-terminus contains two CaM binding motifs: a Ca^{2+} independent (IQ-like) and Ca^{2+} dependent (1-5-10), which are separated by ~ 135 residues [10]. CaM binds to KCNQ channels in the absence or presence of calcium; however, CaM binding requires both motifs to be intact, consistent with *in vitro* studies that indicate a 1:1 stoichiometry for the CaM:KCNQ C-terminus protein-protein interaction [17,84,87]. Fittingly, mutations that disrupt CaM binding to either of these motifs in Q1 and Q2 channels are associated with long QT syndrome (LQTS) and benign

familial neonatal convulsions (BFNC), respectively [81,85-87]. Taken together, these studies indicate that one CaM molecule will simultaneously interact with both CaM binding motifs in the KCNQ C-terminus.

Current structural information for ion channel-CaM complexes is limited to structures of CaM bound to peptides derived from the cytoplasmic parts of ion channels. In many of these high resolution structures, CaM wraps around a single α-helical peptide [143,144]. However for KCNQ subunits harboring two CaM binding motifs, the KCNQ-CaM complex is predicted to be similar to the structures of CaM bound to peptides derived from either the SK Ca^{2+} activated K^+ channel or the pre-IQ domain of Cav1.2 voltage-gated Ca^{2+} channel, where CaM wraps around multiple helices [145-147]. Although these published structures (and the inevitable structure of CaM bound to a KCNQ-derived peptide) are expected to faithfully mirror the structure of CaM when bound to a functioning channel, these isolated structures do not provide any information about the quaternary structure of the full-length ion channel-CaM complex. To determine where CaM resides on a functioning KCNQ channel, we developed an intracellular tethered blocker approach to measure distances between CaM residues and the crystallographically-known quaternary ammonium blocking site on voltage-gated K^+ channels (Kv). Using these distance restraints, we generated three-dimensional structural models of the Q2/Q3 channel-CaM complex in the open state using the $rK_v1.2$ and CaM-$Ca_V1.2$ crystal structures. These models place CaM strikingly close to the cytoplasmic gate where it is well-positioned to communicate changes in intracellular calcium to a functioning Q2/Q3 channel.

Materials and Methods

Molecular Biology

KCNQ2 and KCNQ3 constructs were kindly provided by G. Seebohm (Ruhr University).

Inactivation-removed Shaker (Shaker-IR) was subcloned into pBluescriptII KS (+). The

constructs were linearized with the appropriate restriction enzyme (New England

Biolabs) and cRNA was synthesized using *in vitro* run-off transcription with SP6 or T7

polymerase (Promega). Calmodulin (CaM) DNA was obtained from David Yue (Johns

Hopkins) and subcloned into the pET-DUET1 vector for protein expression and

purification. Cysteine point mutants were introduced by Quikchange site-directed

mutagenesis (Strategene). The CaM binding mutant truncation was generated by PCR

and subcloned into pET-DUET1. Mutations were confirmed by DNA sequencing of the

entire gene.

CaM Expression and Purification

CaM constructs were transformed and expressed in *E.Coli* strain BL21 (DE3)

(Stratagene). Protein expression was induced with 0.4 mM isopropyl-β-D-

thiogalactoside (IPTG) overnight at 20°C. The bacterial pellet was resuspended in lysis

buffer containing (in mM): 2 EDTA, 0.2 phenylmethanesulfonyl fluoride (PMSF), 1 β-

mercaptoethanol (βME), and 50 Tris-HCl, pH 7.5. Cells were lysed by sonification,

clarified by centrifugation, and the supernatant adjusted to a final concentration of 5 mM

$CaCl_2$. Supernatant was applied to a Phenyl-Sepharose CL-4B column (GE Healthcare)

equilibrated with (in mM) 5 $CaCl_2$, and 0.1 NaCl, 1 βME, 50 Tris-HCl, pH 7.5. The

column was washed with 4 column volumes of Wash Buffer #1 containing (in mM): 0.1

CaCl$_2$, 0.1 NaCl, 1 βME, 50 Tris-HCl, pH 7.5 and 4 column volumes of Wash Buffer #2

(in mM): 0.1 CaCl$_2$, 0.5 NaCl, 1 βME, 50 Tris-HCl, pH 7.5. Proteins were eluted in

buffer containing (in mM): 1 EGTA, 1 βME, 50 Tris-HCl, pH 7.5. Purified CaM was

dialyzed against distilled water and lyophilized.

Linker Synthesis, CaM Labeling and Purification

The panel of maleimido-quaternary ammoniums were synthesized and purified as

previously described [109]. To chemically-derivatize CaM with a maleimido-quaternary

ammonium, a CaM cysteine mutant was dissolved in 1 mL of phosphate buffered saline

(PBS) and reacted with 10-fold excess of *tris*(2-carboxyethyl)phosphine (TCEP) for 10

min at room temperature (pH = 7.6). 12-fold excess of the glycine linker was dissolved

in 1 mL of PBS and added dropwise to the CaM solution. Labeling was allowed to

proceed for 2 hours after the addition of linker. To synthesize the N-ethylmaleimide-

capped version (CaM-NEM), the T35C CaM protein was was dissolved in 1 mL of

phosphate buffered saline (PBS) and reacted with 10-fold excess of TCEP for 10 min at

room temperature (pH = 7.6). 12-fold excess of the N-ethylmaleimide was dissolved in 1

mL of PBS and added dropwise to the CaM solution. Labeling was allowed to proceed

for 2 hours after the addition of linker. The reaction mixtures were transferred to a 3 mL

Slide-A-Lyzer (3500 MWCO; Thermo Scientific) and dialyzed against 3 L of PBS at

room temperature. Labeled CaM was separated from unlabeled CaM using a Proto 300

C4 column (250 x 10 mm) composed of 5 μm particles. The aqueous phase contained

(v/v) 95% water, 5% acetonitrile, and 0.1 % trifluoroacetic acid (TFA). The organic

phase was composed of (v/v) 95% acetonitrile, 5% water, and 0.1% TFA. The labeled

proteins were eluted using a linear gradient of 0.4% organic/min between 35 and 50%

organic at a flow rate of 5 mL/min. Fractions containing strong absorption at 214, 260,

and 280 nm were collected and lyophilized. Labeling was confirmed by ESI mass

spectrometry (Table II-1). Calcium Binding Assay: 300 µg of each CaM construct was

preloaded with 5 mM $CaCl_2$ and applied to a Phenyl-Sepharose CL-4B column (GE

Healthcare) as described above. Fractions from the wash and elution buffers were

collected in 5 mL increments. 10 µL of each fraction was diluted with SDS-PAGE

loading buffer containing 100 mM DTT, separated on a 15% SDS-polyacrylamide gel,

and resolved by Coomassie staining.

Electrophysiology

Oocytes were surgically removed from *Xenopus laevis*, defolliculated and stored as

previously described [148]. The extraction procedure and care of *Xenopus laevis* was

approved by the University of Massachusetts Institutional Animal Care and Use

Committee. Oocytes were microinjected with 15.2 ng of mRNA and (27 – 130 ng)

purified CaM 8 – 24 hours after surgery. For Q2/Q3 heteromeric channels, an equal

amount of mRNA (7.6 ng) for each subunit was injected. The final CaM concentration

inside the oocyte (3 – 15 µM) was calculated by assuming a volume of 500 nL for each

oocyte. After 66 – 74 hr (24 hr for *Shaker*), currents were recorded using Warner

Instrument OC-725 two-electrode voltage clamp (TEVC), and the data were acquired

with Digidata 1322A using pClamp 10 (Axon Instruments). Electrodes were filled with:

3 M KCl, 10 mM HEPES, pH 7.6. Currents were measured in ND96 recording buffer

containing (in mM): 96 NaCl, 2 KOH, 0.3 $CaCl_2$, 1 $MgCl_2$, 10 HEPES, pH 7.6. Families

of current were measured by holding at –80 mV and stepping to a series of test potentials

for 4 s (100 ms for *Shaker*) in 20 mV increments, followed by a tail pulse at –30 mV (–80

mV for *Shaker*).

Data Analysis

Analysis of data was performed with Clampfit 10 (Axon Instruments) and Prism 5

software (Graphpad). <u>TEA Injection Studies:</u> Families of Q2/Q3 current were first

measured by holding at –80 mV and stepping to a series of test potentials for 4 s in 20

mV increments, followed by a tail pulse at –30 mV. After recording, oocytes were

injected with TEA so the *in ovo* final concentration was 1 –10 mM and allowed to

recover for 2 h at 16°C. Families of current were then re-measured and the amount of

block was determined for each oocyte. The IC_{50} value for internal block by TEA was

calculated by plotting the amount of block at 40 mV and fitting the data to a hyperbola.

<u>CaM-Gly$_7$-QA Injection Studies:</u> Inhibition by labeled CaM was determined by batch

comparison of oocytes injected with channel mRNA alone versus channel mRNA with

CaM protein. The percent inhibition obtained from each batch was normalized to the

maximal inhibition value. Normalized values were plotted as a function of extended

tether length for each modified CaM. Distance curves were fit to the Boltzmann equation

above to generate a midpoint distance ($d_{1/2}$). <u>Cell Surface Experiments:</u> Families of

Q2/Q3 current were first measured as described for the TEA injection studies. After

recording, oocytes were injected with 27 ng of CaM-Gly$_7$-QA and allowed to recover for

2 h at 16°C. Families of current were then re-measured and the amount of inhibition was

determined for each oocyte. Current remaining after injection was calculated at 40 mV

and normalized to uninjected controls. <u>Binding Site Models:</u> The magnitude of CaM-Gly_n-QA inhibition will depend on the number of tethered blockers that are bound to a Q2/Q3 channel complex. Assuming endogenous CaM and CaM-Gly_n-QA equally compete for binding sites on a Q2/Q3 channel, the incorporation of CaM-Gly_n-QA into a population of Q2/Q3 channels will follow a binomial distribution. Therefore, the amount of inhibition observed can be described by the following equation:

$$F(k;n,P_0) \equiv \sum_{k=0}^{n} (\frac{k \times K_{eff}}{(k \times K_{eff}) + IC_{50}}) \binom{n}{k} P_0^{\,k} (1 - P_0)^{n-k}$$

where n is the number of CaM binding sites on the Q2/Q3 channel, k is the number of Q2/Q3 channel subunits with CaM-Gly_n-QA bound, and P_0, the probability of CaM-Gly_n-QA incorporation based on the concentration of tethered blocker injected. P_0 was calculated using the limits of the range of endogenous CaM that was reported for oocytes (6 or 15 μM) [149,150]:

$$P_0 = \left[\frac{[Injected]}{[Injected] + [CaM]_{endo}} \right]$$

For K_{eff}, we used the range of 2 ± 1 mM as was previously reported for glycine linkers. The IC_{50} of free TEA for Q2/Q3 channels (2 mM) was used as the approximate K_d for CaM-Gly_n-QA block.

KCNQ2/3–CaM Model Generation

The rKv1.2 potassium channel (PDB: 2A79) [9] and CaM–Cav1.2 peptide (PDB: 3G43) [145] o CaM-SK2 peptide (PDB: 1G4Y) [147] crystal structure coordinates were obtained from the Protein Data Bank (<u>www.rcsb.org</u>) and processed using PyMOL

(Schrodinger LLC) to isolate putatively extracellular and intramembranous regions of the rKv1.2 channel and a CaM chain from respective PDB coordinates. Using PyMOL, a dummy atom was placed 20 Å below the quaternary ammonium binding site to indicate the inflection point of a flexible chemical linker as it would angle into the channel pore. Threonine residues (34, 44, 110) in the isolated CaM subunit that correspond to the chemically labeled residues in the purified protein were mutated to cysteine using the mutagenesis wizard within PyMOL, selecting backbone restrained rotamers with minimal van der Waals (VDW) clashes as indicated in the PyMOL graphical user interface. The mutated CaM subunit was positioned at the intracellular end of the isolated potassium channel structure to satisfy the distance restraint between the gamma sulfur atoms of the mutated cysteine residues and the quaternary ammonium binding site. VDW clashes between the channel and CaM were visualized using PyMOL (http://pymolwiki.org/index.php/Show_bumps). Once a CaM orientation was determined that satisfied the measured distance restraints without VDW clashes, the remaining three CaM molecules were generated using basic symmetry operators within PyMOL and confirmed to satisfy the distances without any CaM-channel or CaM-CaM VDW clashes as described above.

Results

To convert CaM binding into a structural reporter for Q2/Q3 channels, we chemically derivatized calmodulin into a "tethered blocker" (Figure II-1A and B) when bound to Q2/Q3 channels. In this intracellular variant, current inhibition requires CaM binding to the channel instead of covalent modification of an extracellular target cysteine residue [109]. Similar to the extracellular version, inhibition of channel function is dependent on tether length; thus, distances between CaM and the blocker's binding site can be determined by comparing the magnitude of current inhibition with a panel of CaM proteins chemically derivatized with different length tethers. For this intracellular tether blocker approach to work as cartooned, three requirements must be met: (1) the binding site of the blocker is known; (2) the blocker binds to Q2/Q3 channels with low affinity such that the freely diffusible tethered blocker does not measurably contribute to channel inhibition; (3) inhibition of Q2/Q3 function depends on CaM binding to increase the local concentration of the tethered blocker for its binding site.
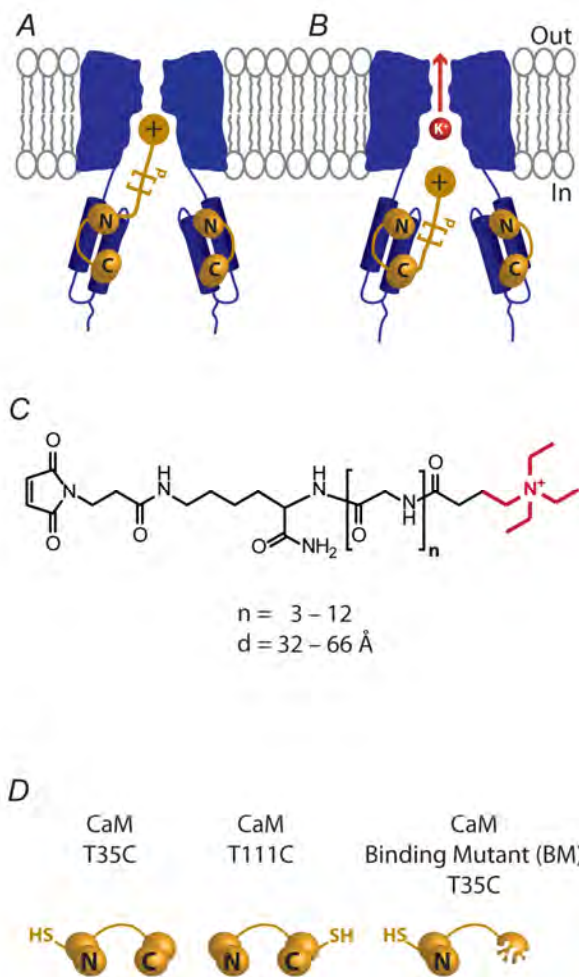
Figure II-1. Tethered blocker strategy for detecting CaM bound to functioning KCNQ channels.
CaM protein chemically derivatized with an internal channel blocker inhibits KCNQ function depending on tether length: if the tether is long enough, (A) the blocker will reach its binding site and block K^+ conduction whereas (B) shorter tethers prevent the blocker from effectively inhibiting channel function. Because the effective concentration of the blocker is dependent on tether length, the magnitude of inhibition provides a distance between a CaM residue and the internal blocker site. (C) Structures of the maleimido-QA linkers: n, number of glycines in the linker; d, extended length of linkers rounded to the nearest angström from the center of the quaternary ammonium (shown in red) to the olefinic carbons on the maleimide. (D) CaM constructs used in this study. Cysteines were introduced into the N- (T35C, T45C) and C-lobes (T111C) of full length CaM and the N-lobe (T35C) of the truncated, binding deficient CaM mutant (BM).

For the blocker, we chose a quaternary ammonium, tetraethylammonium (TEA), because its intracellular binding site on voltage-gated K^+ channels is well-established [4,151] and TEA internally blocks Q2/Q3 channels at millimolar concentrations in excised patches [152]. We chose to perform the tethered blocker experiments in *Xenopus* oocytes to ensure that the chemically-derivatized CaM proteins would co-assemble with KCNQ subunits during biogenesis [17,81,85,86]. Therefore, we determined the IC_{50} value for internal block of Q2/Q3 channels in *Xenopus* oocytes by recording current from individual oocytes before and after injection with various concentrations of TEA. Assuming a cytoplasmic volume of 500 nL [153], the IC_{50} for internal TEA block of Q2/Q3 channels was 2.1 mM, which in contrast to *Shaker* K^+ channels, was essentially independent of voltage (Figure II-2).

With a suitable blocker in hand, we generated a panel of maleimido-quaternary ammoniums (QAs) with various length tethers (32 – 66 Å) by varying the number of glycines between the two moieties using solid-phase peptide synthesis (Figure I-1C) [109]. To transform CaM into a tethered blocker, we engineered individual cysteines into the N- and C-lobes of CaM (Figure I-1D), which does not contain any native cysteines, and labeled the purified mutants with ~ 10-fold molar excess of a maleimido-QA (Methods). The chemically-derivatized CaM proteins were purified by HPLC and the presence of the modification was confirmed by electrospray mass spectrometry (Table II-1). Chemical modification of CaM did not disrupt Ca^{2+} binding, as the QA-derivatized CaM proteins bound phenyl-sepharose only in the presence of Ca^{2+} (Figure II-3).
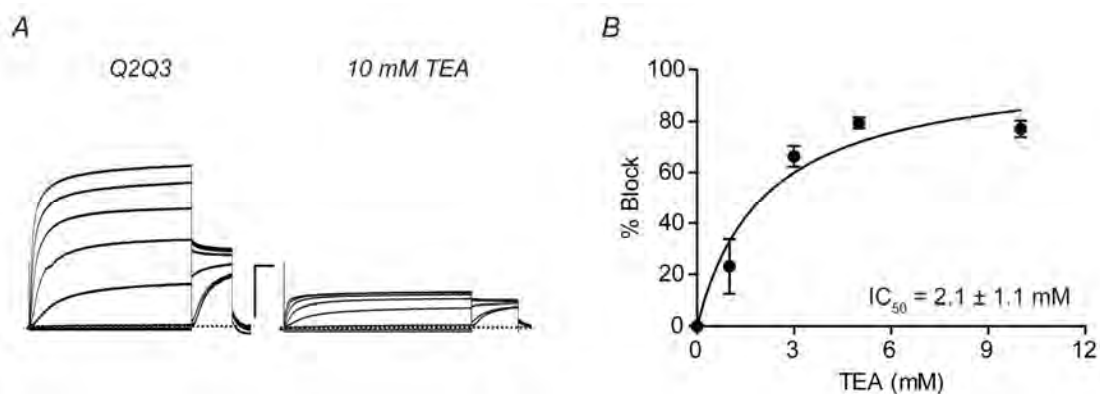
Figure II-2. Free TEA blocks Q2/Q3 channels internally at millimolar concentrations.
(A) Families of currents recorded from *Xenopus* oocytes before and after injection of 10 mM TEA. Currents were elicited by 4 s test potentials from –100 to +40 mV in 20 mV increments from a holding potential of –80 mV followed by a tail pulse to –30 mV. Dashed line indicates zero current. Scale bars represent 0.5 µA and 0.5 s. (B) Percent block at 40 mV was calculated for a range of TEA concentrations (1 – 10 mM). The IC_{50} value is reported as the mean $\pm$ the error of the fit to a hyperbola (n = 4 – 8).

Table II-1. Mass spectrometry data for chemically derivatized CaM

Construct	Fully Extended Tether Length (Å)	Molecular Weight Calculated (Daltons)	Molecular Weight Observed (Daltons)
CaM-Gly$_3$-QA	32	17343	17343
CaM-Gly$_5$-QA	39	17457	17456
CaM-Gly$_6$-QA	43	17516	17518
CaM-Gly$_7$-QA	46	17571	17572
CaM-Gly$_8$-QA	50	17630	17632
CaM-Gly$_9$-QA	54	17687	17687
CaM-Gly$_{10}$-QA	58	17743	17746
CaM-Gly$_{11}$-QA	62	17803	17803
CaM-Gly$_{12}$-QA	66	17857	17860
BM-Gly$_7$-QA	46	11382	11382

Electrospray mass spectrometry results for labeled CaM constructs. Observed masses were the same (within one Dalton) for all three threonine to cysteine mutants (T35C, T45C, and T111C).
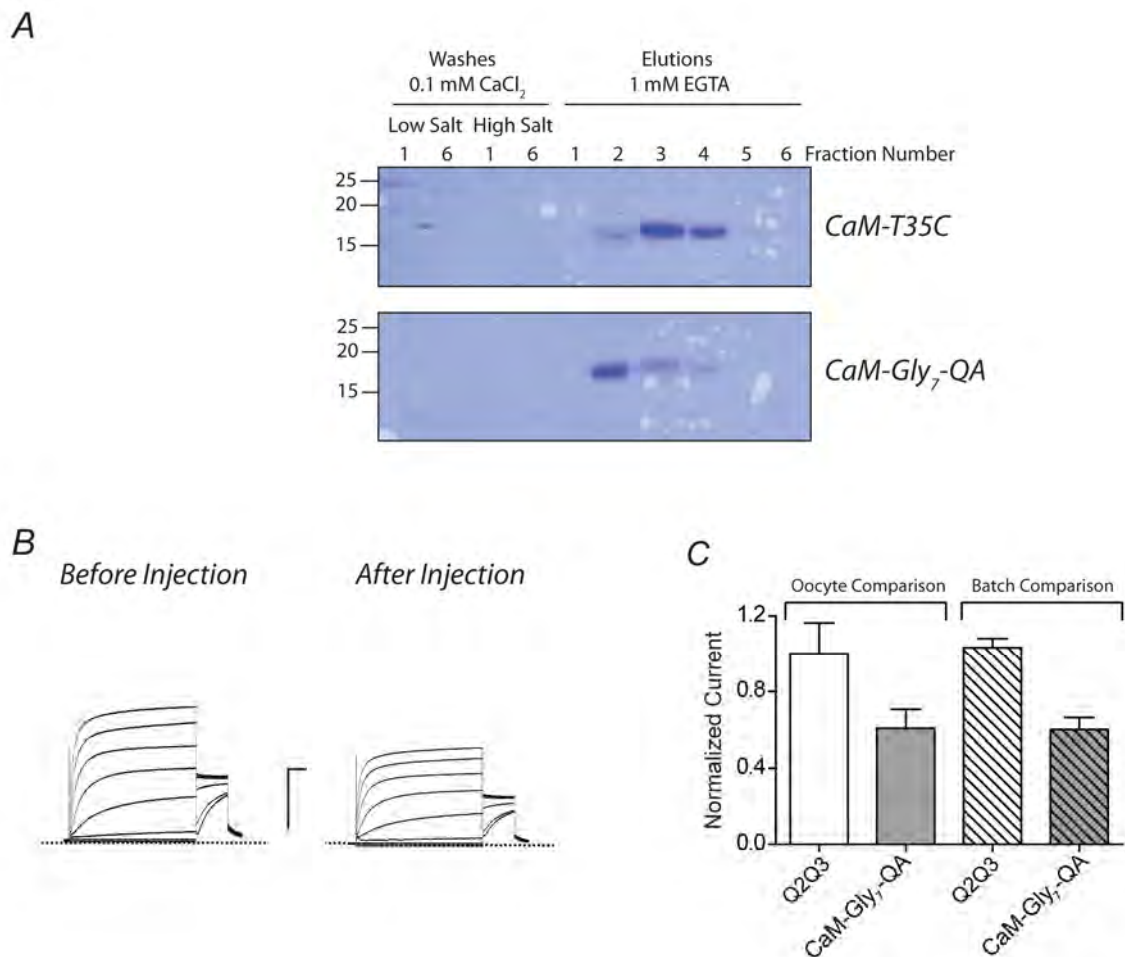
Figure II-3. QA-derivatized proteins retain calcium binding and can exchange with endogenous CaM at the cell surface.
(A) Purified CaM binds to phenyl sepharose in the presence of calcium and dissociates upon chelation with EGTA. SDS-PAGE resolved fractions from a phenyl sepharose column loaded with underivatized or derivatized CaM. (B) Families of Q2/Q3 currents recorded before and after injection of 3 μM CaM-Gly$_7$-QA. Currents were elicited by 4 s test potentials from –100 to +40 mV in 20 mV increments from a holding potential of –80 mV followed by a tail pulse to –30 mV. Dashed line indicates zero current. Scale bars represent 0.5 μA and 0.5 s. (C) Inhibition of Q2/Q3 current by CaM-Gly$_7$-QA is not dependent on time of injection. Quantification of current levels from oocytes injected with CaM-Gly$_7$-QA. For oocyte comparison, values are normalized to current levels before injection. Batch comparison data is from Figure 3 for comparison. Data are presented as the mean ± SEM from 6 individual oocytes.

We first determined whether CaM binding to K^+ channels could be exploited in an intracellular tethered blocker approach by examining CaM derivatized at position T35C (N-lobe) (Figure II-4). To allow the differently derivatized CaM protein to compete with endogenous CaM (6 – 15 µM) [149,154] during Q2/Q3 channel biogenesis, we co-injected CaM protein with channel mRNA. This experimental design required us to compare oocytes injected with derivatized CaM protein to water-injected controls. Oocytes were co-injected with KCNQ channel mRNA and CaM-T35C protein and families of Q2/Q3 currents were measured 3 days after co-injection. Oocytes injected with CaM-Gly$_7$-QA (3 µM *in ovo*) resulted in $43 \pm 4\%$ decrease in current, as compared to water injected control (0 µM) (Figure II-4A and D). Inhibition was dependent on the amount of CaM-Gly$_7$-QA injected (Figure II-4A) and at 13 µM (Figure II-4D) was comparable to maximal block with 10 mM TEA (Figure II-2), consistent with the injected CaM protein competing with endogenous CaM for binding to Q2/Q3 channels. Inhibition of Q2/Q3 current required the presence of the blocker (Figure II-4B) because neither unlabeled CaM-T35C nor an N-ethylmaleimide (NEM)-capped version (CaM-T35C-NEM) reduced the current (Figure II-4B and D).

Figure II-4. Chemically-derivatized CaM proteins behave as intracellular tethered blockers.
(*A*) Families of Q2/Q3 currents recorded from oocytes injected with channel mRNA or co-injected with T35C-Gly$_7$-QA protein. Currents were elicited by 1 s test potentials from –100 to +40 mV in 20 mV increments from a holding potential of –80 mV followed by a tail pulse to –30 mV. Dashed line indicates zero current. Scale bars represent 0.5 μA and 0.2 s. (B) Families of Q2/Q3 currents recorded from oocytes injected with Q2/Q3 mRNA or co-injected with CaM protein. Currents were elicited by 4 s test potentials from –100 to +40 mV in 20 mV increments from a holding potential of –80 mV followed by a tail pulse to –30 mV. Dashed line indicates zero current. Scale bars represent 0.5 μA and 0.5 s. (C) Families of Shaker-IR currents were elicited by test potentials from –100 to +60 mV in 20 mV increments from a holding potential of –80 mV. Scale bars represent 1 μA and 10 ms. (D) Quantification of current levels at 40 mV from oocytes co-injected with CaM. Values are normalized to oocytes injected with only channel mRNA. Data are presented as the mean ± SEM from 2 – 4 batches of oocytes.
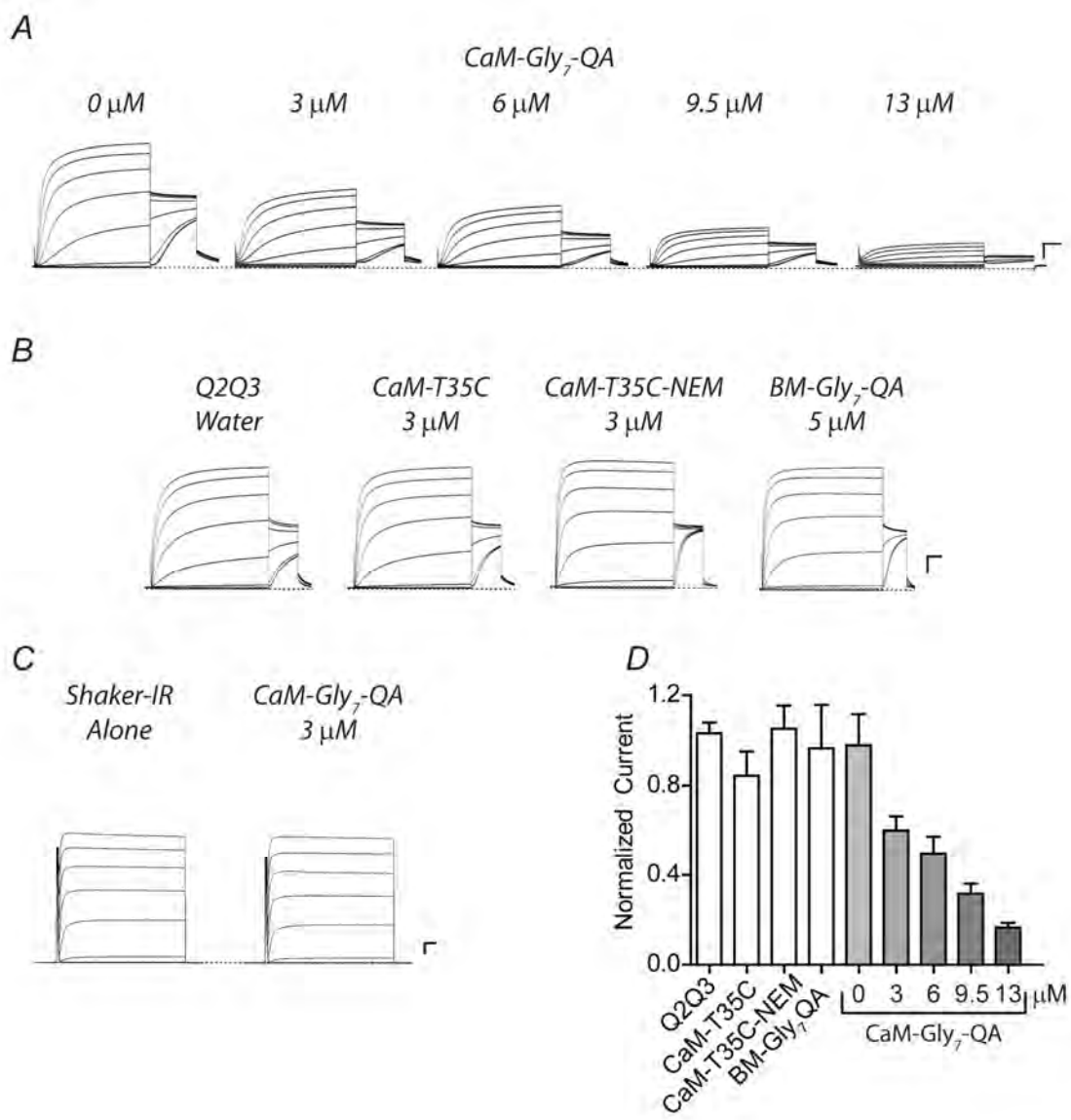
Although Q2/Q3 inhibition with CaM-Gly$_7$-QA was a ~ 1,000-fold more potent

than internal block by TEA (3 μM compared to 2 mM), this increased potency did not

directly demonstrate that the observed inhibition with CaM-Gly$_7$-QA was due to CaM

binding to Q2/Q3 channels. To determine whether CaM binding was required for

inhibition, we first tested CaM-Gly$_7$-QA on Shaker-IR, which is a TEA-sensitive K$^+$

channel that does not directly bind CaM [155]. Co-injection of CaM-Gly$_7$-QA with

Shaker-IR mRNA did not reduce current levels (Figure II-4C) consistent with the notion

that CaM binding is required for inhibition with CaM-Gly$_7$-QA. We also derivatized a

truncated CaM mutant (Figure II-1C) with maleimido-Gly$_7$-QA to generate a tethered

blocker (BM-Gly$_7$-QA) that cannot bind Q2/Q3 channels [10]. Similar to the Shaker-IR

control, BM-Gly$_7$-QA did not inhibit Q2/Q3 currents (Figure II-4B and D).   Together,

these results confirmed that CaM-Gly$_7$-QA requires binding for inhibition, fully

satisfying the requirements of a tethered blocker.

We first used the tethered blockers to determine a distance between the N-lobe of

CaM and the TEA binding site on Q2/Q3 channels. At the N-lobe residue, T35C, six

different tether lengths were tested at 3 μM final oocyte concentration (Figure II-5A). As

expected for a bona fide tether blocker, the magnitude of channel inhibition was

dependent on tether length: the shortest tether, CaM-Gly$_3$-TEA, showed little to no

inhibition; intermediate length tethers showed partial inhibition and all tethers that

contained more than six glycine residues showed maximal inhibition (~ 50%). Plotting

inhibition (normalized to maximal inhibition) as a function of fully extended tether length

(Figure II-5, right panel) resulted in a monophasic curve, indicating that the tethered blockers are reporting from a single CaM binding site on a KCNQ subunit. To calculate a distance, previous tethered blocker studies on the *Shaker* K^+ channel have used the fully extended linker length of the tethered blocker that results in the first sign of inhibition [109]. However, this metric for tether length yields distances that are systematically shorter than the atomic distances in the subsequently published $rK_v1.2$ structure [9]. A reexamination [156] of these data revealed that a better metric for calculating a tethered blocker distance is the end-to-end tether length of the linker that results in half maximal inhibition ($d_{1/2}$). Therefore, we plotted inhibition (normalized to maximal inhibition) as a function of extended tether length (Figure II-5A, right panel) and fit the data to a Boltzmann equation to obtain a $d_{1/2}$ of 40 ± 1 Å between the N-lobe residue, T35C, and the Q2/Q3 TEA binding site. This mathematical fit to a Boltzmann equation has no physical meaning and was solely used to objectively calculate $d_{1/2}$.
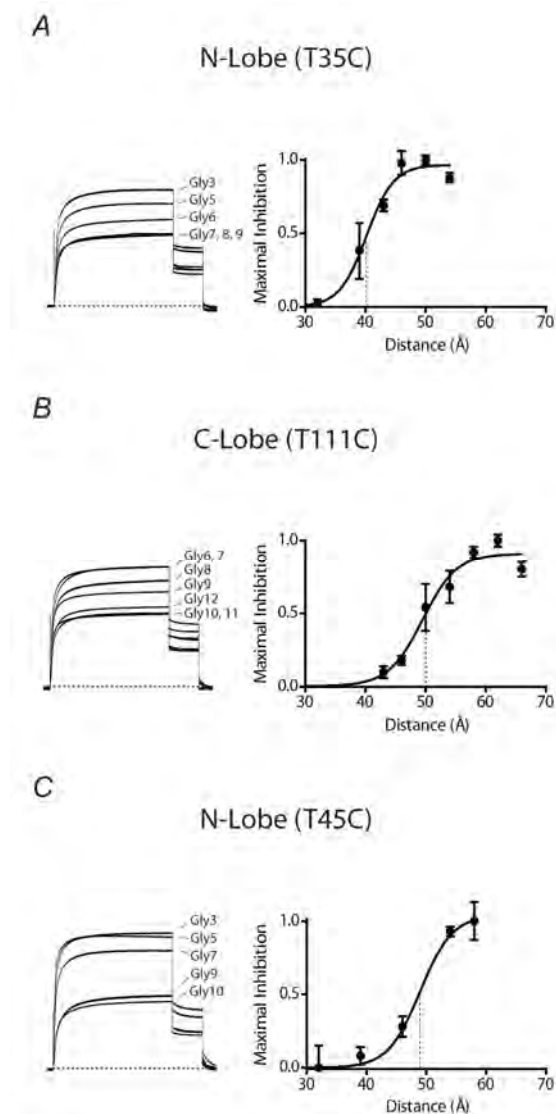
Figure II-5. Distance measurements for CaM residues: T35, T45 and T111.
(*Left*) Superimposed currents recorded from oocytes injected with 3 μM (A) TEA-Gly$_n$-T35C; (B) TEA-Gly$_n$-T111C; (C) TEA-Gly$_n$-T45C. Currents were elicited with 4 s test potentials to +40 mV from a holding potential of –80 mV followed by a tail pulse to –30 mV. Dashed line indicates zero current. (*Right*) Normalized inhibition values plotted as a function of linker length. Data are presented as the mean ± SEM from 2 – 4 batches of oocytes. The data were fitted to a Boltzmann equation to generate the midpoint of inhibition ($d_{1/2}$): (A) 40 ± 1 Å (B) 50 ± 1 Å (C) 49 ± 1 Å. Values are reported as mean ± the error of the fit.

To determine the precision of the measured distance, we also measured the distance from T35C and the Q2/Q3 TEA binding site at different depolarizing potentials and with higher *in ovo* concentrations of derivatized CaM. Repeating the analysis at different test potentials consistently resulted in a $d_{1/2}$ of 40 ± 1 Å (Table II-2), demonstrating that the measured distance is not dependent on the depolarizing pulse. To determine whether the calculated distances were also independent of the amount of injected CaM protein, we repeated the experiments at an *in ovo* concentration of 15 μM (Figure II-6A). As expected, the higher concentration of injected CaM-Gly$_n$-QA that contained more than six glycine residues (n = 7 or 8) resulted in maximal inhibition (~ 85%) that was greater than observed with 3 μM (~ 50%). In addition, this increased inhibition was not due to disrupting CaM homeostasis—as has been observed with CaM overexpression [89]—because CaM protein derivatized with shorter tethers did not inhibit Q2/Q3 channel function (Figure II-6A). Moreover, fitting the 15 μM data to a Boltzmann yielded a $d_{1/2}$ of 43 ± 1 Å, demonstrating that the number of tethered blockers bound to functioning Q2/Q3 channels does not appreciably affect the distance measured between CaM and the TEA binding site. In total, the consistency of the calculated distance at different voltages and *in ovo* concentrations of derivatized CaM bolstered our confidence in both the methodology's robustness and precision of the distance measured with intracellular tethered blockers.

Table II-2. Distances between CaM residues and the Q2/Q3 TEA binding site

Voltage (mV)	$d_{1/2}$ (Å)		
	T35C	T45C	T111C
-20	40	48	49
0	41	48	49
20	41	48	49
40	40	49	50
Average	**41**	**48**	**49**

Data from individual inhibition curves obtained from 2 – 4 batches of oocytes. Curves were fitted to a Boltzmann function to yield $d_{1/2}$ as described for Figure 4.

Figure II-6: Multiple CaM-Gly$_n$-QA subunits assemble with Q2/Q3 channels at the cell surface.

(A) Distance measurement of CaM residue T35 at higher concentrations (13 – 18 μM) of injected CaM-Gly$_n$-QA. Percent inhibition values plotted as a function of end-to-end linker length. Data are presented as the mean ± SEM from 1 – 2 batches of oocytes. The data were fitted to a Boltzmann equation to generate the midpoint of inhibition ($d_{1/2}$): T35C: 43 ± 1 Å. (B) Binding site models for CaM-Gly$_n$-QA using equations described in Methods. Upper limit: 6 μM endogenous CaM; K_{eff} = 3 mM. Lower limit: 15 μM endogenous CaM; K_{eff} = 1 mM. Data are mean ± SEM obtained from 1 – 4 batches of oocytes.
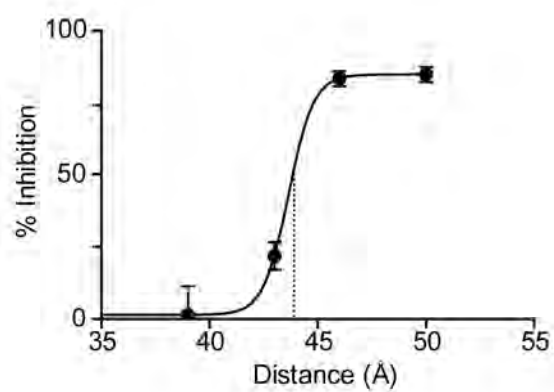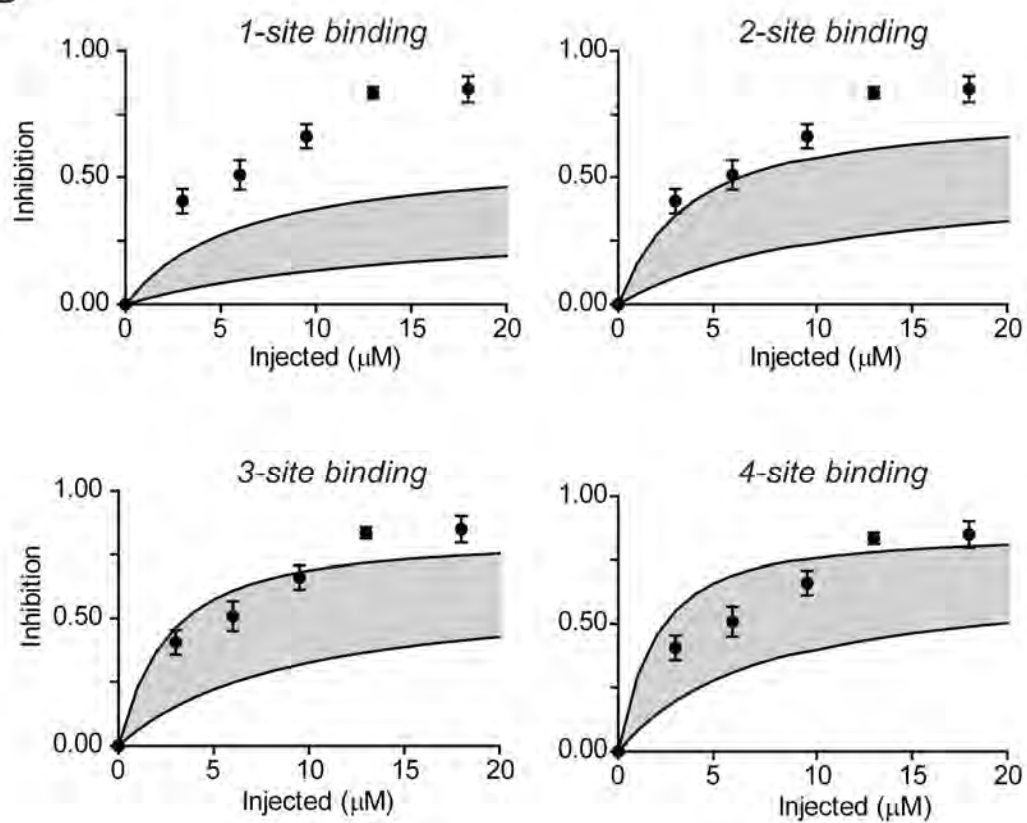
We next switched to the C-lobe of CaM and tested residue, T111C. Compared to T35C, T111C is further away from the TEA binding site, as maximal inhibition required tethers with at least ten glycine residues (Figure II-5B, left panel). Fitting the data to a Boltzmann equation afforded a $d_{1/2}$ of 50 ± 1 Å (Figure II-5, right panel). Lastly, to fully triangulate the position of CaM bound to Q2/Q3 channels, we picked an additional CaM residue, T45C, to generate a third distance restraint. Although this residue is in the N-lobe of CaM, its $d_{1/2}$ (49 ± 1 Å) was comparable to the C-lobe residue, T111C (Figure II-5C).

Since no high resolution structural information exists for the Q2/Q3-CaM complex, we modeled a quaternary structure using ion channel domains with known structures and our distance constraints. For Q2/Q3, we used the membrane-embedded portion of rKv1.2 (PDB: 2A79) [9] to model the S1 – S6 segments and transplanted the crystallographically-determined TEA binding site from the KcsA–tetrabutylantimony structure (PDB: 2HJF) [4]. For CaM, the crystal structure of CaM bound to the Cav1.2 pre-IQ domain (PDB: 3G43) [145] was used for three reasons: (1) both CaM binding motifs must be intact for the KCNQ-CaM protein-protein interaction, suggesting that CaM wraps around a two helices; (2) hydrophobic residues in the pre-IQ domain that make contact with CaM are also present in the KCNQ CaM binding motifs (Figure II-7A). (3) CaM binds to both KCNQ and Cav channels in the absence and presence of calcium [88,146,157]. To apply the radial distance restraints to these high resolution structures, we approximated the trajectory taken by the tethered blocker from CaM to the quaternary ammonium binding site (Figure II-7, large purple sphere). Therefore, the first

20 Å was modeled as a straight line until it emerged from the Kv inner vestibule (depicted as a blue sphere) where it was allowed to splay off at an angle collinear with the S6 helix that enabled the four-fold arrangement of CaM proteins. Four CaM molecules (*sans* Cav1.2 peptides) were modeled because *in vitro* data indicate a 1:1 KCNQ:CaM stoichiometry [17,87] . Two KCNQ-CaM quaternary models satisfied the distance restraints within 1 Å without observable van der Waals clashes (Figure II-7B and C). The lack of a single KCNQ-CaM model arises from the degeneracy with which CaM binds to its targets; thus, Figure II-7B depicts one structural model where T111C faces the channel whereas in Figure II-7C the CaM subunits are essentially inverted (note the position of T111C). In both models, the modeled CaMs are close to the KCNQ channel gate (Figure II-5B and C, left panels).

We also generated quaternary structural models (Figure II-8) of the complex using the crystal structure of CaM bound to a peptide from the SK2 channel (PDB: 1G4Y) [147] because functional data suggests that CaM binds to a continuous KCNQ peptide [92]. Using the SK2-CaM structure as a model of the KCNQ-CaM protein-protein interaction, however, did not fit the distance restraints and required the systematic addition of 5 Å to yield quaternary structures that did not contain non-native contacts. Thus, our experimentally-determined distance restraints indicate the protein fold of CaM in the Cav1.2 pre-IQ domain structure [145] may better represent CaM when it is bound to full-length Q2/Q3 channels.

Figure II-7. Structural models of the Q2/Q3-CaM complex using the Cav1.2 crystal structure (PDB: 3G43). (A) CaM binding motifs from Q2, Q3, Cav1.2, and SK channels. The IQ and 1-5-10 motifs in Q2/Q3 are highlighted. (B) Side and cytoplasmic views of the complex, showing the channel subunits colored grey and the four CaM molecules in different pastels. In the side view, only three subunits are shown for clarity. Residues T35C (red), T45C (green), and T111C (blue) are shown in spacefill. (C) Membrane and cytoplasmic view of the complex with CaM subunits inverted. Colors are the same as in (A).

A

Helix A   *Helix B*

KCNQ2   AAGL**IQ**SAW**R**FYATNLSRT   PG**L**KVS**I**RA**V**C**V**MRF**L**VSKRKFKESLR
KCNQ3   AAEL**IQ**AAW**R**YYATNPNRI   PT**L**KAA**I**RA**V**R**I**LQFRLYKKKFKETLR
Cav1.2   TLFALVRTALRIKTE   LRAIIKKIWKRTSMKLL

B

90°

T111C
T45C

T35C

C

90°

T35C

T45C
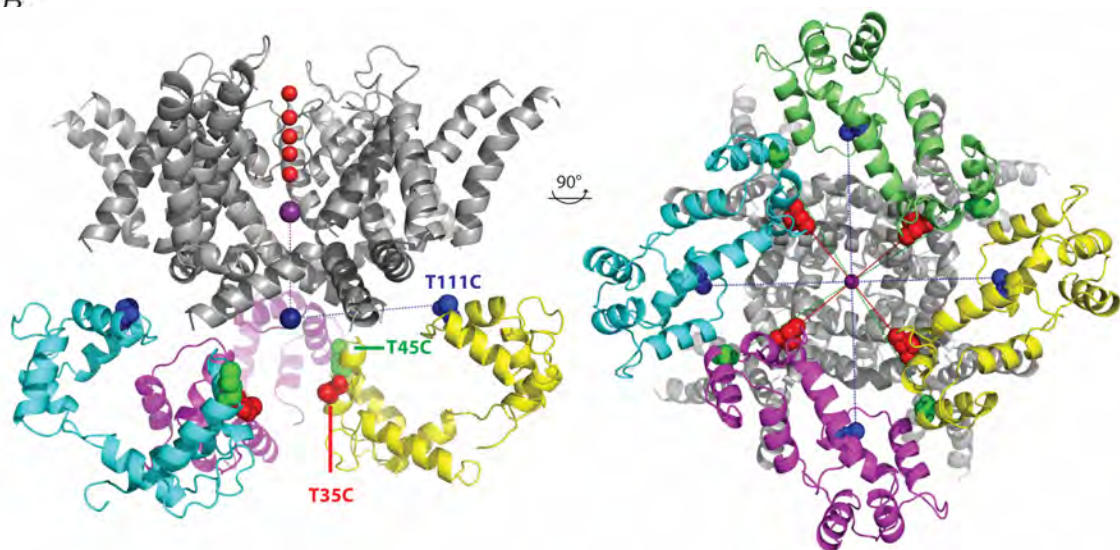
T111C
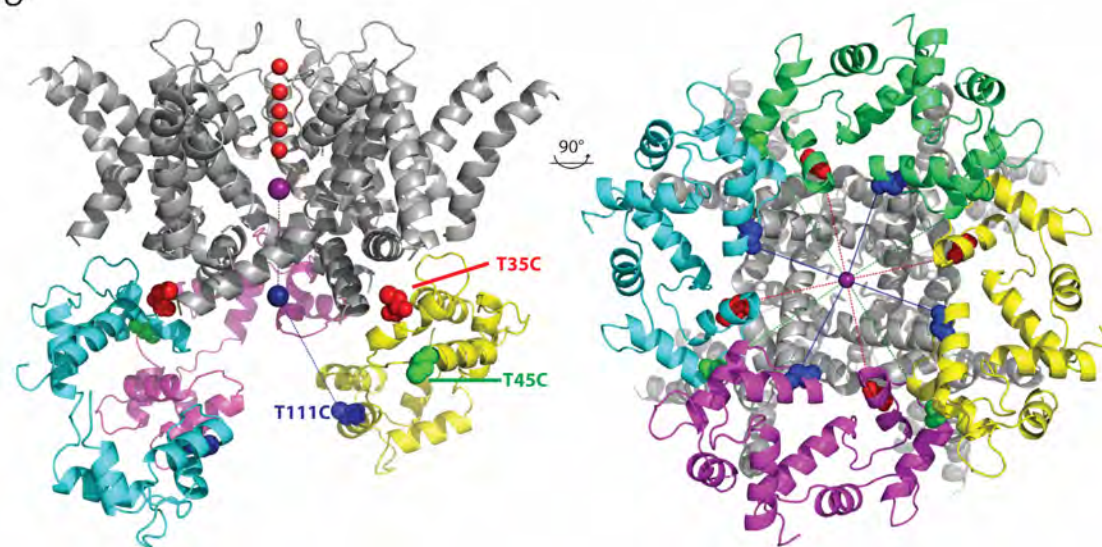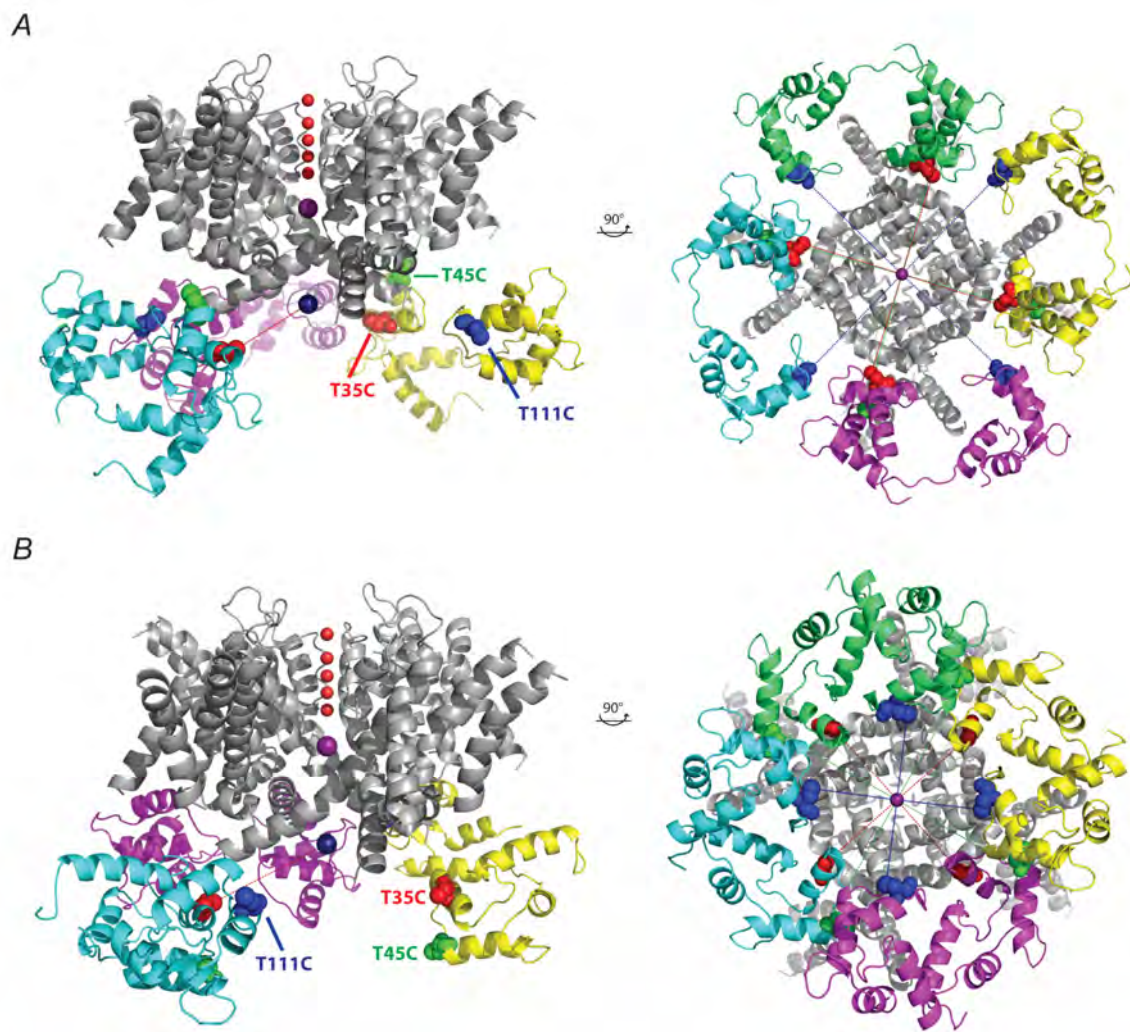
Figure II-8. Structural models of the Q2/Q3-CaM complex using the SK crystal structure (PDB: 1G4Y). Distance restraints were systematically loosened by 5 Å to ensure non-native contacts. (A) Membrane and cytoplasmic views of the complex, showing the channel subunits colored grey and the four CaM molecules in different pastels. In the side view, only three subunits are shown for clarity. Residues T35C (red), T45C (green), and T111C (blue) are shown in spacefill. (B) Membrane and cytoplasmic view of the complex with CaM subunits inverted. Colors are the same as in (A).

Discussion

Motivated by the plethora of high resolution structures of isolated ion channel domains, we developed an intracellular tethered blocker approach to generate quaternary structural models of ion channel-CaM complexes. Using a panel of intracellular tethered blockers to generate distance restraints between CaM and the Kv channel TEA binding site, we generated quaternary models of the Q2/Q3-CaM complex in the open state. In these models, CaM is very close to the cytoplasmic gate of Q2/Q3 channels where it well-positioned to modulate Q2/Q3 channel gating (calmodulation). The juxtaposition of the "CaM ring" to the Q2/Q3 channel gate results in a cytoplasmic vestibule that is continuous with the Q2/Q3 pore domain, which is in contrast to the hanging gondola structure observed in classic Kv channels (Kv1 – 4). This elongated permeation pathway predicts that the potassium ions will enter and exit the Q2/Q3-CaM complex through the center of the CaM ring. Given that the spacing between the first CaM binding motif and the cytoplasmic "bundle crossing" [6] is conserved in the KCNQ family, our quaternary models serve as structural scaffolds for all KCNQ-CaM complexes.

While developing the intracellular tethered blocker approach, we were also able to glean some information about the available CaM binding sites and dynamics of the KCNQ-CaM complex at the plasma membrane. Because the chemically-derivatized CaM proteins compete with endogenous CaM for binding to KCNQ channels (Figure II-4A), we subsequently plotted the magnitude of inhibition versus the concentration of injected tethered blocker and fit the data to different binomial biding site models (Figure II-6B). This post-hoc analysis revealed that there are multiple CaM binding sites

equidistant from the TEA binding site on the full-length KCNQ channel; however, the inability to exquisitely control the total CaM concentration in the cell precluded us from confirming the predicted 4:4 stoichiometry of the KCNQ-CaM complex [17,87]. Similarly, insight into the dynamics of the KCNQ-CaM protein-protein interaction came from experiments where CaM-Gly$_7$-QA was injected into oocytes already expressing Q2/Q3 currents (Figure II-3B). Injecting CaM-Gly$_7$-QA into oocytes already expressing Q2/Q3 currents resulted in a similar magnitude of inhibition compared to co-injection with channel mRNA (Figure II-3C).   The rapid onset (~ 2 hr) indicates that the chemically-derivatized CaM proteins need not co-assemble with Q2 and Q3 channel subunits during biogenesis and can bind to functioning channels at the plasma membrane. These results suggest that at least one CaM binding site is free or the injected CaM rapidly exchanges with KCNQ-bound CaM proteins or other intracellular scaffolding proteins (e.g. Syntaxin 1A and AKAP79/150) [68,91]. Both scenarios illustrate the dynamic nature of the KCNQ-CaM complex.

Although the KCNQ-CaM protein-protein interaction is dynamic, the monophasic inhibition curves indicate that the tethered blockers are reporting from a single location (within ~ 66 Å) on the KCNQ C-terminus and are not oscillating between the two CaM binding motifs. A single CaM on the KCNQ C-terminus is also consistent with previous functional data that suggest the Syntaxin 1A and AKAP79/150 abrogate CaM binding by partially masking only one CaM binding motif [70,92]. In spite of this competition for the KCNQ C-terminus, the distance restraints did not depend on the amount of injected tethered blocker (Figure II-5 and 6), suggesting that KCNQ need not

be fully occupied with QA-derivatized CaM molecules to determine the location of CaM bound to KCNQ channels.

As with all structural determinations that rely on functional measurements, there are some limitations to the intracellular tethered blocker approach. First, the models depict the Q2/Q3-CaM complex in the open state. Second, the distances measured by tethered blockers are radial; thus, the absolute position of CaM with respect to a particular KCNQ subunit cannot be determined. To approximate the position of each CaM molecule in the quaternary structures, we have positioned the KCNQ subunit such that the S6 pore helix bisects the center of each CaM molecule. Given the short distance between the bundle crossing and the first CaM binding domain (~ 15 amino acids), this is a good approximation of the absolute position of CaM in the full-length complex. Third, the approach does not speak to how the KCNQ C-terminus is threaded through the lobes of CaM. With a high resolution structure of a CaM-KCNQ peptide complex, a single Q2/Q3-CaM quaternary model could be generated using tethered blockers; however, the molecular details of the protein-protein interaction inherent to the full-length complex such as whether a single CaM binds to one KCNQ C-terminus or to two adjacent C-termini simultaneously will not be resolvable. Lastly, we do not know whether the measured distances using wild type protein are from fully calcified, half-calcified, uncalcified, or an amalgam of differently calcified CaM proteins. Because injecting micromolar amounts of purified CaM protein does not affect Q2/Q3 function (Figure II-4), our current structural models are most likely representative of the Q2/Q3-CaM complex under endogenous calcium concentrations. Future studies that utilize CaM

calcium binding mutants (CaM$_{12}$, CaM$_{34}$, etc.) [158] will provide insight into how calcification of the different CaM lobes affects its position on the full-length channel.

Given that the number of high resolution structures of CaM bound to peptide fragments from ion channels is steadily increasing, the need to connect these structures to their respective ion-conducting domains is vital for unraveling the mechanisms of calmodulation. By chemically derivatizing CaM with different channel blockers, the intracellular blocker approach can be expanded to determine the location of CaM on a wide variety of ion channels. Moreover, the approach is not limited to CaM, and can be applied to other cytoplasmic regulatory and scaffolding proteins that are essential for ion channel modulation.

CHAPTER III: DISCOVERY OF A NOVEL ACTIVATOR OF KCNQ1-KCNE1 K+ CHANNEL COMPLEXES

Abstract

KCNQ1 voltage-gated K^+ channels associate with the family of five KCNE peptides to form complexes with diverse gating properties and pharmacological sensitivities. The varied gating properties of the different KCNQ1-KCNE complexes enables the same K^+ channel to function in both excitable and non excitable tissues. Small molecule activators would be valuable tools for dissecting the gating mechanisms of KCNQ1-KCNE complexes; however, there are very few known activators of KCNQ1 channels and most are ineffective on the physiologically relevant KCNQ1-KCNE complexes. Here we show that a simple boronic acid, phenylboronic acid (PBA), activates KCNQ1/KCNE1 complexes co-expressed in *Xenopus* oocytes at millimolar concentrations. PBA shifts the voltage sensitivity of KCNQ1 channel complexes to favor the open state at negative potentials. Analysis of different-sized charge carriers revealed that PBA also targets the permeation pathway of KCNQ1 channels. Activation by the boronic acid moiety has some specificity for the KCNQ family members (KCNQ1, KCNQ2/3, and KCNQ4) since PBA does not activate Shaker or hERG channels. Furthermore, the commercial availability of numerous PBA derivatives provides a large class of compounds to investigate the gating mechanisms of KCNQ1-KCNE complexes.

Introduction

The five KCNQ voltage-gated K^+ channels (Kv7.1 – Kv7.5) are responsible for membrane excitability, cardiac rhythmicity, and maintaining salt and water homeostasis. The KCNQ family is divided by their tissue expression: KCNQ1 (Q1) channels are expressed throughout the body, but are noticeably absent from the central nervous system where KCNQ2-5 channels are primarily found [1]. KCNQ2-5 subunits form homo- and heterotetrameric K^+ channels.   KCNQ2/3 (Q2/Q3) channels contribute to the M-current and mutations in these channels cause benign familial neonatal convulsions (BFNC) [61]. Homotetrameric KCNQ4 (Q4) channels have also been implicated in disease. Mutations in Q4 cause an autosomal dominant form of progressive hearing loss in humans [46]. In contrast, Q1 channels only form homotetramers and function in non-excitable as well as excitable tissues [159]. In order to properly function in these diverse tissues, Q1 channels co-assemble with KCNE peptides, affording complexes with different gating properties and pharmacological sensitivities [21]. Although KCNE peptides promiscuously assemble with many voltage-gated K^+ channels in expression systems [21], the physiological relevance of most of the Q1-KCNE (E1, E2, and E3) complexes are well-established. Q1 subunits form a complex with KCNE1 (E1) peptides in the heart and inner ear, generating the cardiac I_{Ks} current and providing an avenue for K^+ to enter the endolymph, respectively [22,23,35]. Mutations in either Q1 or E1 that decrease the conductance of the complex prolong the cardiac action potential, leaving individuals with these mutant proteins susceptible to long QT syndrome [160]. In contrast to the slowly activating and deactivating Q1/E1 complex, both Q1/E2 and Q1/E3 complexes are

constitutively conducting and contribute to K^+ recycling in epithelial cells of the gastrointestinal tract [24,25].

Although the different KCNE peptides have diametrically opposite effects on Q1 channel function, the molecular mechanisms involved in KCNE modulation of Q1 channel gating are starting to be revealed [161-163]. Simple, small molecules that activate Q1-KCNE complexes would be valuable tools for investigating KCNE modulation of Q1 channel gating. Indeed, low-affinity blockers such as the quaternary ammoniums have been instrumental in the biophysical characterization of the permeation pathway of K^+ channels [151,164-166]. However, small molecule activators of voltage-gated K^+ channels are rare [94] and often synthetically challenging to derivatize. Moreover, KCNE peptides are known to affect the sensitivity of pharmacological agents that modulate Q1 function [167]. Inhibitors of Q1 function are typically more potent when the channels are co-assembled with KCNE peptides [120,133,168,169]. Conversely, small molecules that activate homomeric Q1 channels are often ineffective on Q1/E1 complexes. Two known examples of this phenomenon are the Q1-specific activator, R-L3, and the recently discovered KCNQ activator, zinc pyrithione [94,96,97]. The non-specific Cl^- channel blockers, mefanamic acid and DIDS, are the exceptions to the rule as they cross-react with and activate Q1/E1 complexes [98,169]. Thus, there remains a dearth of small molecule activators for the biophysical study of Q1-KCNE complexes.

During our initial efforts to chemically activate Q1 channels by specifically modifying the arginines in the voltage sensor, we serendipitously discovered that some

boronates were modulators of Q1/E1 complexes. Examination of a small panel of boronic acids revealed that the aromatic derivative, phenylboronic acid (PBA), activates Q1/E1 complexes at millimolar concentrations. Activation of Q1/E1 by PBA is due to a shift in the voltage sensitivity of the complex and is specific for the boronic acid moiety. The permeation pathway is also affected by PBA since the magnitude of Q1 channel activation is dependent on the charge carrier. PBA shows some selectivity as it activates other members of the KCNQ family, but does not activate Shaker or hERG K^+ channels. Since derivatives of PBA are common building blocks for organic synthesis, there currently exists a vast array of structurally diverse phenylboronic acids with varied physiochemical properties. The accessibility to thousands of PBA derivatives provides an opportunity to systematically dissect the mechanisms of Q1-KCNE gating and may lead to the discovery of a potent activator of Q1/E1 complexes for the treatment of cardiac arrhythmias.

Materials and Methods

Molecular Biology

cDNA encoding human KCNQ1, E1, and E3 were individually subcloned into the vector

pSG01MX, which contains the 5' and 3'UTRs from the *Xenopus* β-globin gene for

increased protein expression. Inactivation-removed Shaker (Shaker-IR) was in

pBluescriptII KS (+). KCNQ2, Q3, and Q4 were kindly provided by G. Seebohm and

hERG was kindly provided by M. C. Sanguinetti. The constructs were linearized with

the appropriate restriction enzyme (New England Biolabs) and cRNA was synthesized

using *in vitro* run-off transcription with SP6 or T7 polymerase (Promega).

Electrophysiology

Oocytes were surgically removed from *Xenopus laevis*. The extraction procedure and

care of *Xenopus laevis* was approved by the University of Massachusetts Institutional

Animal Care and Use Committee. Oocytes were defolliculated using 2 mg/mL

collagenase (Worthington Biochemical Corp.) in OR2 solution containing (in mM): 82.5

NaCl, 2.5 KCl, 1 $MgCl_2$, 5 HEPES, pH 7.4 for 60-80 minutes. Isolated oocytes were

rinsed and stored in ND96 storage solution containing (in mM): 96 NaCl, 2 KCl, 1.8

$CaCl_2$, 1 $MgCl_2$, 5 HEPES, 50 μg/mL of both gentamicin and tetracycline pH 7.4, at

18°C. Oocytes were microinjected 24 h after surgery with Shaker, Q1, Q4, or hERG

mRNA (15.2 ng). Additionally, Q1 mRNA (7.6 ng) was co-injected with E1 or E3

mRNA (3.8 ng). For Q2/Q3 heteromeric channels, an equal amount of mRNA (7.6 ng)

for each subunit was injected. After 2–4 days, currents were recorded using Warner

Instrument OC-725 two-electrode voltage clamp (TEVC), and the data were acquired

with Digidata 1322A using pClamp 9 (Axon Instruments). Electrodes were filled with: 3

M KCl, 5 mM EGTA, 10 mM HEPES, pH 7.6. Currents were measured in ND96

recording buffer containing (in mM): 96 NaCl, 2 KOH, 0.3 $CaCl_2$, 1 $MgCl_2$, 10 HEPES,

pH 7.6. All chemical compounds were from Sigma Aldrich and dissolved directly into

ND96 recording buffer to a final concentration of 10 mM unless otherwise noted. For the

initial Borax experiments, 10 mM sodium tetraborate was used as a buffer instead of

HEPES. The time courses of current changes upon compound application and washout

were generated by repeatedly depolarizing and measuring the change in current at the end

of the pulse. Channels were held at –80 mV and pulsed to +40 mV (0 mV for hERG) for

2 s (100 ms for Shaker) every 30 s to illicit current. For EC_{50} experiments, current

changes were measured for a range of PBA concentrations (1–10 mM). Current-voltage

relationships were measured in the presence or absence of 10 mM PBA by holding at –80

mV and stepping to a series of test potentials for 4 s in 10 mV increments, followed by a

tail pulse at –30 mV. For Q1/E3 complexes, the current-voltage relationships were

measured in KD50 containing (in mM): 48 NaCl, 50 KOH, 0.3 $CaCl_2$, 1 $MgCl_2$, 10

HEPES, pH 7.6 by holding at –80 mV and pulsing to a series of potentials for 2 s in 20

mV increments, followed by a tail pulse to –80 mV. For charge carrier experiments,

currents were measured in modified KD50 containing either 50 mM KOH, RbCl, or

CsCl.

Data Analysis

Analysis of data was performed with Clampfit 9 (Axon Instruments) and Prism 5

software (Graphpad). The maximal change in current upon PBA washout at 40 mV was

calculated as Δg_{max}. EC_{50} values were calculated by plotting the Δg_{max} values as a

function of PBA concentration and fitting the data to a hyperbola. The amplitude of tail

currents was measured 6 ms (100 ms for Q1) after repolarization to –30 mV (–80 mV for

Q1/E3 and 50 mM external charge carriers) and normalized such that the maximal tail

current in the absence of drug was equal to 1. Normalized tail currents were plotted

versus the test potential to produce activation curves. Activation curves were fit to the

Boltzmann equation: $I_{tail} = A1 + (A2 - A1) / (1 + e^{((V - V_{1/2})*(-zF/RT))})$, where $V_{1/2}$ is the

voltage of half-maximal activation and z is the slope factor. A Student's paired *t*-test was

performed to determine whether PBA activation was significantly different than

activation by benzyl alcohol. Deactivation time constants for Q1 were measured after a

depolarizing pulse to 40 mV and fitting the tail current at –80 mV to a single exponential.

Time constants were fit after recovery from inactivation. For the comparison of outward

and inward currents, the amplitude of the Q1 current was measured 2 s after

depolarization for outward, 100 ms after repolarization for inward. The outward and

inward currents were normalized to 1 after the onset of PBA inhibition (defined as time =

0). Subsequent values were plotted as percent increase as a function of PBA exposure

time.

Results

Borax is a commonly used buffer for protein modification reactions that specifically neutralizes positively charged arginine residues [170]; thus, we initially determined whether borate buffer would have any effect on Q1/E1 complexes. Figure III-1A shows normalized Q1/E1 current elicited by 40 mV, 2 s depolarizations in standard ND96 buffer. Switching the solution to a buffer that contains 10 mM sodium tetraborate resulted in reversible inhibition of the Q1/E1 complex. Intrigued by the inhibitory effect of borate, we determined whether boronic acid derivatives had a similar effect on Q1/E1 complexes. Methylboronic acid in ND96 with HEPES as the buffer had little to no effect on Q1/E1 complex function; however, perfusion of 10 mM phenylboronic acid (PBA) caused a rapid inhibition followed by a slower activation, resulting in a net doubling of current (Figure III-1A). Upon washout of PBA, inhibition was quickly and completely relieved, resulting in a dramatic rise in current amplitude. Although PBA's inhibitory effect was rapidly reversible, activation of Q1/E1 complexes slowly diminished upon removal of PBA, but never fully washed out. To determine whether activation was due to a shift in the voltage sensitivity of Q1/E1 complexes, we measured the effect of PBA at different voltages (Figure III-1B). Tail current analysis (Figure III-1C) in the presence PBA resulted in a left-shift of the midpoint of activation ($V_{1/2}$) and a decrease in the voltage-dependence (z) of Q1/E1 complexes (Table III-1). Since PBA both activates and inhibits Q1/E1 complexes, we utilized the kinetic difference in washout to measure the maximal activation of Q1/E1 complexes by PBA.
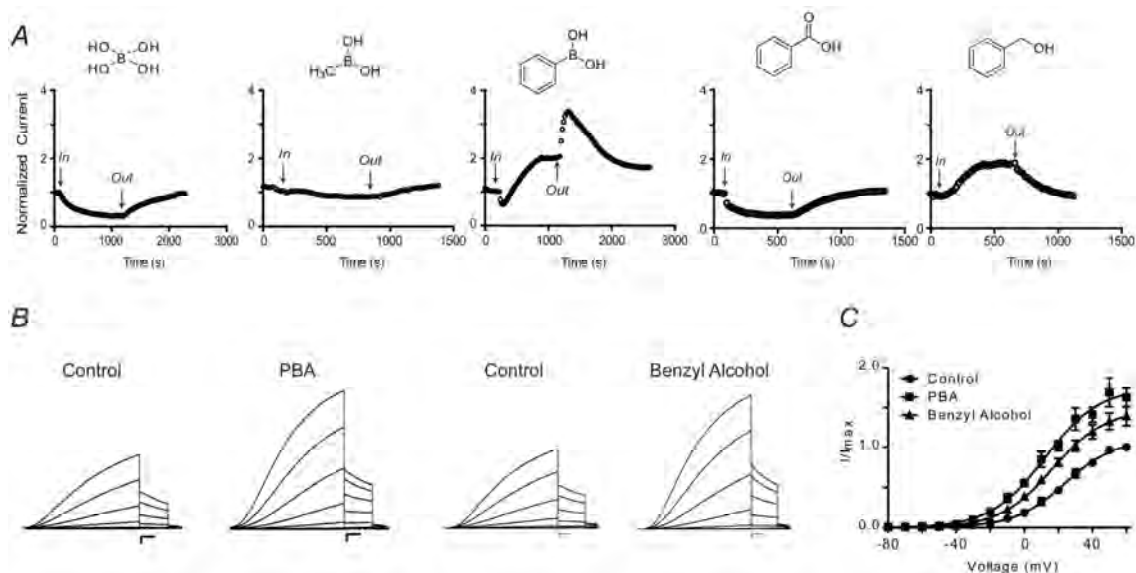
Figure III-1. Modulation of Q1/E1 channels by boronates.
(A) Time course of Q1/E1 current measured in ND96 at +40 mV at the end of a 2 s pulse.
The current was normalized before compound application. Borax reversibly inhibits
while methylboronic acid has little to no effect on channel current. Phenylboronic acid
(PBA) initially inhibits current and then slowly potentiates. Benzoic acid reversibly
reduces Q1/E1 channel current whereas benzyl alcohol reversibly activates the channel
complex. (B) Families of currents recorded before and during treatment with PBA or
benzyl alcohol. Currents were elicited by 4 s step test potentials from −80 to +60 mV in
10 mV increments from a holding potential of −80 mV followed by a tail pulse to −30
mV. Dashed line indicates zero current. Scale bars represent 1 µA and 0.5 s. (C)
Voltage-activation curves for Q1/E1 calculated from tail current analysis. Solid curves
represent Boltzmann fits to the data. Data are presented as the mean ± SEM (n = 10).

Table III-1. Electrophysiological Properties of KCNQ Channels in the presence of PBA or Benzyl Alcohol

	Control		Phenylboronic Acid (PBA)				Benzyl Alcohol	
	$V_{1/2}$ (mV)	z	$\Delta V_{1/2}$ (mV)	Δz	Δg_{max}	EC_{50} (mM)	$\Delta V_{1/2}$ (mV)	Δz
Q1	-31.8 ± 1.6	2.39 ± 0.06	-13.8 ± 1.6*	0.51 ± 0.11	1.5 ± 0.1	0.10 ± 0.02	-4.6 ± 5.5	0.51 ± 0.18
Q1/E1	23.4 ± 1.2	1.70 ± 0.04	-12.6 ± 2.7*	-0.23 ± 0.07	3.0 ± 0.1	1.6 ± 0.5	-4.4 ± 2.4	-0.23 ± 0.07
Q1/E3	26.6 ± 3.0	0.47 ± 0.02	3.3 ± 5.4	0.33 ± 0.04	3.9 ± 0.2	6.1 ± 5.7	2.7 ± 4.9	0.35 ± 0.06
Q2/Q3	-44.6 ± 1.4	3.08 ± 0.11	-9.8 ± 2.3*	-0.32 ± 0.34	3.0 ± 0.3	3.7 ± 1.4	-5.9 ± 2.9	0.31 ± 0.17
Q4	-15.6 ± 1.1	2.45 ± 0.06	-13.7 ± 1.3*	-0.44 ± 0.11	> 10	> 10	-0.8 ± 2.9	-0.53 ± 0.08

Data from individual activation curves obtained from 4–10 oocytes. Activation curves were fit to a Boltzmann function. $V_{1/2}$ is the voltage of half-maximal activation and z is the slope factor. $\Delta V1/2$ and Δz are the changes induced by addition of 10 mM compound. $\Delta gmax$ values were determined during the washout of inhibition, as described in the Materials and Methods. EC50 values were determined during the washout of inhibition for PBA concentrations ranging from 1–10 mM. All values are mean ± SEM except for EC50 values, which are reported as the error of the fit to a hyperbola. *Indicates significant (Student t-test; $p < 0.05$) when compared to benzyl alcohol.

 Upon washout of PBA, inhibition was quickly relieved resulting in a rapid rise in current (Figure III-1A) and the maximum current was measured and defined as Δg_{max} (Table III-1). Making this measurement with different concentrations of PBA afforded an EC_{50} of 1.6 mM for Q1/E1 complexes.

To examine the importance of the boronic acid moiety, we tested the structurally similar compounds: benzoic acid and benzyl alcohol. Perfusion of benzoic acid reversibly inhibited Q1/E1 whereas benzyl alcohol reversibly activated the complex, but to a lesser extent than PBA (Figure III-1). Benzyl alcohol also had a significantly smaller effect on the $V_{1/2}$ of the complex compared to PBA (Figure III-1C and Table III-1). Therefore, we subsequently compared PBA and benzyl alcohol to determine whether the geminal diol of the boronic acid would activate other K^+ channels and Q1-KCNE complexes.

Q1 channels co-expressed with KCNE3 (E3) were also activated by PBA (Figure III-2A). In contrast to Q1/E1, Q1/E3 currents were primarily activated by PBA though a small amount of recovery from inhibition was observed as a rapid increase in current when the reagent was washed out. Since Q1/E3 complexes are open at negative potentials, we used a high external potassium solution (50 mM) to visualize both the outward and inward currents generated from a family of test potentials (Figure III-2B). Although these conditions enabled us to measure the inward currents, Q1/E3-expressing oocytes became unstable during the long time course needed to observe complete activation by PBA (1000 s).
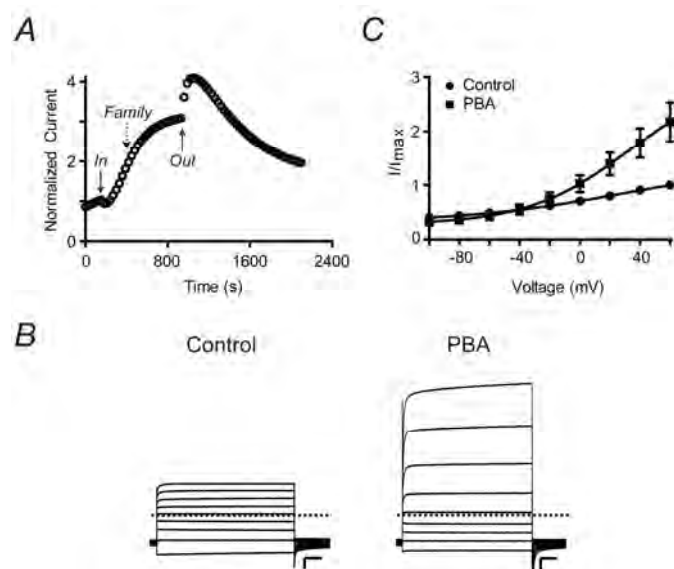
Figure III-2. PBA activates Q1/E3 complexes.
(A) Time course of Q1/E3 current measured in ND96 at +40 mV at the end of a 2 s pulse. The current was normalized before PBA application. PBA initially inhibits then slowly potentiates channel current. (B) Families of currents recorded in high external potassium (50 mM) before and during treatment with PBA. Currents were elicited by 2 s test potentials from −100 to +60 mV in 20 mV increments. The holding and tail potentials were −80 mV. Dashed line indicates zero current. Scale bars represent 1 µA and 0.5 s. (C) Voltage-activation curves for Q1/E3 calculated from tail current analysis. Solid curves represent Boltzmann fits to the data. Data are presented as the mean ± SEM (n = 10).

Therefore, we measured the current-voltage relationships after 500 s of PBA application (dashed arrow in Figure III-2A). Tail current analysis revealed that PBA activation of Q1/E3 complexes occurred only at potentials greater than – 40 mV (Figure III-2C). Accordingly, PBA did not shift the $V_{1/2}$ of the complex, but apparently increased the voltage dependence of the Q1/E3 complex (Table III-1). This effect was not specific for the boronic acid moiety because benzyl alcohol activated Q1/E3 similarly.

Since Q1-KCNE complexes were activated by PBA, we next asked whether activation was KCNE-specific by examining other members of the KCNQ family. Specifically, we examined the physiologically relevant heterotetrameric Q2/Q3 channels and homotetrameric Q4 channels. For homomeric Q1 channels, activation by PBA was offset by inhibition, resulting in a negligible increase in current. However, PBA significantly left-shifted the $V_{1/2}$ of the channel and this activation was observed during washout (Figure III-3, Q1 panel). The overall effect of PBA on Q2/Q3 heterotetrameric channels was activation (Figure III-3, Q2/Q3 panel). Benzyl alcohol also activated Q2/Q3 channels, however, to significantly lesser extent (Table III-1). Strikingly, Q4 channels were *only activated* by PBA (Figure III-3, Q4 panel). A ~ 10-fold increase in current was observed at 40 mV and the $V_{1/2}$ of the complex was significantly left-shifted (Table III-1). Moreover, activation is specific for the boronic acid moiety since benzyl alcohol did not shift the $V_{1/2}$ (Table III-1).
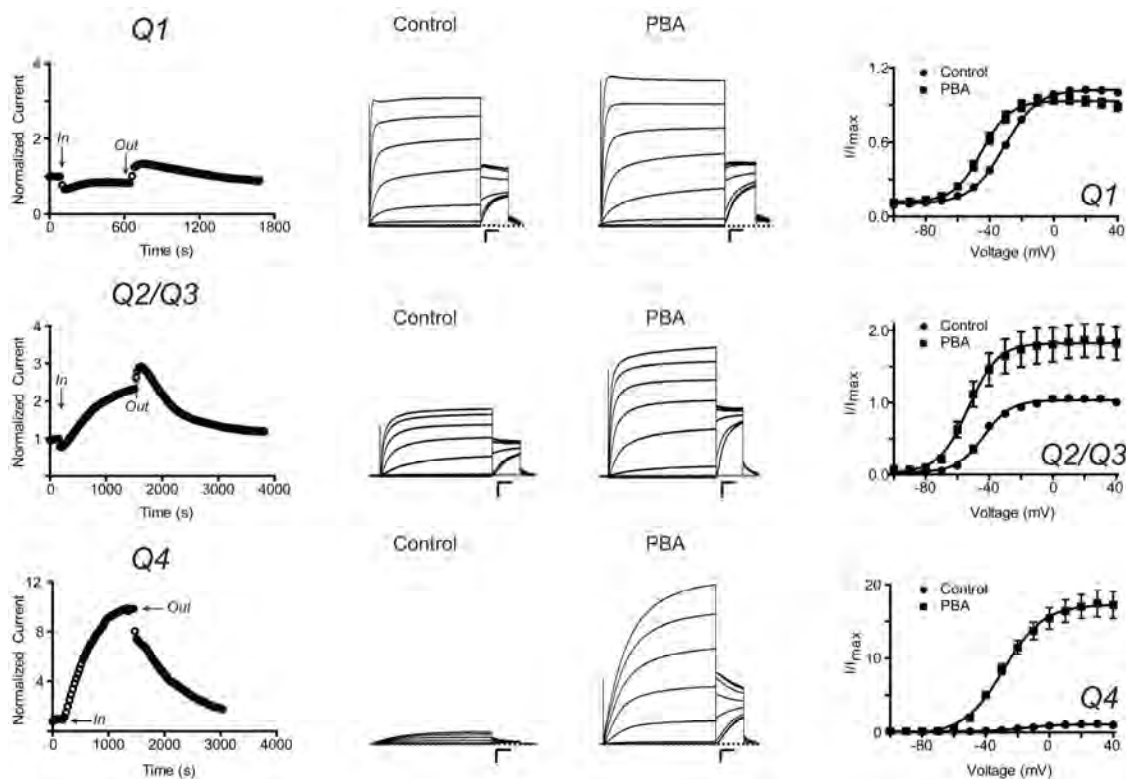
Figure III-3. PBA activates all tested members of the KCNQ family.
Left panel: Time courses of current recorded in ND96 at +40 mV at the end of a 2 s
pulse. The current was normalized before PBA application. PBA initially inhibits and
then slowly potentiates Q1 and Q2/Q3 current. PBA only activates Q4 channels. *Middle
panel:* Families of currents recorded before and during treatment with PBA. Currents
were elicited by 4 s test potentials from −100 to +60 mV in 10 mV increments from a
holding potential of −80 mV followed by a tail pulse to −30 mV. Dashed line indicates
zero current. Scale bars represent 1 µA and 0.5 s. *Right panel:* Voltage-activation
curves calculated from tail current analysis. Solid curves represent Boltzmann fits to the
data. Data are presented as the mean ± SEM (n = 4−6).
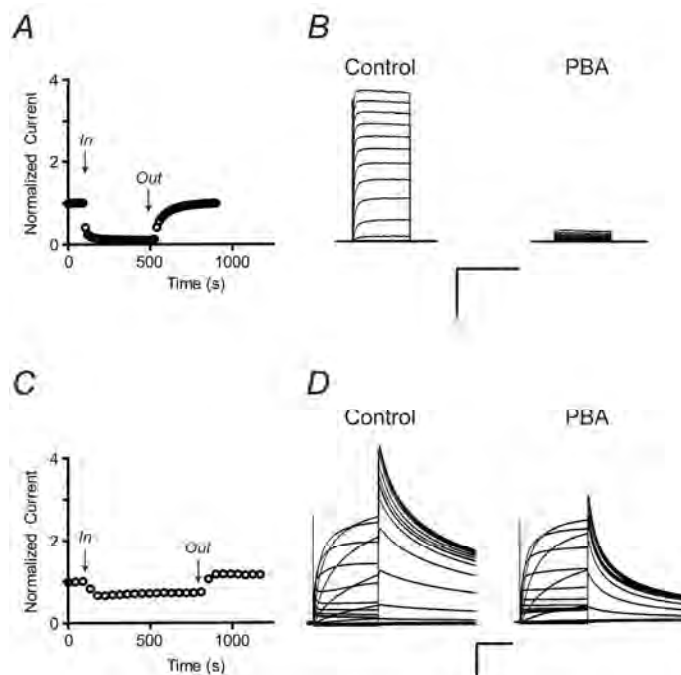
Figure III-4. PBA inhibits other Kv channels.
(*A*) Time course of Shaker (inactivation removed) current measured in ND96 at +40 mV, 100 ms pulse when 10 mM PBA was applied through the bath solution. *(B)* Families of Shaker currents recorded before and during treatment with PBA. Currents were elicited by 100 ms step test potentials from −100 to +60 mV in 10 mV increments from a holding potential of −80 mV. Dashed line indicates zero current. Scale bars represent 1 µA and 0.1 s. (*C*) Time course of hERG current measured in ND96 at 0 mV, 2 s pulse when 10 mM PBA was applied through the bath solution. (*D*) Families of hERG currents recorded before and during treatment with PBA. Currents were elicited by 2 s step test potentials from −100 to +60 mV in 10 mV increments from a holding potential of −80 mV. Dashed line indicates zero current. Scale bars represent 1 µA and 0.5 s.

To determine whether PBA activation was specific for KCNQ family members, we examined two different voltage-gated K^+ channels: *Shaker* and hERG. Both the inactivation removed variant of *Shaker* (*Shaker*-IR) and hERG were only reversibly inhibited by 10 mM PBA (Figure III-4). Therefore, activation by PBA appears to be somewhat specific for KCNQ1-KCNE channel complexes and KCNQ channels.

Because Q1 channels rapidly flicker between open and closed, single channel events cannot be directly observed; therefore, we indirectly determined whether PBA alters the permeation pathway of Q1 channels during the potentiation phase. We examined PBA potentiation in the presence of external cations with diameters larger than K^+ since the Q1 channel pore readily conducts both rubidium (Rb^+) and cesium (Cs^+) [171,172]. Oocytes expressing Q1 channels were initially bathed in 50 mM external K^+, Rb^+, or Cs^+. PBA (10 mM) was added and after the onset of inhibition, the cell was depolarized to 40 mV and returned to – 80 mV to elicit outward and inward currents, respectively (Figure III-5, black traces). The outward and inward currents were normalized and defined the current level at time = 0. During the potentiation phase, outward and inward currents were measured every 30 s until equilibrium was reached (Figure III-5, right graphs); the final trace is shown in gray in the left panel of Figure III-5. For K^+, PBA caused a greater increase in outward than inward current (Figure III-5A) while in Rb^+, both outward and inward current increased equally (Figure III-5B). In contrast, PBA caused a greater increase in inward than outward currents when measured in Cs^+ (Figure III-5C).
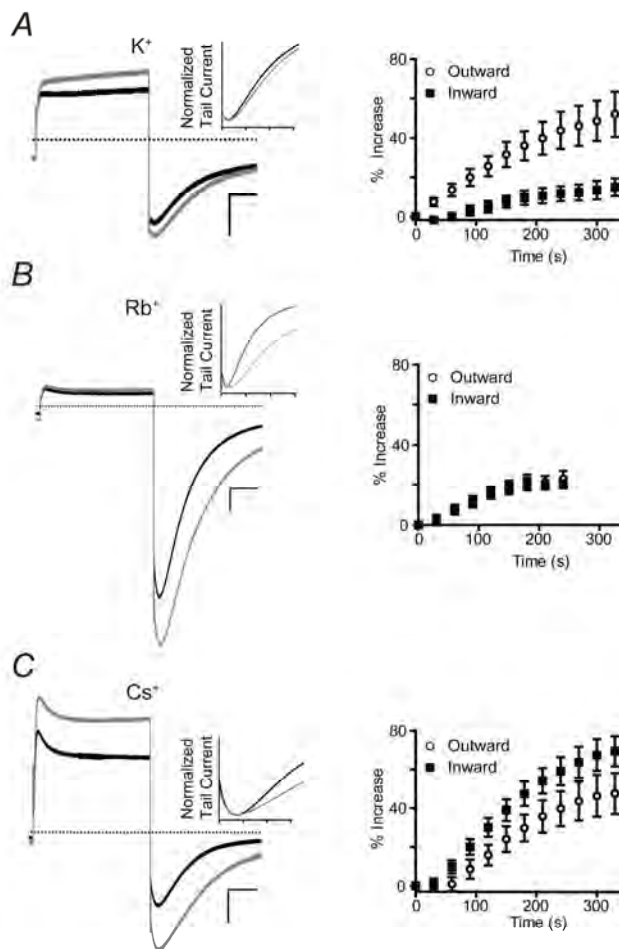
Figure III-5. Activation of Q1 by PBA is dependent on the external charge carrier ion.
Current traces were recorded in (A) 50 mM K$^+$, (B) Rb$^+$, or (C) Cs$^+$. *Left panel:* Representative overlaid traces elicited by a +40 mV test and –80 mV tail pulse before and after the onset of PBA potentiation. *Inset:* Normalized tail currents comparing the deactivation kinetics before and after the onset of PBA potentiation. Tick marks represent 200 ms. *Right panel:* Time course of current recorded during the PBA potentiation phase. Outward current measured at the end of a 2 s pulse to +40 mV; maximal inward current measured during the –80 mV tail pulse. Time zero is the amount of current after initial inhibition but before potentiation by PBA. Data are represented as the mean ± SEM (n = 5–10).

The deactivation kinetics during the potentiation phase (Figure III-5, insets) with the different charge carriers were also measured. PBA slows Q1 channel closing when the larger Rb^+ or Cs^+ ions are charge carriers whereas PBA has no significant effect on closing kinetics with external K^+ (Table III-2). Since permeation and voltage-dependent gating are intrinsically coupled in Q1 channels [172], we also measured the PBA-induced changes in voltage sensitivity with the different charge carriers (Table III-3). PBA caused a –14 mV shift in the $V_{1/2}$ of Q1 channels in both ND96 (2 mM K^+_{ext}) and 50 mM K^+_{ext} (Table III-1 and III-3). However, in the presence of the larger Rb^+ and Cs^+ ions, PBA left-shifted the $V_{1/2}$ an additional 6 mV. In total, these results show that activation of Q1 by PBA is dependent on the external charge carrier.

Table III-2. Deactivation rates of Q1 with different charge carriers

	Deactivation τ (ms)		
	K^+	Rb^+	Cs^+
Before PBA	360 ± 30	480 ± 30	300 ± 20
PBA (inhibition)	510 ± 30	710 ± 90	430 ± 30
PBA (activation)	630 ± 60	1240 ± 200*	650 ± 60*

Rates of deactivation were measured by fitting the tail currents to a single exponential after recovery from inactivation. Data is represented as the mean ± SEM (n = 5–10). *Indicates significant (Student t-test; $p < 0.05$) when compared to inhibition by PBA.

Table III-3. Electrophysiological properties of Q1 with different charge carriers.

	Control		PBA	
	$V_{1/2}$ (mV)	z	$\Delta V_{1/2}$ (mV)	Δz
K^+	-26.8 ± 2.4	1.6 ± 0.1	-14.3 ± 3.1	0.02 ± 0.30
Rb^+	-26.5 ± 1.2	1.7 ± 0.1	-21.6 ± 1.7*	0.6 ± 0.20*
Cs^+	-30.8 ± 1.4	2.2 ± 0.1	-19.3 ± 1.7*	0.4 ± 0.20*

Data from individual activation curves obtained from 5–10 oocytes. Activation curves were fit to a Boltzmann function. $V_{1/2}$ is the voltage of half-maximal activation and z is the slope factor. $\Delta V_{1/2}$ and Δz are the changes induced by addition of 10 mM PBA. All values are mean ± SEM. *Indicates significant (Student t-test; $p < 0.05$) when compared to K^+.

Discussion

Motivated by the fortuitous discovery that borax modulates Q1/E1 complexes, we determined whether the boronic acid moiety was uniquely responsible for modulation of KCNQ channels and KCNQ1-KCNE complexes. By examining structurally different boronic acids, we found that the aromatic derivative, PBA, activates Q1/E1 complexes at millimolar concentrations. PBA activation of Q1/E1 is specific for the boronic acid functional group because other similar aromatic derivatives (benzyl alcohol and benzoic acid) are significantly less effective or inhibitory. In contrast, both PBA and benzyl alcohol similarly activate the Q1/E3 complexes. Activation of the constitutively conducting Q1/E3 complex by PBA is only observed at voltages greater than –40 mV, which ostensibly increases the voltage-dependence of the complex. Homomeric Q1 channels are also modulated by PBA. At positive potentials, PBA inhibits and activates Q1 channels equally, resulting in no net change in current magnitude. Although PBA does not significantly increase the total current, the voltage sensitivity of Q1 channels is shifted with PBA such that they are open at more negative potentials. These results suggest that the presence of the KCNE peptides is not required for PBA to modulate the ion conducting subunit; however, an overall increase in current magnitude is only observed when Q1 channels co-assemble with KCNE peptides. Thus, PBA is a more effective activator of Q1-KCNE complexes.

In addition to Q1 channels, PBA activates the other members of the KCNQ family. Activation appears to be somewhat specific for KCNQ channels, as Shaker and hERG are not activated by PBA. Comparing activation curve data for the KCNQ family

indicated that PBA activates these channels by shifting the midpoint of activation ($V_{1/2}$). The maximal increase of current (Δg_{max}) for KCNQ channels at 40 mV is: Q4 >> Q1/E1 ≈ Q2/Q3 > Q1. This activation trend inversely correlates with the reported open probabilities for KCNQ channels [74,173-175], suggesting a rationale for the varied effectiveness of PBA. Testing this hypothesis, however, is hampered by the flickery nature of Q1/E1 complexes, which precludes the accurate measurement of the open probability of these complexes by either single channel recordings or noise analysis [176,177].

Without the ability to perform traditional single channel analysis, we turned to Rb^+ and Cs^+ as charge carriers to indirectly examine the effect of PBA on the Q1 permeation pathway. We found that the inward and outward Q1 currents were differentially potentiated by PBA. PBA increased Q1 outward currents (compared to inward) when K^+ was in the external bath and inward currents when Cs^+ was present. The asymmetry of PBA activation of Q1 currents cannot be explained by increasing the number of channels and thus points to modulation of the ion conducting subunits. Consistent with this premise was the charge carrier dependence of PBA potentiation: the larger the diameter of the permeant ion, the more PBA increased the inward current (Figure III-5). This result suggests that PBA alters the Q1 selectivity filter such that larger ions are more permeant. The larger Rb^+ and Cs^+ ions also enhanced PBA's effect on the $V_{1/2}$ and deactivation kinetics of Q1 channels compared to K^+. Although the sum of these results do not conclusively rule out an indirect modulatory mechanism, the data in total strongly favor PBA directly interacting with the KCNQ pore forming subunit.

One commonality of PBA modulation of KCNQ channels is the slow onset of potentiation (minutes). If PBA is directly binding to the channel, the slowed kinetics could be explained by a cytoplasmic or buried binding site. PBA binding may in fact be covalent, because boronic acids are known to form covalent, yet reversible bonds with diols [178,179]. A covalent interaction is consistent with the previous observations that chemical modifications activate KCNQ channels [161,162,175,180]. In addition, a slowly reversible covalent interaction may also explain the lack of complete washout with some KCNQ channels (Figures III-1A, 2A and 3). Nonetheless, PBA may still be acting indirectly, activating signaling pathways in the cell. However, these indirect pathways must be specific for KCNQ channels since PBA activation was not observed for Shaker and hERG channels.

While PBA activates KCNQ channels, it does inhibit Kv channels weakly at 10 mM. Rapid inhibition was initially observed for all Kv channels, except Q4. The trend for inhibition is: Shaker > Q1 ≈ hERG ≈ Q1/E1 > Q2/Q3 ≈ Q1/E3. hERG inhibition is a concern for small molecule drug design; however, PBA inhibition of hERG does not appear to occur by classic inner vestibule block [181,182]. First, PBA is not a positively charged molecule, which is typical for hERG blockers that bind to the hydrophobic residues in the S6 helix [183]. Second, inhibition is not specific for hERG, as the other Kv channels are similarly inhibited at this high concentration of PBA. Given that PBA inhibition is already weaker than activation for KCNQ channels, it should be possible to design second generation boronic acid activators that do not inhibit hERG and other Kv channels.

Unlike recently described activators of KCNQ channels, which are rendered less effective when co-assembled with KCNE peptides, PBA activates Q1-KCNE complexes more effectively than homotetrameric Q1 channels [96,97]. Both of these previous studies suggest that co-assembly with KCNE peptides prevents R-L3 and zinc pyrithione from binding to the Q1 channel subunit [94,96,97]. Since PBA activates Q1-KCNE complexes, future structure-function studies with PBA and other boronic acids should provide insight into its binding site and yield new tools to investigate the molecular mechanisms of Q1-KCNE gating. Although the potency of this unoptimized, simple molecule is modest, the non-toxicity of boronic acids (Borax), the catalogues full of boronic acids derivatives, and their synthetic utility makes PBA a potential pharmacophore for building potent activators of Q1/E1 complexes. Moreover, since boronic acid-bearing compounds are used clinically [184], their inclusion into small molecule libraries could generate an array of potential KCNQ activators.

CHAPTER IV: *XENOPUS LAEVIS* OOCYTES INFECTED WITH MULTI-DRUG RESISTANT BACTERIA: IMPLICATIONS FOR ELECTRICAL RECORDINGS

Abstract

The *Xenopus laevis* oocyte has been the workhorse for the investigation of ion transport proteins. These large cells have spawned a multitude of novel techniques that are unfathomable in mammalian cells, yet the fickleness of the oocyte has driven many researchers to utilize other membrane protein expression systems. Here we show that some colonies of *Xenopus laevis* are infected with three multi-drug resistant bacteria: *Pseudomonas fluorescens, Pseudomonas putida,* and *Stenotrophomonas maltophilia.* Oocytes extracted from infected frogs quickly (3 – 4 days) develop multiple black foci on the animal pole, similar to microinjection scars, which render the extracted eggs useless for electrical recordings. Although multi-drug resistant, the bacteria were susceptible to amakacin and ciprofloxacin in growth assays. Supplementing the oocyte storage media with these two antibiotics prevented the appearance of the black foci and afforded oocytes suitable for whole cell recordings. Given that *Pseudomonas fluorescens* associated with *Xenopus laevis* has become rapidly drug resistant, it is imperative that researchers store the extracted oocytes in the antibiotic cocktail and not treat the animals harboring the multi-drug resistant bacteria.

Introduction

Intact oocytes extracted from *Xenopus laevis* are a versatile expression system for the structural and functional investigation of ion channels and transporters. Ion transport proteins expressed in oocytes can be readily studied in the whole cell configuration (two-electrode voltage clamp; TEVC) or in excised patches of membrane: exposing the extracellular side (outside-out) or the intracellular side (inside-out) of the protein (and membrane) to the bath solution in patch clamp recordings [118]. Additionally, cramming inside-out patches back into the egg re-exposes ion transport proteins to intracellular components, allowing for the exploration of ion channel regulation [118]. Cutting open the oocyte simultaneously provides access to the intercellular milieu and reduces the time to charge the membrane, permitting the measurement of fast ionic and gating charge currents [185,186]. The oocyte's physical properties also afford several experimental advantages. Injection of biopolymers into the oocyte cytoplasm is facile, which enables the precise control of protein subunit expression [117], incorporation of unnatural amino acids [114], and examination of ion transport proteins expressed in bacteria [187] and isolated from native cells [116]. The large size of the oocyte also makes single cell biochemistry possible, enabling the direct comparison of cell surface expression and electrical recordings [119-121]. Even the pigmented animal pole is advantageous— blocking light from exciting the intracellular components, which facilitates imaging of plasma membrane proteins with epi-fluorescence[188].

Like any membrane protein expression system, oocytes have a dark side. The vitelline envelope must be removed for many experiments [118] and the endogenous

currents cause some consternation, limiting the ionic composition of the external solution, the range of usable voltages, and the investigation of a few ion transport proteins [189]. In addition, several extrinsic factors can affect egg quality, rendering them unusable for electrophysiological recordings. Frog husbandry conditions such as water quality, population density, and nutrition have been reported to affect oocyte quality [123-125]. Furthermore, many researchers report experiencing unexplained seasonal variations in oocyte quality even in laboratory environments where light and temperature are strictly controlled [122,125,126]. Once extracted, oocytes are susceptible to microbial contaminations, one of which induces marbling of the oocyte pigment and rapid death [190].

Despite good laboratory practices of both our animals and surgically harvested eggs, we recently observed a decline in oocyte quality. A few days post extraction, late stage oocytes (V and VI) formed black foci on the animal pole similar to the pigmented ring scar formed during wound healing [191-193]. The afflicted oocytes had negligible electric resting potentials and poor viability. Unsurprisingly, attempts to record from an injected batch of compromised oocytes were futile. Since frog skin harbors bacteria detrimental for oocyte longevity, we initially made hygienic changes in our animal husbandry and egg handling: none of which were effective and the oocytes remained unsuitable for electrophysiology experiments. Similarly, systematic tinkering with the standard antibiotics—penicillin, streptomycin, gentamicin and tetracycline—in the storage media did not prevent black foci formation. To identify the cause of the black foci, we cultured the compromised oocytes and discovered that they were infected with

multi-drug resistant *Stenotrophomonas maltophilia, Pseudomonas fluorescens* and *Pseudomonas putida*.   Antibiotic testing showed that all three species of bacteria were susceptible to amikacin and ciproflaxin, which when included in the oocyte storage media prevented the appearance of black foci and resulted in oocytes that were usable for electrophysiological recordings.

Materials and Methods

Husbandry

Xenopus laevis were ordered from commercial vendors (Nasco, Fort Atkinson, WI; Xenopus 1, Dexter, MI; Xenopus Express, Brooksville, FL).   Female frogs used for our studies are ordered as adults, with a snout to vent length of 9 cm or greater. The primary Animal Medicine Facility at UMMS only houses frogs from a single vendor, which was our original and current vendor. Upon arrival, frogs are maintained in static tanks for clinical observational and acclimation period lasting a minimum of 5 d.   The maximum housing density of frogs in each static tank is 1 frog per 2 L of artificial pond water. The water in the static frog housing tanks is changed at least twice weekly. The room is maintained at approximately 20˚C, with a humidity of 30% to 70%, and room lights on a 12:12-hr light:dark cycle. Frogs are each fed 5 to 10 pellets of Frog Brittle (Nasco, Ft Atkinson, WI) twice weekly. At the end of the clinical observational period, healthy frogs are released to the standard colony housing area. Colony frogs are housed in either a continuous flow-through system (PharmHouse XLS Rack System, Pharmacal, Naugatuck, CT) or a recirculating frog housing system (X-Mod, Marine Biotech, Beverly, MA). Room environmental conditions and feeding schedules remain the same. The water supplied to the frog housing area is first passed through a 5 micron particulate filter and reverse osmosis system (HP 1200, CUNO/Water Factory Systems, Meriden, CT) prior to entering an intermediate holding tank. Water in the holding tank is treated with a commercial artificial lake salt additive (Cichlid Lake Salt, Seachem Laboratories Inc., Madison, GA) at a concentration of 5.5 g per 37.85 L of water. While in the holding

tank, the water is continually circulated through a 15 watt ultraviolet light system until it

is released. Water conditions in both colony systems are targeted at the following levels:

Water temperature 17 – 19˚C, pH 6.6 – 7.0, conductivity 1550 – 1650 μS, ammonia 0 –

0.8 PPM, nitrites 0 – 0.75 PPM, nitrates 0 – 20 PPM. For the blind study, the animals

from the three vendors were housed in an ancillary facility in static tanks under the same

environmental and aquatic conditions listed above.

Oocyte Extraction

Late stage oocytes (stage V – VI) are removed from the ovaries of adult female frogs in

accordance with the procedures described in our UMMS IACUC-approved protocol.

Specifically, the female is anesthetized by gradually cooling the frog in an ice water bath

at 4˚C over 30 – 45 min. Once anesthetized, the skin on the frog's abdomen is sterilized

by swabbing the surgical site with a 10% povidone iodine solution. Autoclaved

instruments are used for the extraction of ovarian tissue, and harvested oocytes are

defolliculated for 30 – 60 min with 2 mg/mL Type 2 collagenase (290 U/mg dw)

(Worthington Biochemical Corp) in sterile OR2 solution containing (in mM): 82.5 NaCl,

2.5 KCl, 1 $MgCl_2$, 5 HEPES, pH 7.4. The same lot number of Type 2 collagenase was

used for the entire study, which also contained (in U/mg dw): 600 caseinase, 4.6

clostripain, 0.51 tryptic activity based on the manufacturer's certificate of analysis.

Oocyte Storage Conditions

Post collagenase, isolated oocytes are rinsed with OR2 and stored in ND96-GT storage

solution containing (in mM): 96 NaCl, 2 KCl, 1.8 $CaCl_2$, 1 $MgCl_2$, 5 HEPES, 50 μg/mL

of both gentamicin and tetracycline (Sigma) pH 7.4, at 16°C. Oocytes are checked daily

for death and rinsed with ND96 solution with freshly supplemented antibiotics. The

ND96-ACT storage solution is supplemented with 50 µg/mL of tetracycline and 100

µg/mL of both amikacin and ciproflaxicin (Sigma). All solutions containing antibiotics

should be disposed in accordance with state regulations. For the Massachusetts

Department of Environmental Protection, the solution is mixed with a chemical absorbent

powder, autoclaved and then incinerated.

Imaging

Intact oocytes images were captured using SPOT imaging software (Diagnostic Imaging

Inc, Sterling Heights, MI) using a dissecting scope equipped with a color digital camera.

Images were processed in Adobe Photoshop and adjustments were limited to levels and

cropping. For electron microscopy images of oocytes, the samples were fixed by

immersion in 2.5% (v/v) gluteraldehyde in Na Cacodylate buffer (pH=7.2) for a

minimum of 2 hours at room temperature. The fixed oocytes were then washed three

times in the same buffer. Following the third wash, the eggs were dehydrated through a

graded series of ethanol to 100%, then Critical Point Dried in liquid CO_2. The eggs were

then affixed with silver conductive paste to the surface of aluminum SEM stubs and

sputter coated with Au/Pd (80/20). Examination of the specimens was performed using

an FEI Quanta 200 FEG MK II scanning electron microscope at 10 Kv accelerating

voltage. For imaging of individual bacteria cultured from infected oocytes, the bacteria

were stained with 1% Uranyl Acetate and spread onto a carbon stabilized formvar

support film. Images were captured with a Philips CM 10 TEM at 7900X using an 80KV

accelerating voltage.

Bacterial and Fungal Cultures

All cultures were submitted to a commercial diagnostic laboratory (IDEXX Preclinical

Research Services, Grafton, MA). Bacterial culture samples were streaked onto 10%

sheep blood agar with Columbia Blood Agar Base or MacConkey agar and were

incubated at 21°C and 37°C for a minimum of 4 – 6 d. Samples submitted for fungal

culture were streaked on Inhibitory Mold agar and incubated for 21 d.

Histopathology

Oocyte samples were fixed in 10% buffered formalin before preparation with

hematoxylin and eosin stain for histopathological evaluation. The histopathology slides

were submitted to and read by a board certified, contracted veterinary pathologist (Histo-

Scientific Research Laboratories, Mt. Jackson, VA).

Results

As is with many laboratories that use extracted *Xenopus* oocytes, our frog husbandry, surgical procedures, and oocyte handling were an amalgam of established procedures, documented prophylactic measures, and old wives tales (Materials and Methods for complete details). Our *Xenopus laevis* were housed in circulating tanks, fed diligently by animal medicine staff, and bathed in a perfect circadian 12 hr of light per day. We extracted the oocytes using sterilized instruments following our IACUC-approved surgical procedure that enables survival surgeries to minimize animal usage. The extracted oocytes were defoliculated with collagenase and stored in standard ND96 buffer supplemented with gentamicin in a 16°C incubator. Many years ago, we observed the "marbled egg" phenotype described by Iglauer and co-workers [190]; therefore, we included a sterile skin preparation with 10% povidone-iodine solution to our surgical procedure and added tetracycline to the oocyte storage media. With this combination of animal husbandry, surgical procedures and antibiotic cocktail, nine out of ten surgeries afforded experiment-quality oocytes that would last nearly a week with very little effort (daily media change).

About three years ago, we frequently observed that an entire batch of extracted eggs would develop multiple black foci surrounded by an unpigmented halo on the animal pole (Figure IV-1A). The black foci were reminiscent of the pigmented scar ring formed after microinjection [192,193], but would appear on both uninjected and injected eggs three to four days after extraction.

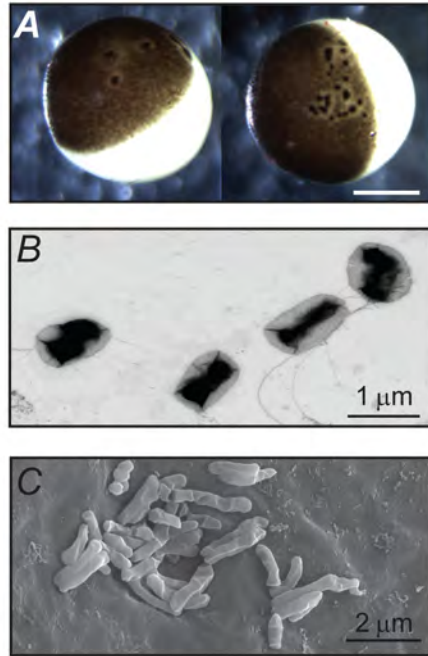**Figure IV-1. *Xenopus laevis* oocytes infected with multiple drug resistant bacteria.** (A) Bright field micrograph of extracted oocytes showing the characteristic black foci and unpigmented halo. White scale bar is 0.5 mm. (B) Transmission electron micrograph of *Pseudomonas fluorescens* cultured from compromised oocytes. (C) Scanning electron micrograph of bacteria on the surface of compromised oocytes.

In addition to morphological changes, these eggs had weak membranes that easily ruptured with typical handling. More distressingly, voltage-clamped, compromised oocytes rapidly developed a large non-specific leak current (> 0.1 μA) within two minutes of establishing a holding potential ($- 80$ mV) (Figure IV-2), which continued to increase until the oocytes became unclampable.

Because oocyte quality can diminish with husbandry conditions [124,125], we initially switched our frogs to static tanks and changed the salt solution of the artificial pond water; however, these husbandry changes did not prevent the formation of the black foci. To rule out contamination from our animal colony and facility, we ordered new frogs from the same vendor that were housed in a different vivarium and a batch of surgically harvested oocytes that were directly shipped overnight to the laboratory. Disappointingly, the eggs from the new animals and the mail-ordered oocytes developed black foci and diminished viability $3 - 4$ days after incubation in ND96 storage solution supplemented with gentamicin and tetracycline (ND96-GT). Because the addition of tetracycline to the storage media and increasing sterile technique previously prevented *Pseudomonas fluorescens* from killing the oocytes [190], we operated using a surgical drape and tried different combinations of antibiotics, including the more traditional penicillin:streptomycin (100 U/mL) antibiotic combination. However, none of these changes were able to thwart the formation of the black spots.
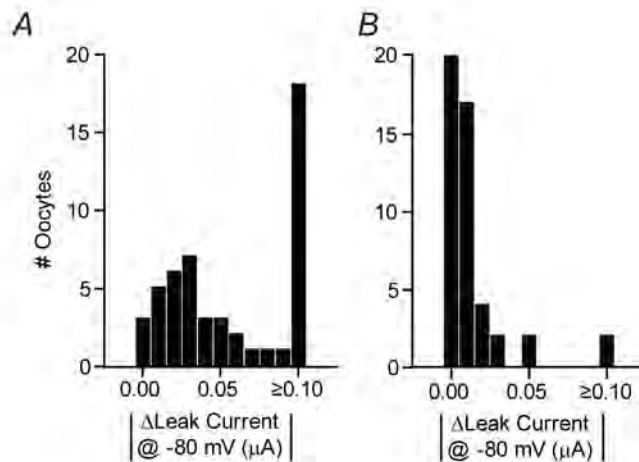
Figure IV-2. Infected oocytes exhibit reduced viability which can be prevented with amikacin:ciproflaxin supplementation. Histographs of the absolute change in leak current of oocytes incubated for 4 days in gentamicin:tetracycline (ND96-GT) or amikacin:ciproflaxin (ND96-ACT) supplemented media. Change in leak current at – 80 mV was calculated by subtracting the initial current value upon clamping from the value at 2 min. Data are from 2 – 5 batches of oocytes.

To determine whether the compromised oocytes were infected, we performed fungal and bacterial cultures on oocytes with black foci. Four batches of oocytes were tested for fungal contamination and all were negative. In contrast, ten different batches of oocytes were infected with bacteria: five were infected with either *Pseudomonas putida* or *Pseudomonas fluorescens* (Figure IV-1B); five were infected with *Stenotrophomonas maltophilia*. Antibiotic susceptibility data showed that all three bacteria were resistant to gentamicin and tetracycline, as well as many other commonly used antibiotics (Table IV-1). Scanning electron microscopy of the oocyte revealed that the bacteria were clustered on the cell surface (Figure IV-1C).

Based on our bacterial culture and sensitivity findings, we modified the antibiotic supplementation in the storage solution from gentamicin and tetracycline, to amikacin and ciprofloxacin. At low levels of these antibiotics, 50 µg/mL, the black foci still formed on the animal pole of the oocytes; therefore, we increased the concentration to 100 µg/mL of amikacin and ciprofloxacin (ND96-ACT), which prevented black foci on a batch of oocytes. To rule out dumb luck, we harvested five batches of oocytes from different animals and stored the eggs in either ND96-GT or ND96-ACT, which was changed daily. Cultures were then performed on the oocytes after four days of incubation in the different antibiotic cocktails. Four out of five batches of oocytes grew multi-drug resistant bacteria when stored in ND96-GT: three grew a *Pseudomonas* species and one grew *Stenotrophomonas maltophilia*. Oocytes in the four samples with bacterial growth all developed the characteristic black spots associated with decreased electric resting potential and viability (Figure IV-3A). In contrast, the oocyte cohorts incubated in

ND96-ACT did not grow any bacteria. Moreover, these oocytes did not exhibit any evidence of morphological or physiological abnormalities after four days in the storage solution (Figure IV-3B) and were useful for electrophysiological studies (Figure IV-2).

To closer examine the morphological changes induced by the multi-drug resistant bacteria, we histopathologically compared the infected and uninfected oocytes. Black foci on the surface of infected oocytes correlated to areas with an increased number of pigmentation granules (Figure IV-3C), surrounded by a region with diminished pigmentation granules (Figure IV-3E). On the other hand, oocytes stored in the ND96-ACT media had continuously smooth membranes with a uniform distribution of pigment granules (Figures IV-3D and IV-3F).

Lastly, we attempted to identify the source of the multi-drug resistant bacteria. Although we were able to repeatedly culture multi-drug resistant bacteria from oocytes incubated for four days in ND96-GT (Table IV-1), in general, most cultures sampled from oocytes directly harvested from the animals were negative for bacterial growth. However, one sample did grow a multi-drug resistant strain of *Pseudomonas putida.* The harvested oocytes from this frog that were not used for culture were collagenased and stored in ND96-GT where they developed multifocal to coalescing black foci on their surfaces. After four days of incubation, cultures from these oocytes demonstrated continued infection with multi-drug resistant *Pseudomonas putida*.

Table IV-I. Susceptibility of bacteria found in *Xenopus* Oocytes

Antibiotic	Bacterial Susceptibility (MIC in µg/ml)	
	Pseudomonas species	*Stenotrophomonas maltophilia*
Amikacin	S 4 (5/5)	S 4 (5/5)
Amoxicillin/Clavulanic	R ≥ 32 (5/5)	R ≥ 32 (5/5)
Amoxicillin	R ≥ 32 (5/5)	R ≥ 32 (5/5)
Cefazolin	R (5/5)	R (5/5)
Cefixime	R (5/5)	R (5/5)
Cefotaxime	R (5/5)	R (5/5)
Cefpodoxime	R (5/5)	R (5/5)
Ceftazidime	S ≤ 8 (3/5), R (1/5), I 16 (1/5)	S ≤ 8 (5/5)
Ceftiofur	R ≥ 8 (5/5)	R ≥ 8 (5/5)
Ceftriaxone	R (4/5), I (1/5)	R (4/5), I (1/5)
Cefuroxime	R (5/5)	R (5/5)
Cefalexin	R ≥ 32 (5/5)	R ≥ 32 (5/5)
Chloramphenicol	R ≥ 32 (5/5)	R ≥ 32 (5/5)
Ciprofloxacin	S ≤ 0.05 (5/5)	S ≤ 0.05 (5/5)
Difloxacin	R (5/5)	R (5/5)
Enrofloxacin	R ≥ 2 (2/5), I 1 (3/5)	R ≥ 2 (5/5)
Gentamicin	R ≥ 16 (5/5)	R ≥ 16 (5/5)
Imipenem	S (5/5)	S (5/5)
Marbofloxacin	R (2/5), I (3/5)	R (4/5), I (1/5)
Ofloxacin	R (3/5), I (2/5)	R (5/5)
Orbifloxacin	R (5/5)	R (5/5)
Piperacillin	I 64 (4/5), I 128 (1/5)	I 64 (5/5)
Tetracycline	R ≥ 16 (5/5)	R ≥ 16 (5/5)
Ticarcillin	R ≥ 256 (5/5)	R ≥ 256 (5/5)
Tobramycin	R ≥ 16 (5/5)	R ≥ 16 (5/5)

Bacterial culture results from ten samples of affected oocytes. Both *Pseudomonas fluorescens* and *Pseudomonas putida* (*Pseudomonas species*) had identical bacterial susceptibility. S = Susceptible, I = Intermediate, R = Resistant. Minimum inhibitory concentration (MIC) is represented in µg/ml. Results without MIC values were performed by disc testing. The number in parentheses represents the number of colonies with the indicated susceptibility / the total number of oocyte samples that grew that species of bacteria.
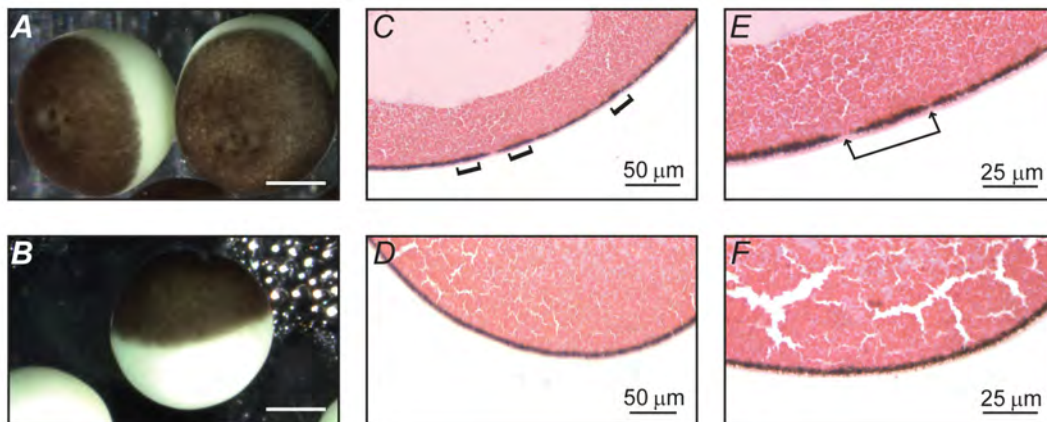
Figure IV-3. Amikacin:ciproflaxin supplementation prevents black foci formation.
Bright field micrographs of extracted oocytes incubated for 4 days in (A)
tetracycline:gentamicin-supplemented (ND96-GT) or (B) amikacin:ciproflaxin-
supplemented media (ND96-ACT). Scale bars are 0.5 mm. (B) Histopathology slices of
a (C) compromised oocyte and (D) a healthy oocyte stored, magnified in (E) and (F),
respectively. Brackets denote areas of increased pigmentation; arrowheads indicate areas
devoid of pigment molecules, both of which were only observed in infected oocytes.

Since only one animal's oocytes were sufficiently infected to test positive for multi-drug resistant bacteria immediately after surgery, we next tested for a contamination source in our laboratory and vivarium. Cultures from our collagenase and OR2 solutions grew no bacteria. Biofilm and water samples from our aquarium grew four ubiquitous bacteria: *Pseudomonas pseudoalcaligenes, Aeromonas hydrophilia, Corynebacterium sp.* and *Alcaligenes sp.*—all of which were not multi-drug resistant and sensitive to gentamicin and tetracycline. Four skin swabs from nine colony frogs also grew bacteria (*Acinobacter baumannii* and *Acinobacter baumannii*) that were similarly sensitive to most antibiotics, including tetracycline and gentamicin. Cultures from the skin of these nine frogs after a surgical preparation with povidone-iodine were all negative, as were the cultures of their coelomic cavities. Having tested all conceivable sources of contamination (and to have experimental quality oocytes during the "black dot" pandemic), we performed a blind study: our animal medicine facility ordered five frogs from three different vendors (our original vendor and two additional vendors), which were housed in separate static tanks in an ancillary animal facility. After performing 15 surgeries and storing the eggs in ND96-GT for four days, we only observed the black foci on oocytes extracted from animals (4 out of 5) ordered from one vendor, which was confirmed by animal medicine to be the original vendor. In total, these data suggest that the animal's ovarian tissue and/or oocytes are the likely source of the multi-drug resistant bacteria.

Discussion

We have shown that *Xenopus laevis* harbor multi-drug resistant bacteria that infect entire batches of surgically harvested oocytes stored in standard antibiotic-supplemented media. By including amikacin and ciprofloxacin in the storage media (ND96-ACT), we were able to prevent black foci formation to afford experimental quality oocytes. In all of our experiments with amikacin– and ciprofloxacin–supplemented media, tetracycline was also included in the storage solutions since we did not know at the time that *Pseudomonas fluorescens* had become resistant to tetracycline. Based on the antibiotic susceptibility of the bacteria that we cultured from oocytes (Table IV-1), amikacin and ciprofloxacin should be sufficient. Nonetheless, we have yet to eliminate tetracycline from our antibiotic cocktail. Given the strong correlation between antibiotic susceptibility and the appearance of the black foci, we believe these multi-drug resistant bacteria are responsible for the diminished resting potential and poor viability oocytes that we observed. Although we could switch to another vendor and use ND96-GT, which is cheaper than ND96-ACT ($9 versus $12 for a 1L solution), we consider the quality of extracted oocytes from our original vendor's animals to be far superior, provided they are not infected with multi-drug resistant bacteria.

The multiple black foci on the animal poles of infected oocytes are highly reminiscent of the pigment changes seen during the process of oocyte healing after puncture: an increased region of pigmentation surrounded by a halo of diminished pigmentation [191,192]. Amphibian oocytes heal by closure of an actomyosin-based purse string [193]. During this process, cytoplasmic pigment granules coalesce to form a

dense spot, referred to as a scar, which can be seen on the cell surface. This scar is most visible on the surface of the animal pole of the oocyte due to the large amount of pigmentation granules; however, similar processes of healing can be observed on the vegetal pole [192]. The striking similarity between wound healing scars and the black foci we observed in compromised oocytes suggests that the bacteria on the oocyte cell surface (Figure IV-1C) are puncturing the membrane to enter the egg. The continual repair of multiple membrane ruptures is consistent with the observed low electric resting potential and cytoplasm leakage from the oocytes.

It is concerning that tetracycline was previously effective against *Pseudomonas fluorescens* when identified as a contaminant of *Xenopus laevis* oocytes [190], but is now ineffective. Although it may be tempting to prophylactically treat the frogs or the frog housing system with amikacin and ciprofloxacin to prevent oocyte contamination, this is not an appropriate course of action. Overuse and inappropriate dosing of antibiotics are considered to be a major cause of the emergence of antibiotic-resistant bacteria [194]. For amphibian medicine, it is a major issue since there is remarkably sparse pharmacokinetic information on safe and effective antibiotic dosing of many species, including *Xenopus laevis* [195-197]. Coincidentally, tetracycline has been one of a few antibiotics that have accumulated a modest amount of dosing guidelines for this species. Whether tetracycline is utilized with any regularity at the vendor's facility for treatment of health conditions in the frogs is unknown. If so, the use of tetracycline with *Xenopus laevis* may have contributed to the development of tetracycline resistant *Pseudomonas fluorescens*. Alternatively, our observation of multi-drug resistant *Pseudomonas*

fluorescens may simply be a reflection of the same global shifts in antibiotic resistance observed in the human health industry, which is presumed to be due to years of antibiotic use. With so few antibiotic options left for treating the *Pseudomonas* and *Stenotrophomonas* species associated with oocyte pathology in *Xenopus laevis*, judicious use of antibiotics *in vitro*, rather than *in vivo*, is warranted.

CHAPTER V: DISCUSSION AND FUTURE DIRECTIONS

Studying the structure and function of Kv channels is difficult due to their membranous lipid environment, multiple regulatory partners, and dynamic nature. High resolution crystal structures provide structural details of Kv channels and their isolated cytoplasmic fragments; however, the relationship between these static images and their dynamic physiological function is still not fully understood. To better define the architecture and dynamics of Kv channels, laboratories have turned to using combinatorial approaches to study Kv channels. The tethered blocker approach has been instrumental in gathering structural information while simultaneously probing channel function. CHAPTER II describes a modified tethered blocker approach that allows for the probing of the intracellular region of Kv channels.

The results in CHAPTER II, which show that CaM is located close to the channel gate, produce a number of questions concerning the calcium sensitivity of KCNQ channels. Although Q1-Q5 channels are all modulated by calcified CaM, the changes in current levels are diametric [89]. The spacing between the KCNQ channel gate and the first CaM binding site on the channels is conserved, suggesting that the differential modulation of KCNQ channels may be due to a Ca^{2+}–induced repositioning of CaM onto KCNQ channels, similar to what is found for voltage-gated calcium channels [198], rather than structural rearrangements within the gate of KCNQ channels. Comparison of the distances reported in CHAPTER II to those generated from a panel of CaM mutants which cannot bind Ca^{2+}: CaM_{12} (apoN-lobe), CaM_{34} (apoC-lobe), and CaM_{1234} (apoCaM) [158] can be used to report on the structural changes induced by calcification of each

CaM lobe when bound to KCNQ channels and thus shed light on the calcium-sensing ability of KCNQ channels.

The intracellular tethered blocker approach described in CHAPTER II is modular in nature allowing for the investigation of additional regulatory proteins which bind to KCNQ channels or other ion channel-calmodulin complexes. Indeed, generating a panel of CaM tethered to the Q1 channel inhibitor chromanol [199,200] allows for the detection of CaM binding to Q1/E1 channel complexes that are insensitive to internal TEA (Figure V-1). Furthermore, as CaM has been shown to directly bind to some KCNEs [201], this approach could be used to probe the structural differences between the Q1-KCNE complexes providing insight into their different gating properties and pharmacological sensitivities.
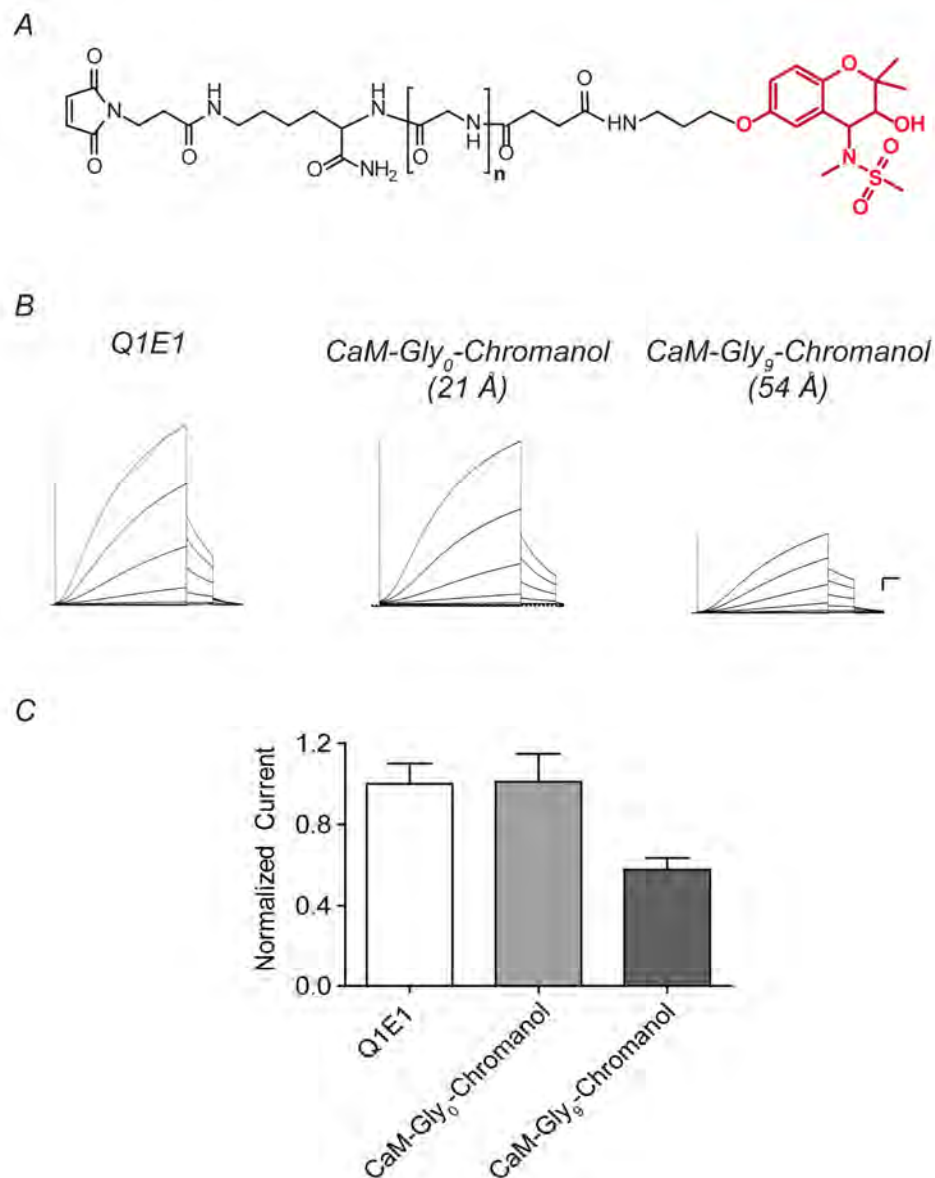
Figure V-1. Tethered blocker strategy for detecting CaM bound to functioning Q1-KCNE channel complexes.
(A) Structure of the maleimido-chromanol linkers: n, number of glycines in the linker.
(B) Families of Q1/E1 currents recorded from oocytes injected with channel mRNA or co-injected with T35C-Gly$_n$-Chromanol protein. Currents were elicited by 4 s test potentials from –100 to +60 mV in 20 mV increments from a holding potential of –80 mV followed by a tail pulse to –30 mV. Dashed line indicates zero current. Scale bars represent 0.5 µA and 0.5 s. (C) Quantification of current levels at 40 mV. Values are normalized to oocytes injected with only channel mRNA. Data are presented as the mean ± SEM from 2 batches of oocytes.

KCNQ channels are essential for normal cardiac and neuronal repolarization. Because many genetic mutations in KCNQ channels lead to a decrease in overall channel conductance, small molecules that activate KCNQ channel complexes could provide a new avenue of pharmacological treatment for KCNQ channelopathies. CHAPTER III describes the identification and characterization of a novel KCNQ activator, PBA. The potency of PBA is modest; however, preliminary studies show that it can activate Q1/E1 complexes harboring a LQTS-associated mutation (S74L) which right-shifts the activation curve of these complexes (Figure V-2) [202]. Although PBA can only partially rescue the S74L LQTS-associated mutation, these preliminary studies demonstrate the promising therapeutic potential PBA has for the treatment and characterization of KCNQ channelopathies.

Traditional high-throughput screens have been largely unsuccessful in identifying KCNQ channel activators [101]. However, since both of the basic structural motifs of PBA – the aromatic ring and the boronic acid – are important for KCNQ activation, structure-function studies on derivatives of PBA may prove useful in characterizing the physiochemical properties of PBA activation and identifying a more potent activator of KCNQ channel complexes. PBA both activates and inhibits KCNQ channels, making traditional Quantitative Structure-Activity Relationship (QSAR) analysis using docking and computational methods unfeasible. Because PBA has different effects on Q1 (inhibition and activation), Q4 (activation), and *Shaker* (inhibition) channels, chimeric channel proteins may be able to differentiate which structural components of the channel (voltage sensing domain or pore domain) are responsible for inhibition versus activation.
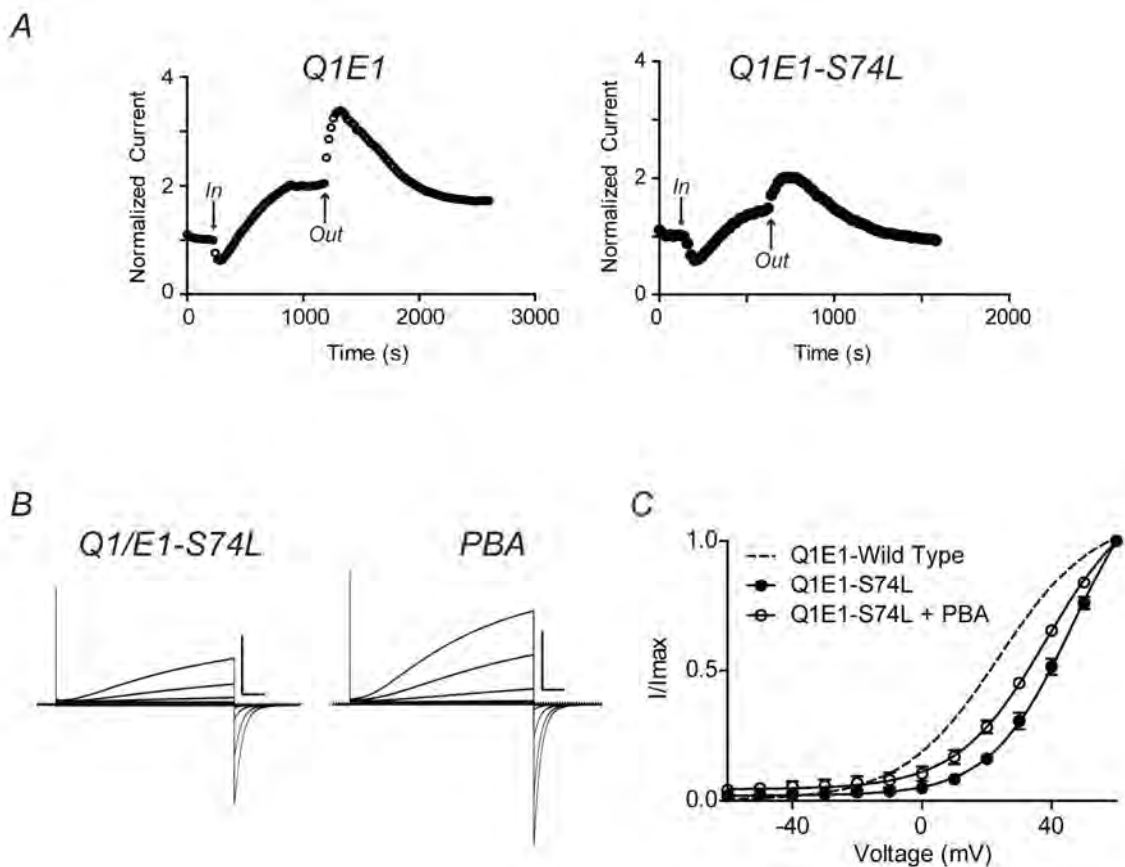
Figure V-2. PBA partially rescues the KCNE1 LQTS-associated mutant S74L.
(A) Time courses of Q1/E1 currents measured in ND96 at +40 mV at the end of a 2 s pulse. The current was normalized to before 10 mM PBA application. PBA initially inhibits current and then slowly potentiates both wild type and mutant channels. (B) Families of currents recorded before and during treatment with PBA in high external potassium (50 mM). Currents were elicited by 4 s step test potentials from −80 to +60 mV in 10 mV increments from a holding potential of −80 mV followed by a tail pulse to −30 mV. Dashed line indicates zero current. Scale bars represent 1 µA and 0.5 s. (C) Voltage-activation curves for Q1/E1 calculated from tail current analysis. Solid curves represent Boltzmann fits to the data. Data are presented as the mean ± SEM (n = 6).

Once the region of the channel responsible for interaction with PBA is established, site-directed mutagenesis could be used to determine specific residues that are required for PBA's interaction, allowing for molecular modeling and docking studies. In complement to mutagenesis studies, qualitative bioisoterism could be used to rationally design PBA derivatives [203] to aid in the elucidation of the mechanism by which PBA activates KCNQ channel complexes. For example, fluorinated boronic acids maintain the overall topology of the molecule as fluorine atoms are similar in size to hydrogen but their electronegativity alters the pKa of the boronic acid moiety allowing for the investigation of the role charge plays in activation. Preliminary studies with fluorinated derivatives of PBA (Figure V-3) suggest that ionization of the boronic acid moiety may be responsible for the quick inhibition initially seen upon PBA application. Additionally, structure-function studies not only provide insight into PBA's binding site but should yield new tools to investigate the molecular mechanisms of KCNQ gating.

CHAPTER IV described the determination of the cause of our poor quality *Xenopus* oocytes after surgical removal. Culturing the afflicted oocytes revealed that they were contaminated with strains of multi-drug resistant bacteria. Our new antibiotic cocktail prevents the contamination of oocytes, allowing for electrophysiological recordings. These results lead to two questions: (1) what is the cause of the recent antibiotic resistance seen in the laboratory setting and (2) what is the source of the microbial contamination?

Compound	pKa	Effect
PBA	8.9	Inhibition + Potentiation
2-fluoro-PBA	8.3	Inhibition + Potentiation
3-fluoro-PBA	7.5	Inhibition
Pentafluoro-PBA	6.1	Inhibition

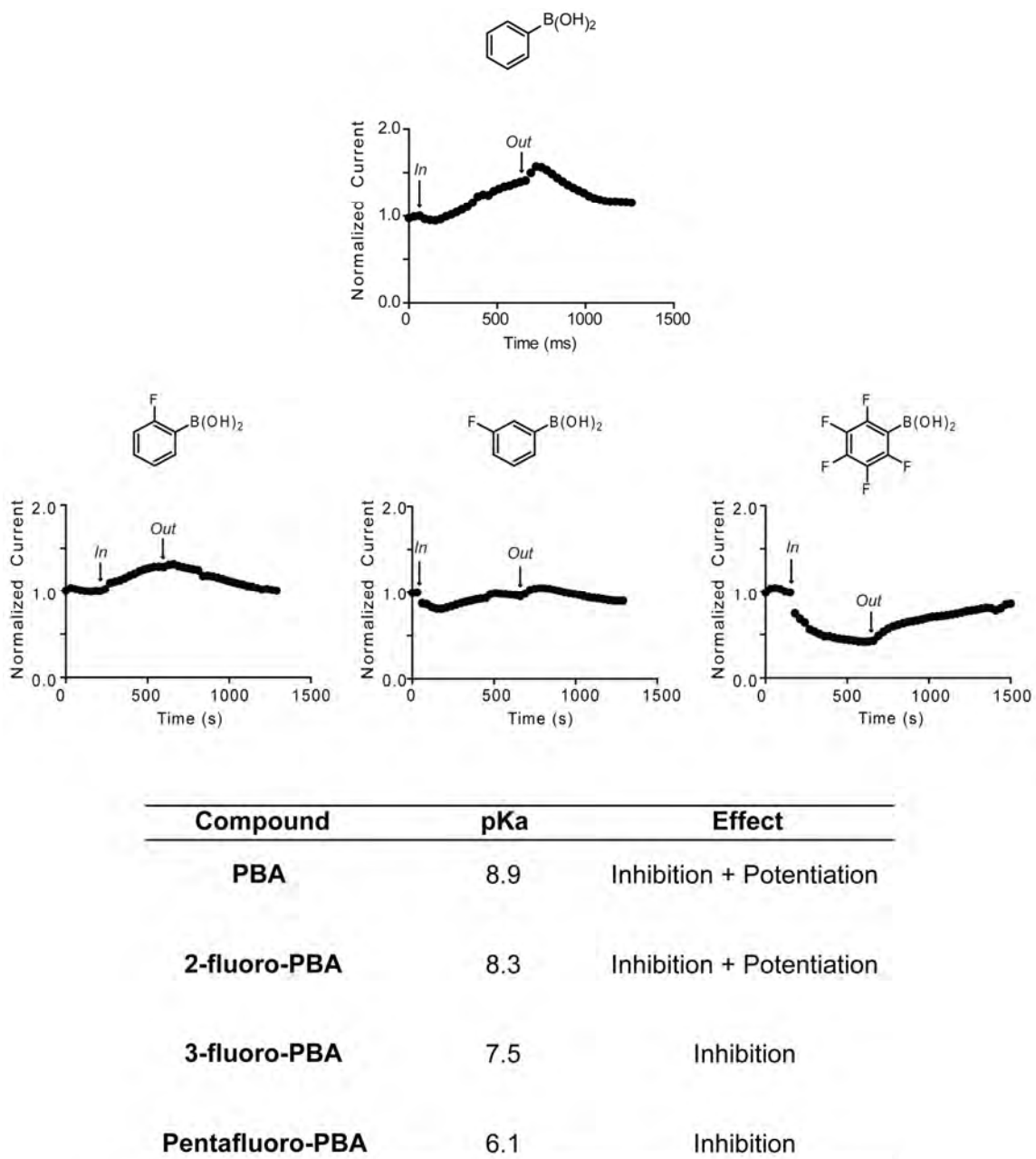**Figure V-3. Preliminary SAR results**
Time courses of Q1/E1 currents measured in ND96 at +40 mV at the end of a 2 s pulse.
The current was normalized to before application of 1 mM boronic acid. Both PBA and
2-fluoroboronic acid initially inhibits current and then slowly potentiates wild type Q1/E1
channel complexes. Both 3-fluoroboronic acid and pentafluoroboronic acid only inhibit.

The widespread misuse and overuse of antibiotics plays a significant role in the emergence of resistant bacteria. Storage media has been supplemented with antibiotics for years, but given that oocytes are discarded after each experiment, it seems unlikely that the environmental pressure to develop antibiotic resistance stems from laboratory use. Rather, it is more likely that husbandry facilities prophylactically treat amphibians with antibiotics. This is consistent with a previous study that showed *P. fluorescens* was present on the *Xenopus* skin [190]. Although the skin cultures were negative for the observed multi-drug resistant strains found in the oocytes, the fact that the black foci were only found on oocytes extracted from animals ordered from one vendor suggests that the animal's ovarian tissue and/or oocytes are the likely source of the multi-drug resistant bacteria. Until the source of the contamination is identified, the judicious use of antibiotics *in vitro*, rather than *in vivo*, is necessary.

Overall, this thesis describes the development of small molecule tools that allow for the dissection of the structure-function relationship of KCNQ channels. Further application and optimization of these tools will allow for the continued examination of Kv channels as a means to better understanding their role in human physiology and disease.

APPENDICES

CHAPTER AI

Determining the Mechanism of Phenyl Boronic Acid Activation of KCNQ Channels

ABSTRACT

KCNQ channels (Q1-Q5) are essential for normal cardiac and neuronal repolarization. Because many genetic mutations in KCNQ channels lead to a decrease in overall channel conductance, small molecules that activate KCNQ channel complexes could provide a new avenue of pharmacological treatment for KCNQ channelopathies. A simple boronic acid, phenylboronic acid (PBA), differently activates KCNQ complexes at millimolar concentrations by shifting the voltage sensitivity of the channel complexes. To determine the KCNQ region(s) important for activation by PBA, chimeric proteins were cloned and treated with PBA. To further characterize which physiochemical properties of PBA are required for activation, derivatives of PBA were tested on wild-type Q1/E1 channel complexes. These preliminary results suggest that ionization of the boronic acid moiety plays a role in modulation of KCNQ channels.

MATERIALS AND METHODS

Molecular Biology

cDNA encoding human KCNQ1 and E1 were individually subcloned into the vector

pSG01MX, which contains the 5' and 3'UTRs from the *Xenopus* β-globin gene for

increased protein expression. Inactivation-removed Shaker (Shaker-IR) was cloned in

pBluescriptII KS (+). Chimeras of Shaker-IR-Q1 and Q1-Q4 were generated by cassette

mutagenesis. All constructs were confirmed by sequencing the entire cDNA. Constructs

were linearized with the appropriate restriction enzyme (New England Biolabs) and

cRNA was synthesized using *in vitro* run-off transcription with SP6 or T7 polymerase

(Promega).

Electrophysiology

Oocytes were surgically removed from *Xenopus laevis*. The extraction procedure and

care of *Xenopus laevis* was approved by the University of Massachusetts Institutional

Animal Care and Use Committee. Oocytes were defolliculated using 2 mg/mL

collagenase (Worthington Biochemical Corp.) in OR2 solution containing (in mM): 82.5

NaCl, 2.5 KCl, 1 $MgCl_2$, 5 HEPES, pH 7.4 for 60-80 minutes. Isolated oocytes were

rinsed and stored in ND96 storage solution containing (in mM): 96 NaCl, 2 KCl, 1.8

$CaCl_2$, 1 $MgCl_2$, 5 HEPES, 50 μg/mL of both gentamicin and tetracycline pH 7.4, at

18°C. Oocytes were microinjected 24 h after surgery with channel mRNA (15.2 ng).

Additionally, Q1 mRNA (7.6 ng) was co-injected with E1 (3.8 ng). After 2–4 days,

currents were recorded using Warner Instrument OC-725 two-electrode voltage clamp

(TEVC), and the data were acquired with Digidata 1322A using pClamp 9 (Axon

Instruments). Electrodes were filled with: 3 M KCl, 5 mM EGTA, 10 mM HEPES, pH

7.6. Currents were measured in ND96 recording buffer containing (in mM): 96 NaCl, 2

KOH, 0.3 CaCl$_2$, 1 MgCl$_2$, 10 HEPES, pH 7.6. All chemical compounds were from

Sigma Aldrich and dissolved directly into ND96 recording buffer. The time courses of

current changes upon compound application and washout were generated by repeatedly

depolarizing and measuring the change in current at the end of the pulse. Channels were

held at –80 mV and pulsed to +40 mV for 2 s every 30 s to illicit current. Current-

voltage relationships were measured in the presence or absence of 10 mM PBA by

holding at –80 mV and stepping to a series of test potentials for 4 s in 10 mV increments,

followed by a tail pulse at –30 mV.

Data Analysis

Analysis of data was performed with Clampfit 9 (Axon Instruments) and Prism 5

software (Graphpad). The amplitude of tail currents was measured 6 ms (100 ms for Q1)

after repolarization to –30 mV (–80 mV for Q1/E3 and 50 mM external charge carriers)

and normalized such that the maximal tail current in the absence of drug was equal to 1.

Normalized tail currents were plotted versus the test potential to produce activation

curves. Activation curves were fit to the Boltzmann equation: $I_{tail} = A1 + (A2 - A1) / (1$

$+ e^{((V - V_{1/2})*(-zF/RT))})$, where $V_{1/2}$ is the voltage of half-maximal activation and z is the slope

factor.

RESULTS AND DISCUSSION

PBA affects the ion selectivity of the Q1 channel suggesting that PBA modulation occurs within the pore domain [204]. Additionally, PBA activates other members of the KCNQ family further indicating that PBA is directly binding to KCNQ channels. In contrast to Q1, PBA only inhibits Shaker-IR channels, and only activates Q4 channels (Figure AI-1A). Because PBA does not modulate Kv channels in the same manner or to the same extent, we designed chimeras between the voltage-sensing domain and the pore domain to determine which regions of the channel confer the varied subunit-specific sensitivities to PBA (Figure AI-1B). We first tested chimeras between Q4 and Shaker-IR because PBA had diametrically opposite effects on current; however, these chimeras were non-functional. Because there is a large amount of homology among the KCNQ channel family (~ 40% amino acid identity), chimeras made between different KCNQ channels are fully functional [205]. Therefore, we generated and cloned chimeras between the voltage-sensing domain and pore domain of Q1 and Q4 channels. These constructs were also non-functional suggesting that such large portions of KCNQ channels are not interchangeable. This is consistent with recent data from the Attali lab that showed that chimeras between the entire voltage-sensing domain of Q1 and Q2 channels are non-functional even though chimeras between single transmembrane domains are [206].
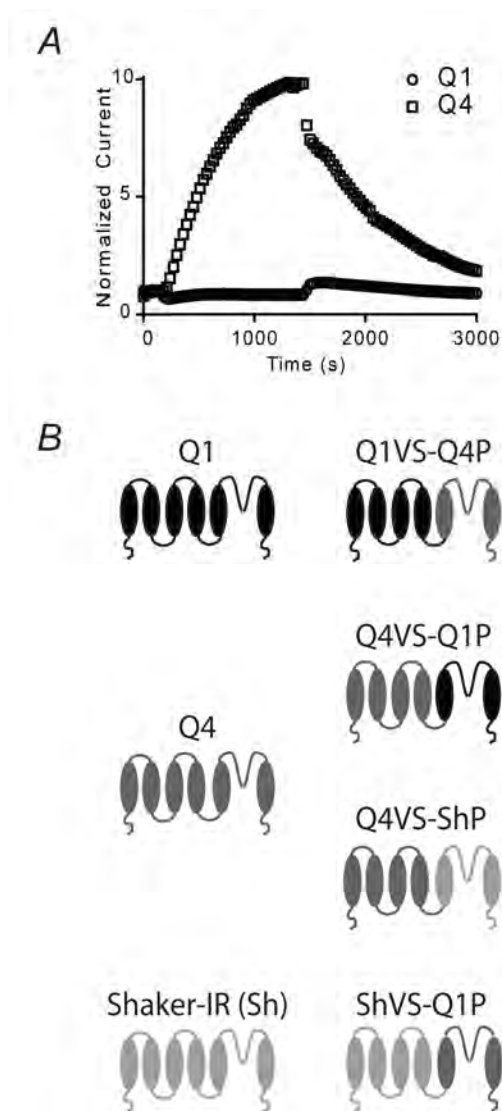
Figure AI-1. PBA activates Q1 and Q4 channels differently.
(A) Time courses of current recorded from Q1 and Q4 channels. The current was normalized before PBA application. PBA initially inhibits and then slowly increases Q1 current. PBA only activates Q4 channels. (B) Schematic of the design of chimeras between Shaker-IR, Q1 and Q4 channels.

Because the chimeras were non-functional, we decided to further characterize the mechanism of activation by PBA using simple structure-activity studies. We first tested fluorinated boronic acids as the fluorine atom is similar in size to the hydrogen atom, keeping the overall topology of the molecule unaffected. 2-fluorophenylboronic acid similarly activated Q1/E1 complexes at 1 mM as PBA (Figure AI-2A). In contrast, both 3-fluorophenylboronic acid and pentafluoroboronic acid only inhibited Q1/E1 complexes (Figure AI-2A). Because fluorine is similar in size to the hydrogen atom but is an electron withdrawing group, the different effect of the fluorinated derivatives of PBA suggest that ionization of the boronic acid moiety may be responsible for the quick inhibition initially seen upon PBA application.

To further establish whether charge may play a role in modulation of Q1/E1 complexes, we tested nitro-substituted PBA derivatives. The electron withdrawing nitro groups will lower the pKa of the boronic acid moiety. At 1 mM, 2-nitrophenylboronic acid slightly reduced Q1/E1 current levels; however, both 3-nitrophenylboronic acid and 4-nitrophenylboronic acid strongly inhibited Q1/E1 complexes (Figure AI-2B). Based on the pKa values (Table AI-I) of the derivitized PBA molecules, it is possible that the negative charged species of PBA is responsible for inhibiting Q1/E1 channel complexes.
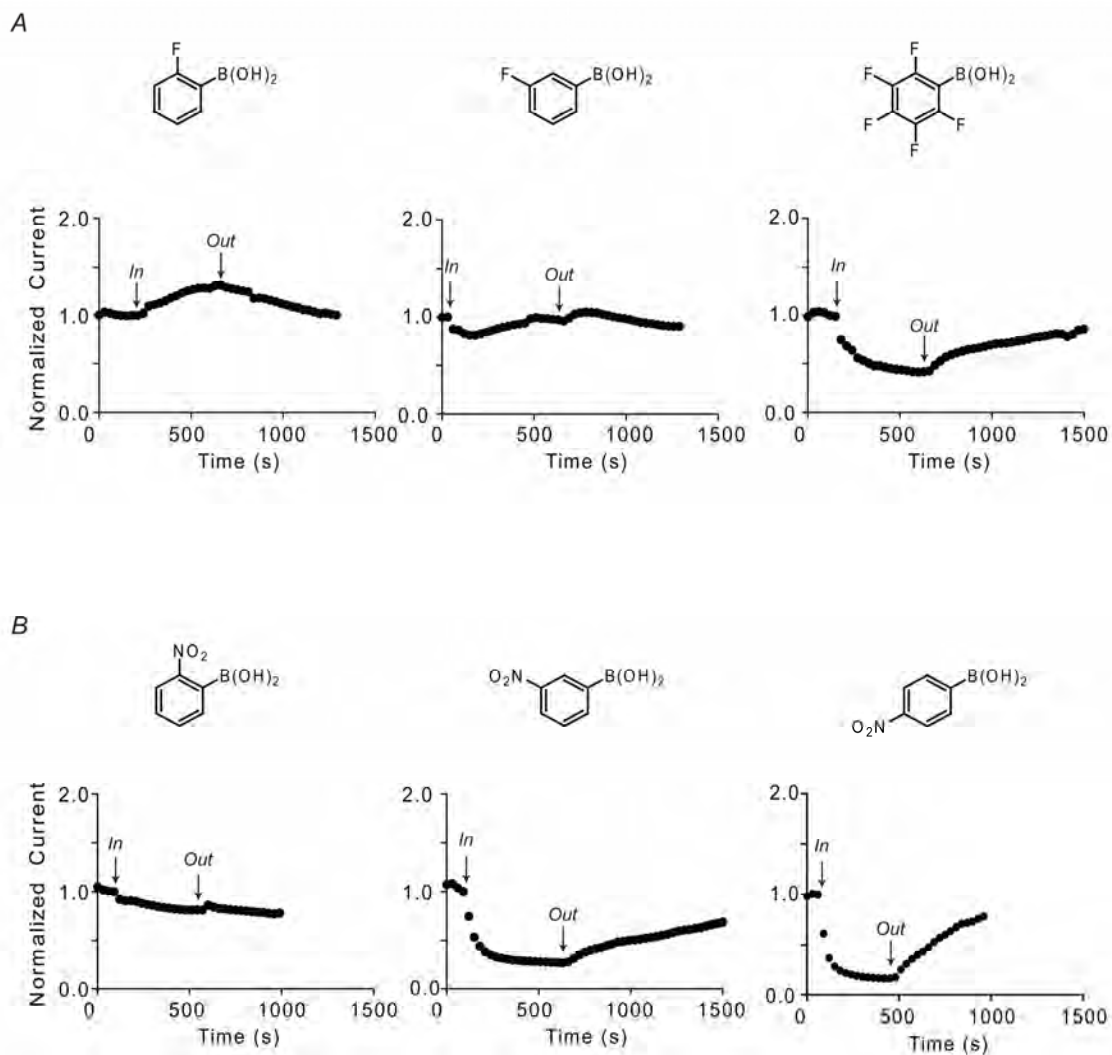
Figure AI-2. Derivatives of PBA also modulate Q1/E1 channels.
(A) Time courses of current recorded from Q1/E1 channels upon treatment and washout of 1 mM fluorinated PBA. The current was normalized before PBA application. 2-fluorophenylboronic acid slightly potentiates Q1/E1 current; both 2-fluoroboronic acid and pentaphenylboronic acid initially inhibits Q1/E1 current. (B) Time courses of current recorded from Q1/E1 channels upon treatment and washout of 1 mM nitro-phenylboronic acid. 2-nitrophenylboronic acid has no significant effect on Q1/E1 current; both 3-nitrophenylboronic acid and 4-nitrophenylboronic acid inhibit Q1/E1 channels.

Table AI-I. Properties of Phenylboronic (PBA) derivatives.

Compound	pKa	Anionic Species Concentration (mM)	Neutral Species Concentration (mM)	Effect
		1 mM Compound		
PBA	8.9	0.05	0.95	Inhibition + Activation
2-fluoroPBA	8.3	0.16	0.84	Inhibition + Activation
3-fluoroPBA	7.5	0.56	0.44	Inhibition
pentafluoroPBA	6.1	0.97	0.03	Inhibition
2-nitroPBA	7.8	0.37	0.63	No effect
3-nitroPBA	7	0.8	0.2	Inhibition
4-nitroPBA	7	0.8	0.2	Inhibition
Benzoic Acid	4.2	1	0	Inhibition
Benzyl Alcohol	15.4	0	1	Activation

PBA activation of KCNQ channels is slow (minutes) which could be explained by a cytoplasmic or buried binding site. However, PBA may be acting indirectly, activating signaling pathways in the cell. To determine whether PBA may be increasing the number of channels on the cell surface, we set out to perform cell-surface luminometry on *Xenopus* oocytes. We choose oocytes because their large size allows for the direct comparison of cell surface expression with the changes observed in current levels upon treatment with PBA. For these experiments, the hemagglutinin A (HA) tag was incorporated into the N terminus of E1 between residues 22 and 23 [121]. Unfortunately, addition of this extracellular tag rendered PBA ineffective on the Q1/E1 complex. We also performed cell-surface biotinylation on *Xenopus* oocytes. However, due to the yolk of the oocytes, it was hard to accurately quantitate Q1 protein. Lastly, we also tried to record from oocytes at 4°C. Similar to what was found in mammalian cells [207], Q1/E1 channel current was abolished at the lower temperature, which could not be rescued by application of PBA. Although it is possible that PBA may be increasing the number of channels on the cell surface, it is unlikely for two reasons: (1) activation of PBA is slow but current levels plateau in minutes which is not enough time for full biogenesis of the Q1/E1 complex and (2) many of the proteins involved in forward trafficking (e.g. Dynein, Syntaxin1A) promote recycling of ion channels which are not activated by PBA [208]. Similarly, since PBA activates all members of the KCNQ family [204] it is unlikely that PBA is acting indirectly as KCNQ channels are differently affected by intracellular signals ([89,209].

Although the molecular mechanism for activation of KCNQ channels by PBA is still unclear, this preliminary data provides a framework for designing future experiments to answer this question. In combination with Chapter III, this work provides additional evidence to support the use of PBA, and its derivatives, as small molecule probes to dissect the mechanism of KCNQ channel function.

CHAPTER AII

Additional Compounds Synthesized by Author

Terpyridine cross-linkers

2,2':6',2"-terpyridine (TYP) is a tridentate ligand that forms a stable

*bis*terpyridine (*bis*TYP) complex through coordination with a transition metal ion [210].

A library of TYP derivatives containing a 4' cysteine reactive group (SS-Pyr) with

varying linker lengths can be synthesized using basic amino coupling strategies (Figure

AII-1).   Our lab has previously showed that the extracellular N-terminus of KCNE1 (E1)

peptides is reactive small molecules [108]. By engineering cysteines into the N-term of

E1, we can modify the N-terminus with TYP derivatives.   If the TYP groups are close

enough in space, the *bis*TYP complex can form in the presence of iron. Formation of the

*bis*TYP complex can be monitored electrophysiologically as a reduction in current.

Plotting inhibition as a function of linker length will generate a distance between the N-

termini of the E1 peptides.

Previous studies have relied on using maleimide to specifically label the cysteines

in E1 as the reaction is fast and forms a irreversible thioether bond [27,108]; however, all

of our attempts to couple TPY to a maleimide we unsuccessful. Therefore, we chose the

pyridyl disulfide which was compatible with TPY. The advantage of the pyridyl

disulfide group is that it is reversible with reducing agents. To estimate the rate of SS-

Pyr reaction with E1, we first measured the reaction rate with βME *in vitro* to obtain a τ

value of 32.5 ± 4.7 s and a rate constant of 360 ± 63 $M^{-1}s^{-1}$. The quick kinetics of the SS-Pyr reaction indicates that these experiments can be monitored while recording from individual oocytes instead of pre-incubating oocytes in the TPY library.
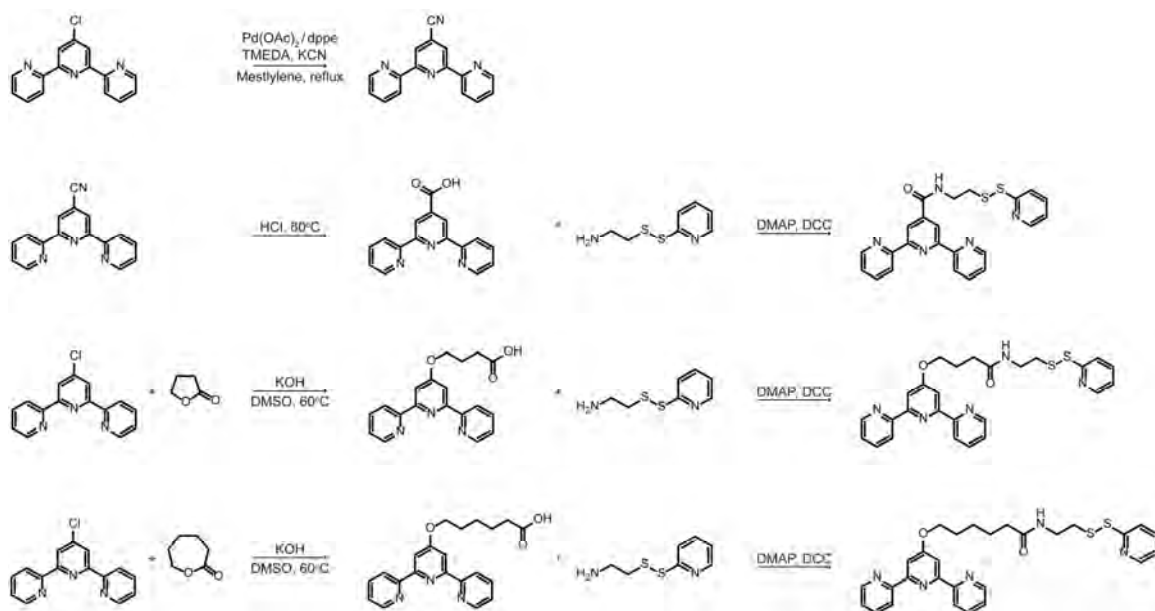
Figure AII-1. Schemes illustrating the synthesis of a panel of 4'-carboxylic acid and 4'-carboxylic acid cysteine reactive derivatives of 2,2':6',2''-terpyridine.

TEA tethered blockers containing PEG linkers

In Chapter II, we chemically derivatized calmodulin (CaM) into a "tethered blocker" using a panel of glycine linkers (Figure AII-1). Generation of the panel of maleimido-quaternary ammoniums (QAs) with glycine linkers requires the use of solid-phase peptide synthesis which is time consuming and the final linkers are hard to purify. To simplify the synthesis of a panel of linkers, we choose to generate a panel of polyethylene glycol (PEG) linkers (Figure AII-1A). PEG linkers are easier to synthesize in larger quantities and more water soluble than their glycine counterparts. A library of maleimido-QA derivatives can be synthesized using basic amino coupling strategies (Figure AII-1B).
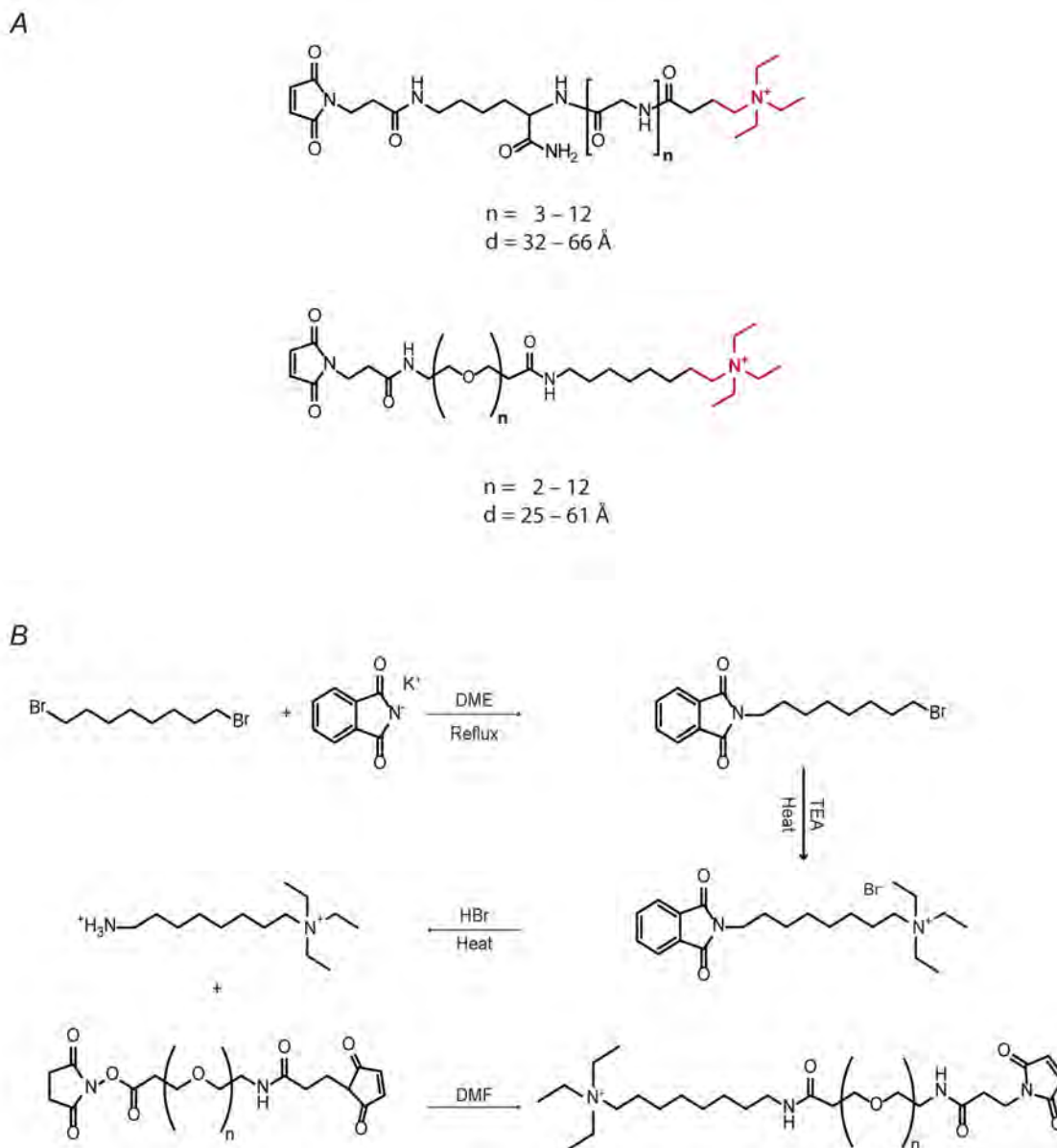
Figure AII-2. Maleimido-Quaternary Ammonium Linkers
(A) Comparison of Glycine and PEG linkers. (B) Scheme illustrating the synthesis of a panel of meleimido-quaternary ammonium linkers containing PEG spacers.

We first determined whether the PEG linkers could be exploited in an intracellular tethered blocker approach by examining CaM derivatized at position T35C (N-lobe) (Figure AII-3) with the shortest linker, CaM-PEG$_2$-QA (21 Å). Oocytes were co-injected with KCNQ channel mRNA and CaM protein and families of Q2/Q3 currents were measured 3 days after co-injection. Oocytes injected with CaM-PEG$_2$-QA (3 μM *in ovo*) resulted in 21 ± 6% decrease in current which was surprising as the longer CaM-Gly3-QA linker did not inhibit Q1/Q3 current (Figure AII-3A). We reasoned that the PEG linker was more flexible than the glycine linker allowing for the linker to reach the QA binding site on Q2/Q3 channels. We next tested CaM-PEG$_8$-QA because its extended length was only 2 Å longer than CaM-Gly$_7$-QA. Inhibition by CaM-PEG$_8$-QA was variable between batches of oocytes (Figure AII-3B) and overall less (29 ± 4%) than what was observed for CaM-Gly$_7$-QA (40 ± 6%) (Figure AII-3C). Lastly, we tested our longest linker, CaM-PEG$_{12}$-QA. Inhibition by CaM-PEG$_{12}$-QA was less than that compared to the glycine linkers and independent of concentration (Figure AII-3D and E). Taken together this data indicates that the PEG linkers cannot be used in an intracellular tethered blocker approach.
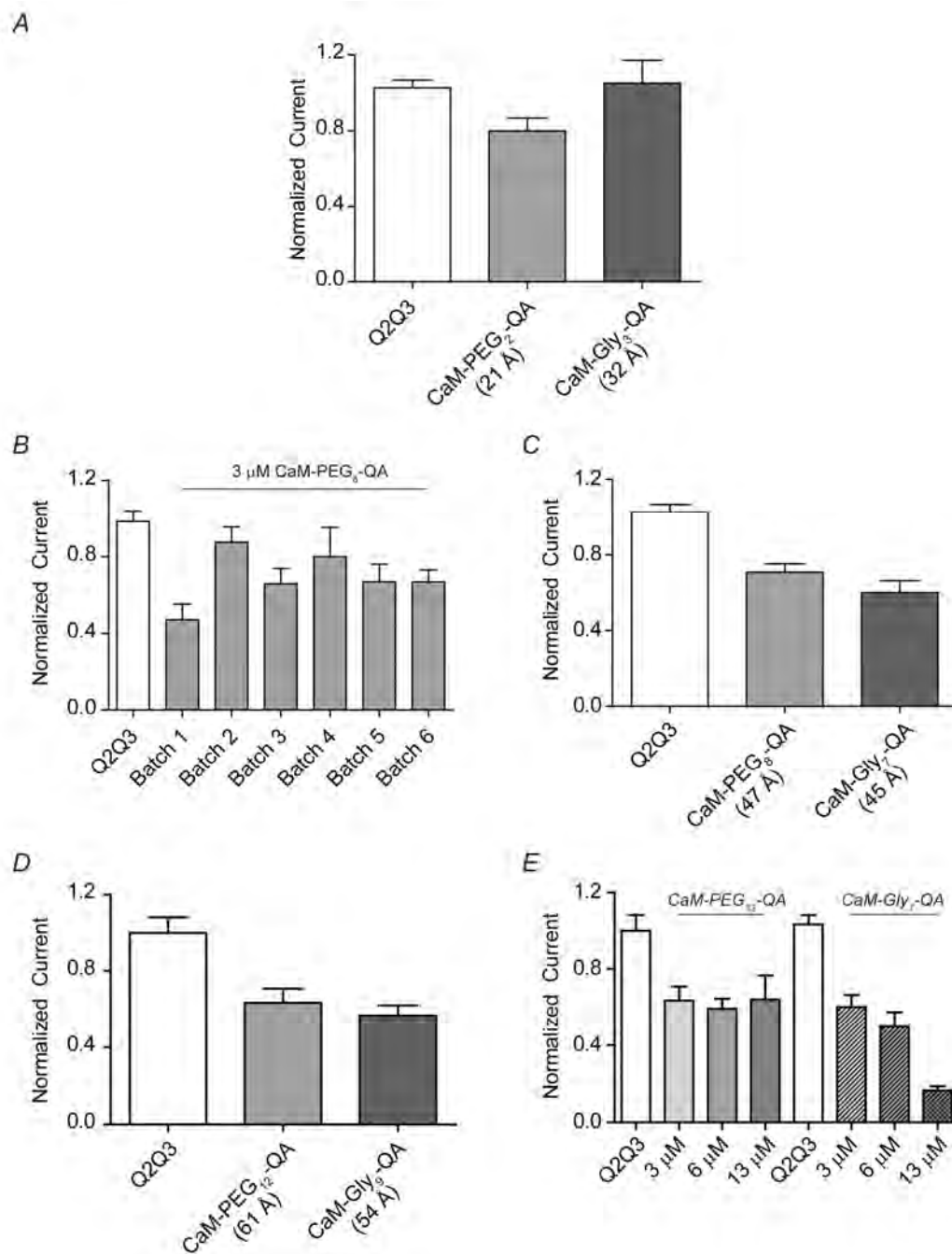
Figure AII-3. PEG-derivatized CaM proteins do not behave as intracellular tethered blockers.
(*A-E*) Quantification of current levels at 40 mV from oocytes co-injected with different CaM proteins. Values are normalized to oocytes injected with only channel mRNA. Data are presented as the mean ± SEM from 2 – 4 batches of oocytes.

BIBLIOGRAPHY

1. Robbins J (2001) KCNQ potassium channels: physiology, pathophysiology, and pharmacology. Pharmacol Ther 90: 1-19.

2. Lehmann-Horn F, Jurkat-Rott K (1999) Voltage-gated ion channels and hereditary disease. Physiol Rev 79: 1317-1372.

3. Doyle DA, Morais Cabral J, Pfuetzner RA, Kuo A, Gulbis JM, et al. (1998) The structure of the potassium channel: molecular basis of K+ conduction and selectivity. Science 280: 69-77.

4. Zhou M, Morais-Cabral JH, Mann S, MacKinnon R (2001) Potassium channel receptor site for the inactivation gate and quaternary amine inhibitors. Nature 411: 657-661.

5. Zhou Y, Morais-Cabral JH, Kaufman A, MacKinnon R (2001) Chemistry of ion coordination and hydration revealed by a K+ channel-Fab complex at 2.0 A resolution. Nature 414: 43-48.

6. Holmgren M, Shin KS, Yellen G (1998) The activation gate of a voltage-gated K+ channel can be trapped in the open state by an intersubunit metal bridge. Neuron 21: 617-621.

7. del Camino D, Holmgren M, Liu Y, Yellen G (2000) Blocker protection in the pore of a voltage-gated K+ channel and its structural implications. Nature 403: 321-325.

8. del Camino D, Yellen G (2001) Tight steric closure at the intracellular activation gate of a voltage-gated K(+) channel. Neuron 32: 649-656.

9. Long SB, Campbell EB, Mackinnon R (2005) Crystal structure of a mammalian voltage-dependent Shaker family K+ channel. Science 309: 897-903.

10. Yus-Najera E, Santana-Castro I, Villarroel A (2002) The identification and characterization of a noncontinuous calmodulin-binding site in noninactivating voltage-dependent KCNQ potassium channels. J Biol Chem 277: 28545-28553.

11. Haitin Y, Attali B (2008) The C-terminus of Kv7 channels: a multifunctional module. J Physiol 586: 1803-1810.

12. Kanki H, Kupershmidt S, Yang T, Wells S, Roden DM (2004) A structural requirement for processing the cardiac K+ channel KCNQ1. J Biol Chem.

13. Schmitt N, Schwarz M, Peretz A, Abitbol I, Attali B, et al. (2000) A recessive C-terminal Jervell and Lange-Nielsen mutation of the KCNQ1 channel impairs subunit assembly. Embo J 19: 332-340.

14. Schwake M, Jentsch TJ, Friedrich T (2003) A carboxy-terminal domain determines the subunit specificity of KCNQ K(+) channel assembly. EMBO Rep 4: 76-81.

15. Schwake M, Athanasiadu D, Beimgraben C, Blanz J, Beck C, et al. (2006) Structural determinants of M-type KCNQ (Kv7) K+ channel assembly. J Neurosci 26: 3757-3766.

16. Howard RJ, Clark KA, Holton JM, Minor DL, Jr. (2007) Structural insight into KCNQ (Kv7) channel assembly and channelopathy. Neuron 53: 663-675.

17. Wiener R, Haitin Y, Shamgar L, Fernandez-Alonso MC, Martos A, et al. (2008) The KCNQ1 (Kv7.1) COOH terminus, a multitiered scaffold for subunit assembly and protein interaction. J Biol Chem 283: 5815-5830.

18. Splawski I, Timothy KW, Vincent GM, Atkinson DL, Keating MT (1997) Molecular basis of the long-QT syndrome associated with deafness. N Engl J Med 336: 1562-1567.

19. Pusch M, Magrassi R, Wollnik B, Conti F (1998) Activation and inactivation of homomeric KvLQT1 potassium channels. Biophys J 75: 785-792.

20. Abbott GW, Goldstein SA (1998) A superfamily of small potassium channel subunits: form and function of the MinK-related peptides (MiRPs). Q Rev Biophys 31: 357-398.

21. McCrossan ZA, Abbott GW (2004) The MinK-related peptides. Neuropharmacology 47: 787-821.

22. Barhanin J, Lesage F, Guillemare E, Fink M, Lazdunski M, et al. (1996) K_VLQT1 and IsK (minK) proteins associate to form the I_{Ks} cardiac potassium current. Nature 384: 78-80.

23. Sanguinetti MC, Curran ME, Zou A, Shen J, Spector PS, et al. (1996) Coassembly of K_VLQT1 and minK (IsK) proteins to form cardiac I_{Ks} potassium channel. Nature 384: 80-83.

24. Roepke TK, Anantharam A, Kirchhoff P, Busque SM, Young JB, et al. (2006) The KCNE2 potassium channel ancillary subunit is essential for gastric acid secretion. J Biol Chem 281: 23740-23747.

25. Schroeder BC, Waldegger S, Fehr S, Bleich M, Warth R, et al. (2000) A constitutively open potassium channel formed by KCNQ1 and KCNE3. Nature 403: 196-199.

26. Grunnet M, Jespersen T, Rasmussen HB, Ljungstrom T, Jorgensen NK, et al. (2002) KCNE4 is an inhibitory subunit to the KCNQ1 channel. J Physiol 542: 119-130.

27. Morin TJ, Kobertz WR (2007) A Derivatized Scorpion Toxin Reveals the Functional Output of Heteromeric KCNQ1-KCNE K^+ Channel Complexes. ACS Chem Biol 2: 469-473.

28. Manderfield LJ, George AL, Jr. (2008) KCNE4 can co-associate with the I(Ks) (KCNQ1-KCNE1) channel complex. Febs J 275: 1336-1349.

29. Angelo K, Jespersen T, Grunnet M, Nielsen MS, Klaerke DA, et al. (2002) KCNE5 induces time- and voltage-dependent modulation of the KCNQ1 current. Biophys J 83: 1997-2006.

30. Peroz D, Rodriguez N, Choveau F, Baro I, Merot J, et al. (2008) Kv7.1 (KCNQ1) properties and channelopathies. J Physiol 586: 1785-1789.

31. Bokil NJ, Baisden JM, Radford DJ, Summers KM (2010) Molecular genetics of long QT syndrome. Mol Genet Metab 101: 1-8.

32. Wilde AA, Bezzina CR (2005) Genetics of cardiac arrhythmias. Heart 91: 1352-1358.

33. (2010) The Gene Connection for the Heart. 2010 ed.

34. Hedley PL, Jorgensen P, Schlamowitz S, Wangari R, Moolman-Smook J, et al. (2009) The genetic basis of long QT and short QT syndromes: a mutation update. Hum Mutat 30: 1486-1511.

35. Neyroud N, Tesson F, Denjoy I, Leibovici M, Donger C, et al. (1997) A novel mutation in the potassium channel gene KVLQT1 causes the Jervell and Lange-Nielsen cardioauditory syndrome. Nat Genet 15: 186-189.

36. Nicolas M, Dememes D, Martin A, Kupershmidt S, Barhanin J (2001) KCNQ1/KCNE1 potassium channels in mammalian vestibular dark cells. Hear Res 153: 132-145.

37. Wangemann P (2002) K+ cycling and the endocochlear potential. Hear Res 165: 1-9.

38. Rivas A, Francis HW (2005) Inner ear abnormalities in a Kcnq1 (Kvlqt1) knockout mouse: a model of Jervell and Lange-Nielsen syndrome. Otol Neurotol. United States. pp. 415-424.

39. Dedek K, Kunath B, Kananura C, Reuner U, Jentsch TJ, et al. (2001) Myokymia and neonatal epilepsy caused by a mutation in the voltage sensor of the KCNQ2 K+ channel. Proc Natl Acad Sci U S A. United States. pp. 12272-12277.

40. Charlier C, Singh NA, Ryan SG, Lewis TB, Reus BE, et al. (1998) A pore mutation in a novel KQT-like potassium channel gene in an idiopathic epilepsy family. Nat Genet 18: 53-55.

41. Wang HS, Pan Z, Shi W, Brown BS, Wymore RS, et al. (1998) KCNQ2 and KCNQ3 potassium channel subunits: molecular correlates of the M-channel. Science 282: 1890-1893.

42. Maljevic S, Wuttke TV, Lerche H (2008) Nervous system KV7 disorders: breakdown of a subthreshold brake. J Physiol 586: 1791-1801.

43. Maljevic S, Wuttke TV, Seebohm G, Lerche H (2010) KV7 channelopathies. Pflugers Arch 460: 277-288.

44. Wuttke TV, Jurkat-Rott K, Paulus W, Garncarek M, Lehmann-Horn F, et al. (2007) Peripheral nerve hyperexcitability due to dominant-negative KCNQ2 mutations. Neurology. United States. pp. 2045-2053.

45. Kubisch C, Schroeder BC, Friedrich T, Lutjohann B, El-Amraoui A, et al. (1999) KCNQ4, a novel potassium channel expressed in sensory outer hair cells, is mutated in dominant deafness. Cell 96: 437-446.

46. Kharkovets T, Hardelin JP, Safieddine S, Schweizer M, El-Amraoui A, et al. (2000) KCNQ4, a K+ channel mutated in a form of dominant deafness, is expressed in the inner ear and the central auditory pathway. Proc Natl Acad Sci U S A. United States. pp. 4333-4338.

47. Marcotti W, Kros CJ (1999) Developmental expression of the potassium current IK,n contributes to maturation of mouse outer hair cells. J Physiol. England. pp. 653-660.

48. Strutz-Seebohm N, Seebohm G, Fedorenko O, Baltaev R, Engel J, et al. (2006) Functional coassembly of KCNQ4 with KCNE-beta- subunits in Xenopus oocytes. Cell Physiol Biochem 18: 57-66.

49. Nie L (2008) KCNQ4 mutations associated with nonsyndromic progressive sensorineural hearing loss. Curr Opin Otolaryngol Head Neck Surg 16: 441-444.

50. Kharkovets T, Dedek K, Maier H, Schweizer M, Khimich D, et al. (2006) Mice with altered KCNQ4 K+ channels implicate sensory outer hair cells in human progressive deafness. EMBO J. England. pp. 642-652.

51. Lerche C, Scherer CR, Seebohm G, Derst C, Wei AD, et al. (2000) Molecular cloning and functional expression of KCNQ5, a potassium channel subunit that may

contribute to neuronal M-current diversity. J Biol Chem. United States. pp. 22395-22400.

52. Schroeder BC, Hechenberger M, Weinreich F, Kubisch C, Jentsch TJ (2000) KCNQ5, a novel potassium channel broadly expressed in brain, mediates M-type currents. J Biol Chem. United States. pp. 24089-24095.

53. Roura-Ferrer M, Etxebarria A, Sole L, Oliveras A, Comes N, et al. (2009) Functional implications of KCNE subunit expression for the Kv7.5 (KCNQ5) channel. Cell Physiol Biochem. Switzerland: 2009 S. Karger AG, Basel. pp. 325-334.

54. Walsh KB, Kass RS (1988) Regulation of a heart potassium channel by protein kinase A and C. Science 242: 67-69.

55. Marx SO, Kurokawa J, Reiken S, Motoike H, D'Armiento J, et al. (2002) Requirement of a macromolecular signaling complex for beta adrenergic receptor modulation of the KCNQ1-KCNE1 potassium channel. Science. United States. pp. 496-499.

56. Chen L, Kass RS A-kinase anchoring protein 9 and IKs channel regulation. J Cardiovasc Pharmacol 58: 459-413.

57. Piippo K, Swan H, Pasternack M, Chapman H, Paavonen K, et al. (2001) A founder mutation of the potassium channel KCNQ1 in long QT syndrome: implications for estimation of disease prevalence and molecular diagnostics. J Am Coll Cardiol. United States. pp. 562-568.

58. Chen L, Marquardt ML, Tester DJ, Sampson KJ, Ackerman MJ, et al. (2007) Mutation of an A-kinase-anchoring protein causes long-QT syndrome. Proc Natl Acad Sci U S A. United States. pp. 20990-20995.

59. Schroeder BC, Kubisch C, Stein V, Jentsch TJ (1998) Moderate loss of function of cyclic-AMP-modulated KCNQ2/KCNQ3 K+ channels causes epilepsy. Nature 396: 687-690.

60. Chambard JM, Ashmore JF (2005) Regulation of the voltage-gated potassium channel KCNQ4 in the auditory pathway. Pflugers Arch 450: 34-44.

61. Jentsch TJ (2000) Neuronal KCNQ potassium channels: physiology and role in disease. Nat Rev Neurosci 1: 21-30.

62. Higashida H, Brown DA (1986) Two polyphosphatidylinositide metabolites control two K+ currents in a neuronal cell. Nature 323: 333-335.

63. Marrion NV (1996) Calcineurin regulates M channel modal gating in sympathetic neurons. Neuron. United States. pp. 163-173.

64. Shapiro MS, Roche JP, Kaftan EJ, Cruzblanca H, Mackie K, et al. (2000) Reconstitution of muscarinic modulation of the KCNQ2/KCNQ3 K(+) channels that underlie the neuronal M current. J Neurosci 20: 1710-1721.

65. Nakajo K, Kubo Y (2005) Protein kinase C shifts the voltage dependence of KCNQ/M channels expressed in Xenopus oocytes. J Physiol 569: 59-74.

66. Cooper EC, Aldape KD, Abosch A, Barbaro NM, Berger MS, et al. (2000) Colocalization and coassembly of two human brain M-type potassium channel subunits that are mutated in epilepsy. Proc Natl Acad Sci U S A. United States. pp. 4914-4919.

67. Hoshi N, Zhang JS, Omaki M, Takeuchi T, Yokoyama S, et al. (2003) AKAP150 signaling complex promotes suppression of the M-current by muscarinic agonists. Nat Neurosci. United States. pp. 564-571.

68. Higashida H, Hoshi N, Zhang JS, Yokoyama S, Hashii M, et al. (2005) Protein kinase C bound with A-kinase anchoring protein is involved in muscarinic receptor-activated modulation of M-type KCNQ potassium channels. Neurosci Res 51: 231-234.

69. Hoshi N, Zhang JS, Omaki M, Takeuchi T, Yokoyama S, et al. (2003) AKAP150 signaling complex promotes suppression of the M-current by muscarinic agonists. Nat Neurosci 6: 564-571.

70. Bal M, Zhang J, Hernandez CC, Zaika O, Shapiro MS (2010) Ca2+/calmodulin disrupts AKAP79/150 interactions with KCNQ (M-Type) K+ channels. J Neurosci 30: 2311-2323.

71. Loussouarn G, Park KH, Bellocq C, Baro I, Charpentier F, et al. (2003) Phosphatidylinositol-4,5-bisphosphate, PIP2, controls KCNQ1/KCNE1 voltage-gated potassium channels: a functional homology between voltage-gated and inward rectifier K+ channels. Embo J 22: 5412-5421.

72. Zhang H, Craciun LC, Mirshahi T, Rohacs T, Lopes CM, et al. (2003) PIP(2) activates KCNQ channels, and its hydrolysis underlies receptor-mediated inhibition of M currents. Neuron. United States. pp. 963-975.

73. Lopes CM, Rohacs T, Czirjak G, Balla T, Enyedi P, et al. (2005) PIP2 hydrolysis underlies agonist-induced inhibition and regulates voltage gating of two-pore domain K+ channels. J Physiol. England. pp. 117-129.

74. Li Y, Gamper N, Hilgemann DW, Shapiro MS (2005) Regulation of Kv7 (KCNQ) K+ channel open probability by phosphatidylinositol 4,5-bisphosphate. J Neurosci. United States. pp. 9825-9835.

75. Suh BC, Hille B (2005) Regulation of ion channels by phosphatidylinositol 4,5-bisphosphate. Curr Opin Neurobiol 15: 370-378.

76. Park KH, Piron J, Dahimene S, Merot J, Baro I, et al. (2005) Impaired KCNQ1-KCNE1 and phosphatidylinositol-4,5-bisphosphate interaction underlies the long QT syndrome. Circ Res 96: 730-739.

77. Matavel A, Medei E, Lopes CM PKA and PKC partially rescue long QT type 1 phenotype by restoring channel-PIP2 interactions. Channels (Austin). United States. pp. 3-11.

78. Ekberg J, Schuetz F, Boase NA, Conroy SJ, Manning J, et al. (2007) Regulation of the voltage-gated K(+) channels KCNQ2/3 and KCNQ3/5 by ubiquitination. Novel role for Nedd4-2. The Journal of biological chemistry 282: 12135-12142.

79. Jespersen T, Membrez M, Nicolas CS, Pitard B, Staub O, et al. (2007) The KCNQ1 potassium channel is down-regulated by ubiquitylating enzymes of the Nedd4/Nedd4-like family. Cardiovasc Res 74: 64-74.

80. Krzystanek K, Rasmussen HB, Grunnet M, Staub O, Olesen SP, et al. (2012) Deubiquitylating enzyme USP2 counteracts Nedd4-2-mediated downregulation of KCNQ1 potassium channels. Heart rhythm : the official journal of the Heart Rhythm Society 9: 440-448.

81. Shamgar L, Ma L, Schmitt N, Haitin Y, Peretz A, et al. (2006) Calmodulin is essential for cardiac IKS channel gating and assembly: impaired function in long-QT mutations. Circ Res 98: 1055-1063.

82. Bai CX, Namekata I, Kurokawa J, Tanaka H, Shigenobu K, et al. (2005) Role of nitric oxide in Ca2+ sensitivity of the slowly activating delayed rectifier K+ current in cardiac myocytes. Circ Res 96: 64-72.

83. Gamper N, Shapiro MS (2003) Calmodulin mediates Ca2+-dependent modulation of M-type K+ channels. J Gen Physiol 122: 17-31.

84. Gomez-Posada JC, Aivar P, Alberdi A, Alaimo A, Etxeberria A, et al. (2011) Kv7 channels can function without constitutive calmodulin tethering. PLoS One 6: e25508.

85. Alaimo A, Gomez-Posada JC, Aivar P, Etxeberria A, Rodriguez-Alfaro JA, et al. (2009) Calmodulin activation limits the rate of KCNQ2 K+ channel exit from the endoplasmic reticulum. J Biol Chem 284: 20668-20675.

86. Etxeberria A, Aivar P, Rodriguez-Alfaro JA, Alaimo A, Villace P, et al. (2008) Calmodulin regulates the trafficking of KCNQ2 potassium channels. Faseb J 22: 1135-1143.

87. Ghosh S, Nunziato DA, Pitt GS (2006) KCNQ1 assembly and function is blocked by long-QT syndrome mutations that disrupt interaction with calmodulin. Circ Res 98: 1048-1054.

88. Wen H, Levitan IB (2002) Calmodulin is an auxiliary subunit of KCNQ2/3 potassium channels. J Neurosci 22: 7991-8001.

89. Gamper N, Li Y, Shapiro MS (2005) Structural requirements for differential sensitivity of KCNQ K+ channels to modulation by Ca2+/calmodulin. Mol Biol Cell 16: 3538-3551.

90. Hernandez CC, Zaika O, Tolstykh GP, Shapiro MS (2008) Regulation of neural KCNQ channels: signalling pathways, structural motifs and functional implications. J Physiol. England. pp. 1811-1821.

91. Regev N, Degani-Katzav N, Korngreen A, Etzioni A, Siloni S, et al. (2009) Selective interaction of syntaxin 1A with KCNQ2: possible implications for specific modulation of presynaptic activity. PLoS One 4: e6586.

92. Etzioni A, Siloni S, Chikvashvilli D, Strulovich R, Sachyani D, et al. (2011) Regulation of neuronal M-channel gating in an isoform-specific manner: functional interplay between calmodulin and syntaxin 1A. J Neurosci 31: 14158-14171.

93. Asada K, Kurokawa J, Furukawa T (2009) Redox- and calmodulin-dependent S-nitrosylation of the KCNQ1 channel. J Biol Chem. United States. pp. 6014-6020.

94. Xiong Q, Gao Z, Wang W, Li M (2008) Activation of Kv7 (KCNQ) voltage-gated potassium channels by synthetic compounds. Trends Pharmacol Sci 29: 99-107.

95. Xiong Q, Sun H, Li M (2007) Zinc pyrithione-mediated activation of voltage-gated KCNQ potassium channels rescues epileptogenic mutants. Nat Chem Biol 3: 287-296.

96. Salata JJ, Jurkiewicz NK, Wang J, Evans BE, Orme HT, et al. (1998) A novel benzodiazepine that activates cardiac slow delayed rectifier K+ currents. Mol Pharmacol 54: 220-230.

97. Gao Z, Xiong Q, Sun H, Li M (2008) Desensitization of chemical activation by auxiliary subunits: Convergence of molecular determinants critical for augmenting KCNQ1 potassium channels. J Biol Chem 283: 22649-22658.

98. Abitbol I, Peretz A, Lerche C, Busch AE, Attali B (1999) Stilbenes and fenamates rescue the loss of I(KS) channel function induced by an LQT5 mutation and other IsK mutants. Embo J 18: 4137-4148.

99. Slack M, Kirchhoff C, Moller C, Winkler D, Netzer R (2006) Identification of novel Kv1.3 blockers using a fluorescent cell-based ion channel assay. J Biomol Screen 11: 57-64.

100. Belardetti F, Tringham E, Eduljee C, Jiang X, Dong H, et al. (2009) A fluorescence-based high-throughput screening assay for the identification of T-type calcium channel blockers. Assay Drug Dev Technol 7: 266-280.

101. Seebohm G (2005) Activators of cation channels: potential in treatment of channelopathies. Mol Pharmacol 67: 585-588.

102. Shah MM, Mistry M, Marsh SJ, Brown DA, Delmas P (2002) Molecular correlates of the M-current in cultured rat hippocampal neurons. J Physiol. England. pp. 29-37.

103. Hadley JK, Passmore GM, Tatulian L, Al-Qatari M, Ye F, et al. (2003) Stoichiometry of expressed KCNQ2/KCNQ3 potassium channels and subunit composition of native ganglionic M channels deduced from block by tetraethylammonium. The Journal of neuroscience : the official journal of the Society for Neuroscience 23: 5012-5019.

104. Kurokawa J, Motoike HK, Kass RS (2001) TEA(+)-sensitive KCNQ1 constructs reveal pore-independent access to KCNE1 in assembled I(Ks) channels. J Gen Physiol 117: 43-52.

105. MacKinnon R (1991) Determination of the subunit stoichiometry of a voltage-activated potassium channel. Nature 350: 232-235.

106. MacKinnon R, Aldrich RW, Lee AW (1993) Functional stoichiometry of Shaker potassium channel inactivation. Science 262: 757-759.

107. Chen H, Kim LA, Rajan S, Xu S, Goldstein SA (2003) Charybdotoxin binding in the I_{Ks} pore demonstrates two MinK subunits in each channel complex. Neuron 40: 15-23.

108. Morin TJ, Kobertz WR (2008) Counting Membrane-Embedded KCNE β-subunits in Functioning K^+ Channel Complexes. Proc Natl Acad Sci USA 105: 1478-1482.

109. Blaustein RO, Cole PA, Williams C, Miller C (2000) Tethered blockers as molecular 'tape measures' for a voltage-gated K^+ channel. Nat Struct Biol 7: 309-311.

110. Kramer RH, Chambers JJ, Trauner D (2005) Photochemical tools for remote control of ion channels in excitable cells. Nat Chem Biol 1: 360-365.

111. Kramer RH, Fortin DL, Trauner D (2009) New photochemical tools for controlling neuronal activity. Curr Opin Neurobiol. England. pp. 544-552.

112. Fortin DL, Dunn TW, Fedorchak A, Allen D, Montpetit R, et al. (2011) Optogenetic photochemical control of designer K+ channels in mammalian neurons. J Neurophysiol 106: 488-496.

113. Hua Z, Lvov A, Morin TJ, Kobertz WR (2011) Chemical control of metabolically-engineered voltage-gated K+ channels. Bioorg Med Chem Lett 21: 5021-5024.

114. Nowak MW, Gallivan JP, Silverman SK, Labarca CG, Dougherty DA, et al. (1998) In vivo incorporation of unnatural amino acids into ion channels in Xenopus oocyte expression system. Methods Enzymol 293: 504-529.

115. Vanoye CG, Welch RC, Tian C, Sanders CR, George AL, Jr. (2010) KCNQ1/KCNE1 assembly, co-translation not required. Channels (Austin) 4: 108-114.

116. Marsal J, Tigyi G, Miledi R (1995) Incorporation of acetylcholine receptors and Cl-channels in Xenopus oocytes injected with Torpedo electroplaque membranes. Proc Natl Acad Sci U S A 92: 5224-5228.

117. Wang KW, Goldstein SA (1995) Subunit composition of minK potassium channels. Neuron 14: 1303-1309.

118. Stuhmer W (1998) Electrophysiologic recordings from Xenopus oocytes. Methods Enzymol 293: 280-300.

119. Zerangue N, Schwappach B, Jan YN, Jan LY (1999) A new ER trafficking signal regulates the subunit stoichiometry of plasma membrane K(ATP) channels. Neuron 22: 537-548.

120. Gage SD, Kobertz WR (2004) KCNE3 Truncation Mutants Reveal a Bipartite Modulation of KCNQ1 K^+ Channels. J Gen Physiol 124: 759-771.

121. Rocheleau JM, Gage SD, Kobertz WR (2006) Secondary Structure of a KCNE Cytoplasmic Domain. J Gen Physiol 128: 721-729.

122. Goldin AL (1992) Maintenance of Xenopus laevis and oocyte injection. Methods Enzymol 207: 266-279.

123. Green SL (2002) Factors affecting oogenesis in the South African clawed frog (Xenopus laevis). Comp Med 52: 307-312.

124. Godfrey EW, Sanders GE (2004) Effect of water hardness on oocyte quality and embryo development in the African clawed frog (Xenopus laevis). Comp Med 54: 170-175.

125. Delpire E, Gagnon KB, Ledford JJ, Wallace JM (2011) Housing and Husbandry of Xenopus laevis Affect the Quality of Oocytes for Heterologous Expression Studies. J Am Assoc Lab Anim Sci 50: 46-53.

126. Wu M, Gerhart J (1991) Raising Xenopus in the laboratory. Methods Cell Biol 36: 3-18.

127. Giorgetti A, Carloni P (2003) Molecular modeling of ion channels: structural predictions. Curr Opin Chem Biol. England. pp. 150-156.

128. Smith JA, Vanoye CG, George AL, Jr., Meiler J, Sanders CR (2007) Structural models for the KCNQ1 voltage-gated potassium channel. Biochemistry 46: 14141-14152.

129. Van Horn WD, Vanoye CG, Sanders CR (2011) Working model for the structural basis for KCNE1 modulation of the KCNQ1 potassium channel. Curr Opin Struct Biol 21: 283-291.

130. Faraldo-Gomez JD, Smith GR, Sansom MS (2002) Setting up and optimization of membrane protein simulations. Eur Biophys J 31: 217-227.

131. Lipkind GM, Fozzard HA (1997) A model of scorpion toxin binding to voltage-gated K+ channels. J Membr Biol 158: 187-196.

132. Shiau YS, Huang PT, Liou HH, Liaw YC, Shiau YY, et al. (2003) Structural basis of binding and inhibition of novel tarantula toxins in mammalian voltage-dependent potassium channels. Chem Res Toxicol 16: 1217-1225.

133. Seebohm G, Chen J, Strutz N, Culberson C, Lerche C, et al. (2003) Molecular determinants of KCNQ1 channel block by a benzodiazepine. Mol Pharmacol 64: 70-77.

134. Decher N, Pirard B, Bundis F, Peukert S, Baringhaus KH, et al. (2004) Molecular basis for Kv1.5 channel block: conservation of drug binding sites among voltage-gated K+ channels. J Biol Chem 279: 394-400.

135. Strutz-Seebohm N, Pusch M, Wolf S, Stoll R, Tapken D, et al. (2011) Structural basis of slow activation gating in the cardiac I Ks channel complex. Cell Physiol Biochem 27: 443-452.

136. Rhoads AR, Friedberg F (1997) Sequence motifs for calmodulin recognition. Faseb J 11: 331-340.

137. Schonherr R, Lober K, Heinemann SH (2000) Inhibition of human ether a go-go potassium channels by Ca(2+)/calmodulin. Embo J 19: 3263-3271.

138. Ziechner U, Schonherr R, Born AK, Gavrilova-Ruch O, Glaser RW, et al. (2006) Inhibition of human ether a go-go potassium channels by Ca2+/calmodulin binding to the cytosolic N- and C-termini. Febs J 273: 1074-1086.

139. Hirschberg B, Maylie J, Adelman JP, Marrion NV (1998) Gating of recombinant small-conductance Ca-activated K+ channels by calcium. J Gen Physiol 111: 565-581.

140. Black DJ, LaMartina D, Persechini A (2009) The IQ domains in neuromodulin and PEP19 represent two major functional classes. Biochemistry 48: 11766-11772.

141. DeMaria CD, Soong TW, Alseikhan BA, Alvania RS, Yue DT (2001) Calmodulin bifurcates the local Ca2+ signal that modulates P/Q-type Ca2+ channels. Nature 411: 484-489.

142. Maylie J, Bond CT, Herson PS, Lee WS, Adelman JP (2004) Small conductance Ca2+-activated K+ channels and calmodulin. J Physiol 554: 255-261.

143. Mori MX, Vander Kooi CW, Leahy DJ, Yue DT (2008) Crystal structure of the CaV2 IQ domain in complex with Ca2+/calmodulin: high-resolution mechanistic implications for channel regulation by Ca2+. Structure 16: 607-620.

144. Contessa GM, Orsale M, Melino S, Torre V, Paci M, et al. (2005) Structure of calmodulin complexed with an olfactory CNG channel fragment and role of the central linker: residual dipolar couplings to evaluate calmodulin binding modes outside the kinase family. J Biomol NMR 31: 185-199.

145. Fallon JL, Baker MR, Xiong L, Loy RE, Yang G, et al. (2009) Crystal structure of dimeric cardiac L-type calcium channel regulatory domains bridged by Ca2+* calmodulins. Proc Natl Acad Sci U S A 106: 5135-5140.

146. Kim EY, Rumpf CH, Van Petegem F, Arant RJ, Findeisen F, et al. (2010) Multiple C-terminal tail Ca(2+)/CaMs regulate Ca(V)1.2 function but do not mediate channel dimerization. Embo J 29: 3924-3938.

147. Schumacher MA, Rivard AF, Bachinger HP, Adelman JP (2001) Structure of the gating domain of a Ca2+-activated K+ channel complexed with Ca2+/calmodulin. Nature 410: 1120-1124.

148. O'Connell D, Mruk K, Rocheleau JM, Kobertz WR (2011) Xenopus laevis Oocytes Infected with Multi-drug Resistant Bacteria: Implications for Electrical Recordings. *J Gen Physiol (in press)*.

149. Cartaud A, Ozon R, Walsh MP, Haiech J, Demaille JG (1980) Xenopus laevis oocyte calmodulin in the process of meiotic maturation. J Biol Chem 255: 9404-9408.

150. Cicirelli MF, Smith LD (1986) Calmodulin synthesis and accumulation during oogenesis and maturation of Xenopus laevis oocytes. Dev Biol 113: 174-181.

151. Yellen G, Jurman ME, Abramson T, MacKinnon R (1991) Mutations affecting internal TEA blockade identify the probable pore-forming region of a K+ channel. Science 251: 939-942.

152. Suh BC, Hille B (2007) Electrostatic interaction of internal Mg2+ with membrane PIP2 Seen with KCNQ K+ channels. J Gen Physiol 130: 241-256.

153. Cicirelli MF, Robinson KR, Smith LD (1983) Internal pH of Xenopus oocytes: a study of the mechanism and role of pH changes during meiotic maturation. Dev Biol 100: 133-146.

154. Cicirelli MF, Smith LD (1986) Calmodulin Synthesis and Accumulation during Oogenesis and Maturation of Xenopus laevis Oocytes. Developmental Biology 113: 171-181.

155. Cukovic D, Lu GW, Wible B, Steele DF, Fedida D (2001) A discrete amino terminal domain of Kv1.5 and Kv1.4 potassium channels interacts with the spectrin repeats of alpha-actinin-2. FEBS Lett 498: 87-92.

156. Morin TJ, Kobertz WR (2008) Tethering Chemistry and K^+ Channels. J Biol Chem 283: 25105-25109.

157. Erickson MG, Liang H, Mori MX, Yue DT (2003) FRET two-hybrid mapping reveals function and location of L-type Ca2+ channel CaM preassociation. Neuron 39: 97-107.

158. Klevit RE, Dalgarno DC, Levine BA, Williams RJ (1984) 1H-NMR studies of calmodulin. The nature of the Ca2+-dependent conformational change. Eur J Biochem 139: 109-114.

159. Jespersen T, Grunnet M, Olesen SP (2005) The KCNQ1 potassium channel: from gene to physiological function. Physiology (Bethesda) 20: 408-416.

160. Splawski I, Shen J, Timothy KW, Lehmann MH, Priori S, et al. (2000) Spectrum of mutations in long-QT syndrome genes. KVLQT1, HERG, SCN5A, KCNE1, and KCNE2. Circulation 102: 1178-1185.

161. Rocheleau JM, Kobertz WR (2008) KCNE Peptides Differently Affect Voltage Sensor Equilibrium and Equilibration Rates in KCNQ1 K^+ Channels. J Gen Physiol 131: 59-68.

162. Nakajo K, Kubo Y (2007) KCNE1 and KCNE3 Stabilize and/or Slow Voltage Sensing S4 Segment of KCNQ1 Channel. J Gen Physiol 130: 269-281.

163. Panaghie G, Abbott GW (2007) The role of S4 charges in voltage-dependent and voltage-independent KCNQ1 potassium channel complexes. J Gen Physiol 129: 121-133.

164. MacKinnon R, Yellen G (1990) Mutations affecting TEA blockade and ion permeation in voltage-activated K+ channels. Science 250: 276-279.

165. Choi KL, Aldrich RW, Yellen G (1991) Tetraethylammonium blockade distinguishes two inactivation mechanisms in voltage-activated K+ channels. Proc Natl Acad Sci U S A 88: 5092-5095.

166. Baukrowitz T, Yellen G (1996) Use-dependent blockers and exit rate of the last ion from the multi-ion pore of a K+ channel. Science 271: 653-656.

167. Gutman GA, Chandy KG, Grissmer S, Lazdunski M, McKinnon D, et al. (2005) International Union of Pharmacology. LIII. Nomenclature and molecular relationships of voltage-gated potassium channels. Pharmacol Rev 57: 473-508.

168. Lerche C, Seebohm G, Wagner CI, Scherer CR, Dehmelt L, et al. (2000) Molecular impact of MinK on the enantiospecific block of I(Ks) by chromanols. Br J Pharmacol 131: 1503-1506.

169. Busch AE, Busch GL, Ford E, Suessbrich H, Lang HJ, et al. (1997) The role of the IsK protein in the specific pharmacological properties of the IKs channel complex. Br J Pharmacol 122: 187-189.

170. Patthy L, Smith EL (1975) Reversible modification of arginine residues. Application to sequence studies by restriction of tryptic hydrolysis to lysine residues. J Biol Chem 250: 557-564.

171. Seebohm G, Sanguinetti MC, Pusch M (2003) Tight coupling of rubidium conductance and inactivation in human KCNQ1 potassium channels. J Physiol 552: 369-378.

172. Pusch M, Bertorello L, Conti F (2000) Gating and flickery block differentially affected by rubidium in homomeric KCNQ1 and heteromeric KCNQ1/KCNE1 potassium channels. Biophys J 78: 211-226.

173. Schwake M, Pusch M, Kharkovets T, Jentsch TJ (2000) Surface Expression and Single Channel Properties of KCNQ2/KCNQ3, M-type K+ Channels Involved in Epilepsy. J Biol Chem 275: 13343-13348.

174. Selyanko AA, Hadley JK, Brown DA (2001) Properties of single M-type KCNQ2/KCNQ3 potassium channels expressed in mammalian cells. J Physiol 534: 15-24.

175. Li Y, Gamper N, Shapiro MS (2004) Single-channel analysis of KCNQ K+ channels reveals the mechanism of augmentation by a cysteine-modifying reagent. J Neurosci 24: 5079-5090.

176. Sesti F, Goldstein SA (1998) Single-channel characteristics of wild-type IKs channels and channels formed with two minK mutants that cause long QT syndrome. J Gen Physiol 112: 651-663.

177. Yang Y, Sigworth FJ (1998) Single-channel properties of IKs potassium channels. J Gen Physiol 112: 665-678.

178. Yan J, Springsteen G, Deeter S, Wang B (2004) The relationship among pKa, pH, and binding constants in the interactions between boronic acids and diols--it is not as simple as it appears. Tetrahedron 60: 11205-11209.

179. Springsteen G, Wang B (2002) A detailed examination of boronic acid-diol complexation. Tetrahedron 58: 5291-5300.

180. Roche JP, Westenbroek R, Sorom AJ, Hille B, Mackie K, et al. (2002) Antibodies and a cysteine-modifying reagent show correspondence of M current in neurons to KCNQ2 and KCNQ3 K+ channels. Br J Pharmacol 137: 1173-1186.

181. Mitcheson JS, Chen J, Sanguinetti MC (2000) Trapping of a methanesulfonanilide by closure of the HERG potassium channel activation gate. J Gen Physiol 115: 229-240.

182. Mitcheson J, Perry M, Stansfeld P, Sanguinetti MC, Witchel H, et al. (2005) Structural determinants for high-affinity block of hERG potassium channels. Novartis Found Symp 266: 136-150; discussion 150-138.

183. Mitcheson JS, Chen J, Lin M, Culberson C, Sanguinetti MC (2000) A structural basis for drug-induced long QT syndrome. Proc Natl Acad Sci U S A 97: 12329-12333.

184. Bunn PA, Jr. (2004) The potential role of proteasome inhibitors in the treatment of lung cancer. Clin Cancer Res 10: 4263s-4265s.

185. Kaneko S, Akaike A, Satoh M (1998) Cut-open recording techniques. Methods Enzymol 293: 319-331.

186. Stefani E, Bezanilla F (1998) Cut-open oocyte voltage-clamp technique. Methods Enzymol 293: 300-318.

187. Maduke M, Williams C, Miller C (1998) Formation of CLC-0 chloride channels from separated transmembrane and cytoplasmic domains. Biochemistry 37: 1315-1321.

188. Sonnleitner A, Mannuzzu LM, Terakawa S, Isacoff EY (2002) Structural rearrangements in single ion channels detected optically in living cells. Proc Natl Acad Sci U S A 99: 12759-12764.

189. Weber W (1999) Ion currents of Xenopus laevis oocytes: state of the art. Biochim Biophys Acta 1421: 213-233.

190. Elsner HA, Honck HH, Willmann F, Kreienkamp HJ, Iglauer F (2000) Poor quality of oocytes from Xenopus laevis used in laboratory experiments: prevention by use of antiseptic surgical technique and antibiotic supplementation. Comp Med 50: 206-211.

191. Gingell D (1970) Contractile Responses at the Surface of an Amphibian Egg. J Embryol exp Morph 23: 583-609.

192. Merriam RW, Christensen K (1983) A Contractile Ring-like Mechanism in Wound Healing and Soluble Factors Affecting Structural Stability in the Cortex of *Xenopus* Eggs and Oocytes. J Embryol exp Morph 75: 11-20.

193. Bement WM, Mandato CA, Kirsch MN (1999) Wound-induced assembly and closure of an actomyosin purse string in Xenopus oocytes. Curr Biol 9: 579-587.

194. Sosa A (2007) The Threat of Antibiotic-resistant Bacteria and the Development of new Antibiotics. In: Amabile-Cuevas C, editor. Antimicrobial Resistance in Bacteria. Norfolk, UK: Horizon Bioscience. pp. 7-24.

195. Reavill DR (2001) Amphibian Skin Diseases. Vet Clin North Am Exot Anim Pract 4: 413-440.

196. Wright KM, Whitaker BR (2001) Pharmacotherapeutics. In: Wright KM, Whitaker BR, editors. Amphibian Medicine and Captive Husbandry. Malabar, FL: Krieger Publishing Co. pp. 309-330.

197. Green S (2010) The Laboratory Xenopus sp.; M. S, editor. Boca Raton, FL: CRC Press. 180 p.

198. Tadross MR, Dick IE, Yue DT (2008) Mechanism of local and global Ca2+ sensing by calmodulin in complex with a Ca2+ channel. Cell 133: 1228-1240.

199. Bett GC, Morales MJ, Beahm DL, Duffey ME, Rasmusson RL (2006) Ancillary subunits and stimulation frequency determine the potency of chromanol 293B block of the KCNQ1 potassium channel. J Physiol 576: 755-767.

200. Lerche C, Bruhova I, Lerche H, Steinmeyer K, Wei AD, et al. (2007) Chromanol 293B binding in KCNQ1 (Kv7.1) channels involves electrostatic interactions with a potassium ion in the selectivity filter. Mol Pharmacol 71: 1503-1511.

201. Ciampa EJ, Welch RC, Vanoye CG, George AL, Jr. (2011) KCNE4 juxtamembrane region is required for interaction with calmodulin and for functional suppression of KCNQ1. J Biol Chem 286: 4141-4149.

202. Splawski I, Tristani-Firouzi M, Lehmann MH, Sanguinetti MC, Keating MT (1997) Mutations in the hminK gene cause long QT syndrome and suppress IKs function. Nat Genet 17: 338-340.

203. Lima LM, Barreiro EJ (2005) Bioisosterism: a useful strategy for molecular modification and drug design. Curr Med Chem 12: 23-49.

204. Mruk K, Kobertz WR (2009) Discovery of a Novel Activator of KCNQ1-KCNE1 K^+ Channel Complexes. *PLoS ONE* 4: e4236.

205. Melman YF, Um SY, Krumerman A, Kagan A, McDonald TV (2004) KCNE1 Binds to the KCNQ1 Pore to Regulate Potassium Channel Activity. Neuron 42: 927-937.

206. Peretz A, Pell L, Gofman Y, Haitin Y, Shamgar L, et al. (2010) Targeting the voltage sensor of Kv7.2 voltage-gated K+ channels with a new gating-modifier. Proc Natl Acad Sci U S A 107: 15637-15642.

207. Unsold B, Kerst G, Brousos H, Hubner M, Schreiber R, et al. (2000) KCNE1 reverses the response of the human K+ channel KCNQ1 to cytosolic pH changes and alters its pharmacology and sensitivity to temperature. Pflugers Arch 441: 368-378.

208. Balse E, Steele DF, Abriel H, Coulombe A, Fedida D, et al. (2012) Dynamic of ion channel expression at the plasma membrane of cardiomyocytes. Physiol Rev 92: 1317-1358.

209. Bentzen BH, Schmitt N, Calloe K, Dalby Brown W, Grunnet M, et al. (2006) The acrylamide (S)-1 differentially affects Kv7 (KCNQ) potassium channels. Neuropharmacology 51: 1068-1077.

210. Ulrich S. Schubert HH, George R. Newkome (2006) Modern Terpyridine Chemistry: Wiley-VCH. 229 p.